A NETWORK APPROACH FOR THE PREDICTION OF FLOW AND FLOW SPLITS WITHIN A GAS TURBINE COMBUSTOR

By

Johannes Jacobus Pretorius

Presented in partial fulfilment of the requirements for the degree

Master of Mechanical Engineering

In the Faculty of Engineering, Building Environment and Information Technology
University of Pretoria
Pretoria

March

2005

Abstract

A NETWORK APPROACH FOR THE PREDICTION OF FLOW AND FLOW SPLITS WITHIN A GAS TURBINE COMBUSTOR

By

Johannes Jacobus Pretorius

Promotors:

Dr A.G. Malan, Prof. J.A. Visser

Department of Mechanical and Aeronautical Engineering

Degree: *Master of Mechanical Engineering*

The modern gas turbine engine industry needs a simpler and faster method to facilitate the design of gas turbine combustors due to the enormous costs of experimental test rigging and detailed computational fluid dynamics (CFD) simulations. Therefore, in the initial design phase, a couple of preliminary designs are conducted to establish initial values for combustor performance and geometric characteristics. In these preliminary designs, various one-dimensional models using analytical and empirical formulations may be used. One of the disadvantages of existing models is that they are typically geometric dependant, i.e. they apply only to the geometry they are derived for. Therefore the need for a more versatile design tool exists.

In this work, which constitutes the first step in the development of such a versatile design tool, a single equation-set network simulation model to describe both steady state compressible and incompressible isothermal flow is developed. The continuity and momentum equations are solved through a hybrid type network model analogy which makes use of the SIMPLE pressure correction methodology. The code has the capability to efficiently compute flow through elements where the loss factor K is highly flow dependant and accurately describes variable area duct flow in the case of incompressible flow. The latter includes ducts with discontinuously varying flow

cross-sectional areas. Proper treatment of flow related non-linearities, such as flow friction, is facilitated in a natural manner in the proposed methodology.

The proposed network method is implemented into a *Windows* based simulation package with a user interface. The ability of the proposed method to accurately model both compressible and incompressible flow is demonstrated through the analyses of a number of benchmark problems. It will be shown that the proposed methodology yields similar or improved results as compared to other's work.

The proposed method is applied to a research combustor to solve for isothermal flows and flow splits. The predicted flows were in relatively close agreement with measured data as well as detailed CFD analysis.

Keywords:

Pipe network analysis
Gas turbine combustors
Computational fluid dynamics
Compressible and incompressible flow
Gas dynamics
Flow splits
SIMPLE method
Variable area ducts

Uittreksel

‘N NETWERK METODE VIR DIE VOORSPELLING VAN VLOEI EN VLOEI VERDELINGS BINNE GASTURBIEN VERBRANDINGSRUIME

Deur

Johannes Jacobus Pretorius

Studieleiers:

Dr A.G. Malan, Prof. J.A. Visser

Department van Meganiese en Lugvaartkundige Ingenieurswese

Graad: *Magister in Meganiese Ingenieurswese*

Die moderne gas turbien industrie benodig vinniger en eenvoudiger metodes om die ontwerp van gas turbien verbrandingsruime te fasiliteer as gevolg van die enorme koste verbonde aan experimentele toets opstellings en gedetaileerde berekenings vloei dinamika (BVD) simulasies. Gevolglik word daar in die aanvangsontwerp fase ‘n paar konsep ontwerpe gegenereer om sodoende die aanvangswaardes vir verbrander prestasie en geometriese karakteristieke te bepaal. In hierdie konsep ontwerp fase word verskeie een-dimensionele modelle gebruik wat uit analitiese en empiriese formuleerings bestaan. Een nadeel van huidige modelle is dat hulle oor die algemeen geometries beperk is en dus slegs gebruik kan word vir die geometrie waarvoor hulle afgelei is. Gevolglik bestaan daar ‘n behoefte aan ‘n meer algemene ontwerpshulpmiddel.

In hierdie werkstuk, wat beskou kan word as die eerste stap in die ontwikkeling van so ‘n ontwerpshulpmiddel, word ‘n enkel-vergelyking-stel netwerk-simulasie-model wat gestadigde isotermiese samedrukbare en onsamedrukbare vloeie kan beskryf, ontwikkel. Die kontinuteits- en momentum vergelykings word deur ‘n gemengde tipe netwerk model analogie opgelos deur gebruik te maak van die SIMPLE druk-korreksie metode. Die kode het die vermoeë om vloei deur elemente waar die verlies-

faktor hoogs afhanklik is van die vloei effektief op te los as ook die simulasie van onsamedrukbare vloeie waar die area van die kanaal verander. Laasgenoemde sluit kanale met varieerbare diskontinuele deursnit areas in. Die handtering van vloei verwante nie-lineariteite soos vloei wrywing word op ‘n natuurlike wyse deur die voorgestelde metodiek gehandteer.

Die voorgestelde metode is geimplementeer in ‘n *Windows* gebaseerde simulasie pakket met ‘n gebruikersintervlak. Die vermoeë van die voorgestelde metode om beide samedrukbare en onsamedrukbare vloeie akkuraat te modeleer word gedemonstreer deur die oplos van ‘n aantal verwysingsprobleme. Dit sal ook uitgewys word dat die voorgestelde metode eenderse en selfs beter resultate lewer as in vergelyking met die van ander navorsers.

Die voorgestelde metode word toegepas op ‘n navorsingsverbrander om isotermiese vloeie en vloei verdelings te simuleer. Die voorspelde vloeie is in relatiewe goeie vergelyking met gemete data asook die resultate van gedetaileerde BVD analises.

Sleutelterme:

Pyp netwerk analise
Gas turbiene verbranding
Berekenings vloei dinamika
Samedrukbare- en onsamedrukbare vloei
Gas dinamika
Vloei verdelings
SIMPLE metode
Varieerbare area kanale

Acknowledgements

I would like to thank the following for their assistance, contribution or influence on me throughout the course of this dissertation:

- Firstly, my Creator, for giving me so much opportunities and chances. Thank you Lord for making this dissertation possible.

- Dr. A.G. Malan for all the assistance, support, suggestions and time he spent assisting me during this dissertation. I sincerely appreciate all the help and encouragement.

- Prof. Josua Meyer for his insight, assistance and diligence overseeing this dissertation to succession.

- Dr. J.E van Niekerk for very helpful discussions and recommendations regarding fluid flow and gas dynamics during the development of this simulation package.

- Thomas Roos for his interest in this research and the many helpful discussions and ideas.

- Armscor for funding this research project.

- Lastly I would like to thank my close family, in particular my parents, for their never ending interest, support, understanding and encouragement during this study and their comfort, through a very difficult time, in the end, I had to face.

SOLI DEO GLORIA

Table of Contents

CHAPTER 1

Introduction

*Chapter 1 serves as an **Introduction** to the simulation of physical problems using a flow network methodology. The method is to be capable of dealing with both compressible and incompressible flow. The work objectives are stated, and some background on certain components found in gas turbine propulsion given. The need and objectives for this study is explained, and an outline of the study is provided.*

1.1 The problem under consideration

The main development goal in the modern gas turbine industry is the enhancement of the efficiency of these engines. Therefore, one will find that modern gas turbine engines operate progressively at higher compression ratios, lower specific fuel consumptions, higher turbine inlet temperatures and lower carbon oxide emission. These gas turbine engines are more compact in layout and also features higher thrust to weight ratios, while being considerably less noisy than their older counter parts. The design-process related costs to furnish improved engines are becoming more costly as technological boundaries are pushed further, and therefore more effective design methods are required [1].

One of the critical components in obtaining a highly efficient engine is the combustor. When designing a gas turbine combustor, important overall performance requirements such as combustion efficiency, lean lightoff and blowoff limits, exit temperature traverse and CO and NO_x emissions, among others, have to be taken into consideration. In the past, empirical and semi-empirical models combined with full-scale experimental investigations were used to design gas turbine combustors. With the recent improvement of computational fluid dynamic (CFD) models, CFD analysis added a new dimension to combustor design. The use of CFD analysis is usually undertaken after completing the initial design and before starting with the experimental phase. CFD has the advantage that detailed design information can be obtained at a fraction of the costs of experiments. Design changes may follow this more complicated combustor analysis, in which case, the analysis process has to be repeated. Although advanced CFD analyses are more cost effective than experimental tests, it is still expensive [2]. The designer therefore requires accurate simplified empirical and semi-empirical models for the preliminary design phase prior to the initiation of such advanced analysis. Such methods provide first order information regarding quantities like pressure loss, heat transfer and mass-flow splits.

The preliminary design of a gas turbine is a tedious task and may normally require the use of cumbersome and in some cases, geometrically restrictive, semi-empirical models [2]. Over the years successful evolutionary combustor improvements have been established with such empirically based procedures [2]. When different configurations and new technological designs are required that differs significantly from proven concepts, these empirical procedures can prove extremely limited.

Most of the empirical models provide details about the overall sizing of the combustor and the design of the individual combustor zones as separate units. The problem facing the modern design engineer is that these zones do not operate in isolation and affects one another in practice. The requirement therefore, exists for an improved empirical model that can be used for the initial overall geometrical design of gas turbine combustors by accounting for the effect that the different zone layouts will have on each another.

1.2 Review of related literature

1.2.1 Empirical and Analytical models

The goal in gas turbine combustor design and development is to obtain an acceptable trade-off between the conflicting design objectives such as combustion efficiency, gaseous emissions, smoke, ignition, restart, lean blowout, burner exit temperature quality, structural durability and life cycle costs [1]. For many years component testing and benchmark tests were conducted to effect a balanced design. The tests were backed by empirically and experience based correlations. The ultimate goal has been to develop a reliable combustor design model that can provide quantitatively accurate predictions of the complex combustion flow field so that an optimum combustion system can be designed within reasonable cost and time constraints [1]. Over the years numerous empirical based procedures and models have been developed to design combustors, which led to successful evolutionary combustor improvements [1]. A typical empirical gas turbine combustor design approach is built

on experience and empirical correlations obtained from extensive component and subcomponent testing [2]. However, when combustor design requirements are significantly different from those in current technology engines, these empirical methods become unsuitable. Some critical areas in which empirical methods exhibit limitations are [2]:

- Empirical based design methods have shown severe limitations in scaling combustors.
- Combustion engineers are hesitant to use existing empirical correlations when significant advances in technology levels are required.
- The applicability of experience-based correlations (for a particular concept) is limited in their use for new or revolutionary combustion design concepts.
- With the ever improving design requirements of advanced technology combustors, better design tools are needed to achieve an optimum solution to satisfy conflicting combustor design requirements.

Analytical combustor modeling methods have been developed to reduce the amount of empirical development work required as well as to predict the air pollutant emissions [3]. Existing analytical models may be subdivided into three groups. The first of these is the turbulent flame speed model, where the calculation of the turbulent flame speed is based on turbulence parameters of the flow and the chemical reaction rate is obtained by using the laminar flame speed. Second is the microvolume burning model, where each zone is assumed to contain a homogenous reacting mixture whereas the mixing and chemical reaction processes are accounted for in a series of turbulent eddies within small cubes in the first model. Third is the stirred reactor model, where turbulence is so high that mixing is instantaneous. A brief discussion of each group follows.

Turbulent flame speed combustor theories have one general point in common: the calculation of the turbulent flame speed is assumed analog to the laminar flame speed, which accounts for the turbulence in the combustion process. Flame propagation from

various sources is then calculated via the turbulent flame speed in order to determine the required combustor dimensions and performance. In the highly turbulent combustor situation, burning is postulated to occur in a discrete zone. The thickness of the zone, i.e. between the flame front and the end of the burning zone, is determined by the chemical reaction rate, which implies that the gas moves through the zone in a streamline like flow fashion (Figure 1.1). The size of the burning zone and its position relative to the flame holder determines the combustion efficiency. The determination of latter is important in the design of a combustor.

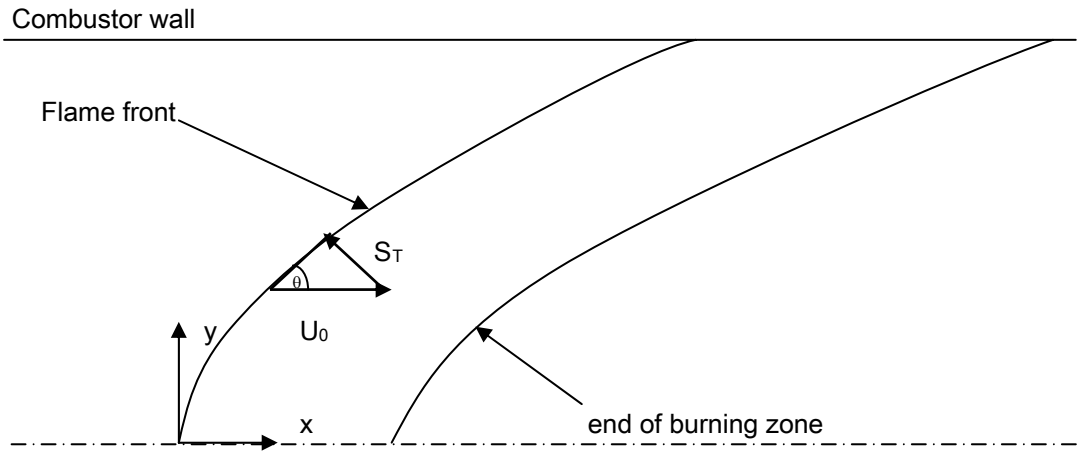

Figure 1.1 Turbulent flame speed combustor model [3]

Several problems arise when attempting to apply the burning velocity analysis to gas turbine combustors. Irregular combustion flames deviates substantially from the reasonably smooth flame concept. All burning is considered to be the result of the primary flame propagation out of the flameholder and the effect of secondary air penetration jets are omitted due to the fact that these analyses focused primarily on ramjet combustors. The latter effect will most certainly influence downstream burning and results in a considerably more complex flame propagation pattern. Since the entire analysis is based on the turbulent flame speed, several methods to determine the turbulent flame speed S_T have been proposed, although great controversy still exists in the determination thereof.

The microvolume burning model, describes the simultaneous phenomenon of mixing and chemical reaction quite successfully [3]. Here it is being postulated that the formation and dissipation of turbulent eddies characterizes mixing, and that these eddies move as particles relative to each other. Turbulent fluctuations in the combustor zone carries these eddies, which contain burned or partially burned gases, out of the combustor zone where it mixes with eddies of fresh gas. This mixing behavior is modeled by means of a grid of microvolume cubes (Figure 1.2).

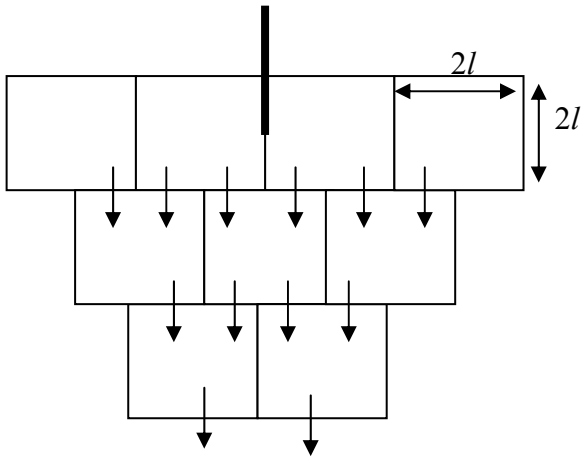

Figure 1.2 Microvolume burning model [3]

The lifetime of an eddy is defined as

$$t_f = \frac{l}{U'}$$

where l is the mixing length and U' the turbulence intensity. The available time for combustion is

$$t_c = t_f - t_{mix} - t_{ign}$$

where t_{mix} is a measure of mixing rate within the eddy and t_{ign} the ignition delay time. The diffusion processes within the eddy smooth out the composition and the

temperature, although surface and volume burning do not ensure homogeneity. Chemical reaction rate considerations therefore become important within an eddy and a compromise has to be reached. This type of analysis approximates the physical process of eddy formation and decay in a certain mixing length. However, the treatment of eddy sizes as homogeneous rather than a statistical size-distribution is a rather severe approximation. No consensus regarding a preferred formulation for mixing lengths and turbulent fluctuations has been reached [3]. The evaluation of t_{mix} and t_{ign} also remains a serious problem [3] because of the different conditions present in each eddy.

A stirred reactor is a zone containing a homogeneous reacting mixture [3]. The temperature, pressure and chemical composition taken at any point within the zone would consequently be identical to each other. Flow entering the volume is mixed instantaneously and exhaust products leaves the zone with the same composition as the reactor. Continuity is assured through the equality of mass flow into and out of the reactor.

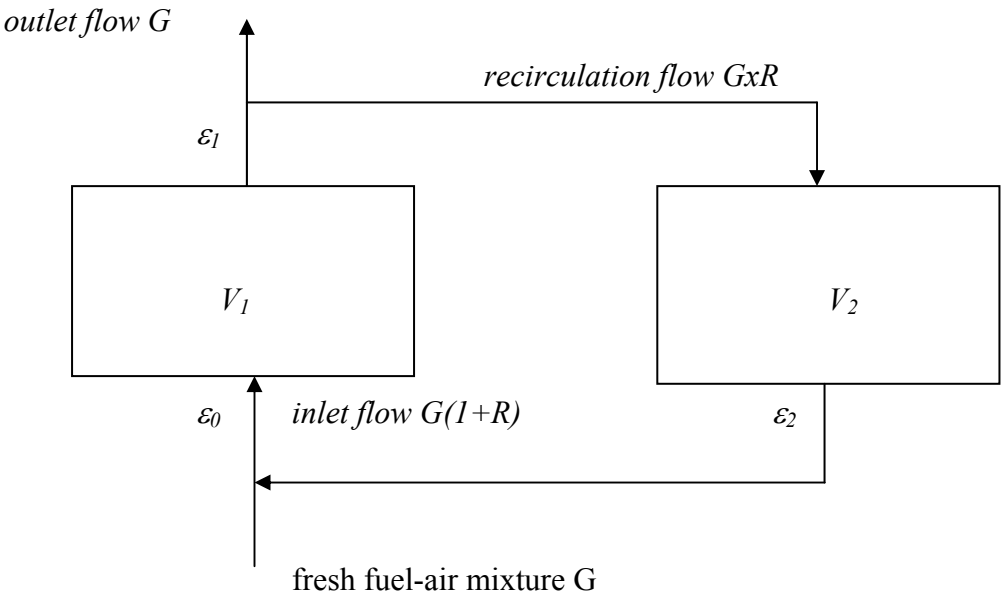

Figure 1.3 Recirculatory stirred reactor model [3].

A dimensionless parameter, the completeness of reaction parameter ε, is defined to describe the completeness of the chemical reaction in the stirred zone because this reaction will not progress to completion in general. For an unreacted mixture ε = 0 and for a completely reacted mixture ε = 1. Many stirred reactor models have been developed to date and references to other models may be found in reference [3]. Figure 1.3 shows one of these models.

Here V_1 and V_2 are stirred reactor volumes. Reactor V_1 represents the combustion in the main flow and reactor V_2 the combustion in the recirculatory flow. G is the fuel feed rate into the system and R an indication of the ratio of flow to G going through V_2. The phenomenon of blow out and a residual flame are predicted quantitatively [3]. However, the quantitative accuracy of the model has not been evaluated and burning in the secondary combustion zones must be accounted for by some other means if this model is to be applied in the analysis of gas turbine combustors. The use of a series of plugged flow reactors proved to be a possible method [3].

1.2.2 Detailed multi-dimensional CFD analysis

Gas turbine combustor flows have been simulated with reasonable success with computational fluid dynamics (CFD) due to advances in CFD modeling. This provides an additional tool in the design process, which may have a powerful influence on future designs. In these codes, combustion system subcomponents such as diffusers, fuel injectors and combustor liners need to be modeled accurately. Therefore physical sub-models and accurate numerical schemes must describe the various aerothermochemical processes (e.g. turbulence and combustion) occurring within the combustion chamber. Some of these sub-models have already been developed although a need for newer and more accurate sub-models exists. The accuracy of CFD simulations remains limited by the submodels they utilize [1,2]. In the following paragraphs some CFD aerothermal models used in combustor aerothermal modeling are discussed briefly [2].

A model suitable for calculating recirculating flows is the k-ε turbulence model. This model attains closure through a gradient transport model for Reynolds stresses with an isotropic eddy viscosity. Corrections to this model for low Reynolds numbers, additional strain due to streamline curvature and swirl (Richardson number correction), and other ad hoc assumptions for changing empirical constants have been made [2]. Conclusions regarding the general capabilities of the k-ε turbulence model are [2]:

- Gives good correlations for simple flows.
- Requires low Reynolds number correction for predicting wall shear flow.
- Model modifications are required to predict curved boundary layers accurately.
- Gives reasonable correlations for most of the flow region created by a confined swirler.
- Predicts the trends for an unconfined swirler.
- Gives good correlations for non-recirculating swirling flows and reasonable results for recirculating nonswirling flows.

The mean flow predictions of the Algebraic Stress Model (ASM) correlate well with those of the k-ε turbulence model. Comments regarding the previous paragraph apply where the mean flow field is concerned. In addition, the ASM gives quantitatively satisfactory predictions for the Reynolds stress components, consistent with the strengths and limitations of the k-ε turbulence model. In several continuing studies the accuracy of the standard k-ε turbulence model and the algebraic and differential Reynolds stress models for use in combustor CFD simulation are being investigated by workers around the world [2].

The k-ε turbulence model with specific Prandtl numbers predicts scalar fluxes reasonably well for flows where the gradient diffusion approximation is valid. Indications are that the algebraic Scalar Transport Model (STM) has the capability to give more accurate predictions as compared to the k-ε model, but its validity for swirling flows is yet to be determined [2].

Another important deficiency that has been identified in the assessment of gas turbine combustor CFD simulation was the accuracy of numerical discretization [2]. The accuracy of the calculation is limited by the numerical approximation wherein the false diffusion is of the same magnitude as the turbulent diffusion. This masked the differences between the various models in such a way that very different turbulence models essentially gave the same result, sometimes resulting in unmerited good agreement between the predictions and the data [2]. In general, if false diffusion is present, the numerical solution will be dependent on the grid density and distribution.

1.2.3 One-dimensional CFD techniques

Even though there are some deficiencies in CFD analyses as mentioned above, a reasonable solution can still be achieved. In some cases, CFD is however just too computational expensive if used in isolation as a design tool and simpler solutions are needed in addition. Empirically based procedures and CFD methodologies have shown great promise when used in combination [1]. Examples of successful application of such methodologies on specific combustors have been published [2]. Historical trend lines and one-dimensional procedures were used to develop a preliminary combustor design. This preliminary design was augmented by a three-dimensional empirical/analytical procedure that resulted in a good qualitative analysis using available sub-models of turbulent reactive flow. Satisfactory preliminary results for different combustors under different operating conditions were obtained.

Another method that proved to be a useful tool in the preliminary analysis of a gas turbine combustor is the characteristic time model [4]. Goals such as combustion efficiency, exit temperature traverse and emission requirements were, among others, were calculated successfully. The model provided details of the preliminary and secondary air requirements and comparisons to test rig data proved reasonably accurate. This form of analysis, which provides predictions for the mass flow splits, pressure loss and heat transfer modes, offers a sound basis for more detailed

computations. The initial design process efficiency may therefore be improved by using such results.

Burrus et al. [5] described one-dimensional models that proved to be successful in the preliminary design and sizing of a combustor. For a given airflow distribution target, the required flow areas could be calculated. Or for given flow areas, the required flow splits and pressure drops could be computed. These one-dimensional models incorporate numerous experimental data and empirically derived correlations to support the simplified governing equations [6].

Due to the success of the above one-dimensional approaches, it is evident that a one-dimensional model has the potential of providing information required for combustor design in less time than a more comprehensive three- dimensional approach such as CFD. Amongst one-dimensional approaches, network models allow for the simple modeling of complex geometries and remove many of the restrictions placed upon conventional one-dimensional methods. The sub models within these procedures such as radiation models, film-cooling models etc. can be combined with relative ease. Therefore the network approach offers a simple procedure of incorporating the latest sub-models in an algorithm, while enabling the complete modeling of a combustor. Network analysis schemes such as the algorithms proposed by Osiadacz [7], Greyvenstein and Laurie [8], and Greyvenstein [20] have to be investigated to find a suitable algorithm for combustion simulation.

1.2.4 Gas network approaches

In the last three decades, there have been numerous attempts to generate numerical solvers to simulate the flow of gas through a pipe network. Most of the solvers were used to simulate the transport of natural gas and fluids in distribution networks. The earliest methods proposed for the simulation of distribution networks dates back to the 1930s when Hardy Cross had published his well-known pipe network methods [33]. Two methods were proposed. One method utilizes a node-based equation to ensure

continuity. The other method utilizes the loop equations to satisfy the pressure balance around closed loops.

Other factors that affect the analysis of pipeline networks are the inclusion of non-pipe elements into the network. The initial fluid stream loses its energy because of frictional losses and heat extraction, while compressors installed in compressor stations compensate for the resultant loss in pressure. In the field of gas turbine combustor analysis, losses through combustor components such as liner holes, swirlers and cooling slots are analogous to these non-pipe elements in gas network analysis.

The simulation of networks is divided into two types; steady state simulation and unsteady state simulation. A network is in the steady state when the values characterizing the flow of gas in the system are not dependant on time. Values of nodal pressures and of flow in the branch elements are computed for known sources, exit pressures and gas mass flow in and out of the system. A common feature of steady state simulation algorithms is that they all solve a set of non-linear algebraic equations by means of the multidimensional Newton Method [10-13], and with good results compared to the well-known Hardy-Cross method. It has also been shown by many authors that the one-dimensional assumption on the gas flow model yielded accurate results for steady and slow varying pipe network flows [13, 14]. The types of methods exploited today to simulate the flow of fluids in networks include the nodal methods, loop methods, element methods and hybrid methods. These are discussed next

The nodal method is shown in Figure 1.4. It utilizes the continuity equation to establish a mass balance at each node of the network. The pressure at each node is provided via a pressure drop-flow relationship across pipe elements, which is established through the momentum equations.

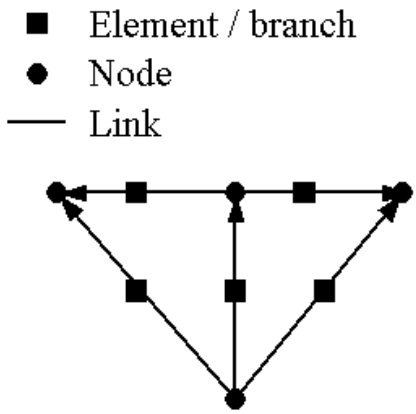

Figure 1.4 Graphical representation of the nodal method [15]

The advantage of the nodal methods lies in the fact that it is straightforward to implement and requires less storage space than the element based methods [8]. There is also no need to specify loops or initial flows that do not violate the continuity equation as with the loop based method, and the method can also deal with mixed boundary conditions that are in the form of either pressure or flow. The other advantage of the nodal method is the high degree of sparsity of the solution matrix [7]. However, the main disadvantage of the traditional nodal method is the poor convergence characteristic that it poses. The method is extremely sensitive to initial pressure values, and the solution diverges when these initial values are far removed from the solution. This makes the traditional method unattractive for combustor simulation.

The loop method is shown in Figure 1.5. This method uses the same basic set of equations as the nodal method but with different boundary conditions [11].

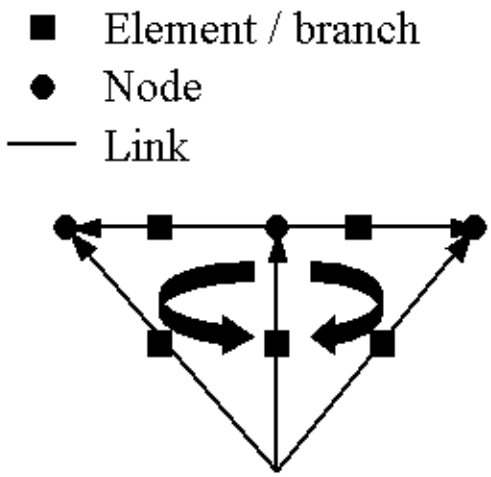

Figure 1.5 Graphical representation of the loop method [15]

This method involves constructing a number of loops representing the flow through a network. Kirchoff's second law, from which it follows that the sum of the pressure-drops around any loop equals zero, is applied. These so-called loop flows represent the flow correction to be added to the branch flows to give the true flow values. By employing a pressure drop-flow relationship, the corrected flows are calculated. The advantage of this method is that the storage requirement is less than that of the other methods. The method also poses very good convergence characteristics. However, the most prevalent disadvantage of this method comes from having to define loops. Because of the many different combinations in which the loops may be generated, it is very difficult to obtain the optimal combination numerically. The manner in which loops are defined effect the sparsity as well as the conditioning of the solution matrix. In other words, the solution matrix is well posed or ill conditioned, depending on whether or not an appropriate loop generating method was used. Oziadac and Pienkosz proposed some loop-generating methods [16]. Another disadvantage is that the initial "guessed" flows have to satisfy continuity (as stated above), which may not be as straightforward as initially envisaged.

In the element-based method employed to simulate pipe networks, nodes are still used in a similar manner to the previous two methods, but the pipes themselves are regarded as elements [17]. A pipe element has a downstream and an upstream node, which supply the nodal fluid head (or potential). Firstly, a potential function is selected for the chosen pipe segment. A gradient/potential and a velocity/gradient relationship are then defined. This relationship is similar to the pressure drop-flow relationship that will be defined in Chapter 4. A stiffness matrix **K**, (also the permeability coefficient in the case of fluids) is subsequently derived for the pipe element, and the element equations are assembled to obtain the global matrix. The boundary conditions are applied, and the global nodal potentials or pressures are solved [17]. The advantages of this method are its rapid convergence and the fact that it is not necessary to specify initial flows that satisfy continuity. A disadvantage is that the method uses more storage space than the previous methods [8].

The last method to be discussed is a hybrid method, which combines the node and loop-based methods. Osiadacz [7] describes this method where each loop flow is made identical to a particular branch flow, and hence to a particular chord flow. Although the loop equations will subsequently solve the chord flows, the loop equations are not solved but transformed into a set of nodal equations. The nodal equations are solved to yield the nodal pressures. From the nodal pressures, one will then be able to calculate the chord flows, from which the branch flows can be established. The nodal formulation makes the network definition much easier and yields a sparser matrix, while the good convergence characteristics of loop formulation are preserved.

Another hybrid method quite analogous to Osiadacz's hybrid method is a technique pioneered by Greyvenstein and Laurie [8]. This technique was actually a spin-off result from pressure-based nodal methods utilized in CFD to solve the Navier-Stokes equations [18]. This hybrid method is analogous to the work of Patankar [18] insofar as the pressure equations are solved at the nodes from which the branch flows are calculated using the updated pressures. Greyvenstein and Laurie [8] adapted

Patankar's original SIMPLE method for incompressible flows to handle compressible flows as well. In their paper, they define compressible flow as a subsonic flow with varying density, but Greyvenstein and Meyer [19] adapted the method to handle supersonic flows with shocks. It has also been shown that for incompressible flows, the method [8] is almost identical to the Newton-Nodal [7] method. Due to the relative straightforward formulation and good convergence characteristics of this type of hybrid method, it is viewed as the most suitable gas network method to simulate flows and flow spits in a combustor chamber.

1.3 The need for this study

From the literature study, it is evident that the preliminary design of gas turbine combustors is an important step during the development of a new combustor chamber. Important performance requirements such as combustion efficiency, total pressure loss requirements, combustion exit temperature pattern factor requirements, emission requirements etc. can be determined with reasonable accuracy during this preliminary design phase [4].

Empirically and analytical based procedures have led to successful evolutionary combustion improvements, however, when significantly different technological designs are required, these procedures shows evidence of under performance. However, the successful simulation of gas turbine flows is possible due to advances in CFD modeling. The downside to comprehensive CFD simulations are that of time consuming grid generation procedures, complexity of boundary condition specification and time intensive solution calculations, which is undesirable in the preliminary combustor design phase.

A flexible geometrically independent one-dimensional model, while lacking the resolution of the three-dimensional models, offers reasonable accuracy. The flexibility of the network analysis allows the modeling of complex geometries and removes many of the limitations placed on conventional one-dimensional models. The sub-

models within these solution procedures such as equilibrium models, film-cooling models, linerhole flow models etc. further continue to be improved upon. The network approach offers a simple procedure of incorporating the latest sub-models in an algorithm enabling the complete modeling of a combustor. Rapid execution times, in the order of a few seconds, while offering a good first order solution, are the main advantage of these one-dimensional network models. This is an advantage for the design engineer as it allows optimization of the combustor with relatively little computational cost. The more accurate the preliminary design process the more rapid the phases to follow will be. In the final analysis, an effective network approach will contribute to less initial development costs.

1.4 Objectives

From the literature survey, the development of a network based gas turbine combustor simulation tool is both justified and promising. As previously mentioned the network method compromises a number of sub-flows that are linked together to simulate the physical process, which naturally facilitates modeling multi-dimensional flows. Every sub-flow can further be defined by semi-empirical pressure drop-flow rate relationships making the modeling of combustor flow components such as liner-holes, possible and sudden expansion type elements possible. In the case of gas turbine combustors the latter is subject to essentially incompressible flow.

Although impressive network-flow capabilities based on hybrid methods exists [8, 20, 21], further work is required to furnish a suitable network simulation methodology for application to gas-turbines. Not all of the aforementioned solves a single set of equations, which models both compressible and incompressible flows with significant dynamic pressure fluctuations across the elements. Note that the set of governing equations should in addition be applicable to pipe elements with large area changes in the case of incompressible flow, i.e. to model essentially incompressible flow through duct elements with discontinuities such as sudden expansion type elements. The formulation should further be such that combustor type components

e.g. linerholes may be modeled as an element in the network. To effect this all flow related non-linearities such as frictional loss as a function of the flow need to be properly taken into consideration. This is not done in a natural and straight forward manner in existing simulation methodologies [8, 20]. Note that as this work constitutes the first step in the development in 1-D combustor technology, the development of the network model is limited to isothermal flow.

In the light of the above, the objectives for this study are as follows:

- Development of a single equation network simulation model to describe both steady incompressible and compressible flow where the dynamic pressure component is fully taken in consideration.
- Capability to compute flows through sudden expansions and liner holes in the case of incompressible flow.
- Capability to efficiently compute elements where the loss factor K is highly flow dependant. This implies the proper treatment of flow related non-linearities such as flow friction in the formulation and solution of the pressure correction equation.

1.5 An outline of this study

Chapter 2: Chapter 2 gives a theoretical background on the theory of combustor modeling. A number of aspects in combustor design which are applicable to this study are described and the relevant illustrations are provided.

Chapter 3: Chapter 3 describes the derivation of the strong form of 1-D general governing equations as well as the discretization strategy for a pipe network.

Chapter 4: Chapter 4 discusses the numerical implementation of the theoretical network model derived in Chapter 3. Different applicable numerical schemes are reviewed, and a proposed numerical scheme is explained in detail and compared to the other numerical methods in terms of complexity and applicability.

Chapter 5: Chapter 5 considers the simulation package and the validation thereof. A brief description of the package is given as well as the simulations of published networks to validate the accuracy of the proposed method.

Chapter 6: Chapter 6 describes the application of the network model to a gas turbine combustor and discusses the results that were obtained.

Chapter 7: The conclusion summarises the achievements and limitations of the proposed pipe network methodology. Recommendations are made for further work.. The References and the Appendices follow Chapter 7.

CHAPTER 2

Combustor Design Principles

Chapter 2 gives a theoretical background on the theory of combustor modelling. A number of aspects in combustor design which are applicable to this study are described and the relevant illustrations are provided.

2.1 Preamble

The previous chapter provided an overview of research that has been undertaken in the field of combustor analysis and in the field of pipe network analysis. Difficulties and limitations that have been encountered in these were also illustrated. The requirements for a network-based simulation methodology for combustor design were defined.

This chapter provides a short overview of some of the aerodynamic processes found in gas turbine combustors. Attention is given to the aerodynamic features and the associated nonlinearities which will be modelled via the propose network methodology. More detailed information on gas turbine combustor flows may be found in well-known texts authored by Harman [22] and Levebre [23] respectively. Note that these texts were extensively consulted throughout this study.

2.2 Gas turbine combustor theory

Figure 2.1 shows a schematic representation of the evolution of gas turbine combustors. In the early stages of combustor design, fuel was added to a free air stream within a straight duct (schematic (a)). The excessive pressure loss induced in this arrangement rendered it unfeasible, to say the least, and a diffuser was introduced to reduce the pressure drop (schematic (b)). Although the diffuser reduced the pressure drop satisfactorily (by a factor of approximately 5), the flame could not be sustained, and a baffle was placed into the combustor to shield the flame from the oncoming airflow while simultaneously sustaining the flame by means of a low velocity region provided as a result of flow reversal (schematic (c)). Establishing the desired combustor temperature rise, the air-fuel ratio should be approximately 50, which is well outside the flammability limits of air-hydrocarbon mixtures. Therefore, to overcome this problem, a perforated liner has replaced the baffle and provides a region of low velocity so that combustion is sustained through recirculatory flow of burned products that provide an uninterrupted source of ignition for the incoming combustible mixture (schematic (d)). Exhaust gases are cooled by air not used during the combustion process, and pressure losses resulting from chemical dissociation are thereby recovered.

The requirements driving combustor design these days include, amongst others, the following:

- High combustion efficiency
- Reliability and durability
- Wide stability limits
- Low pressure loss and smoke emissions
- Excellent maintenance characteristics
- Multifuel capability (industrial engines)

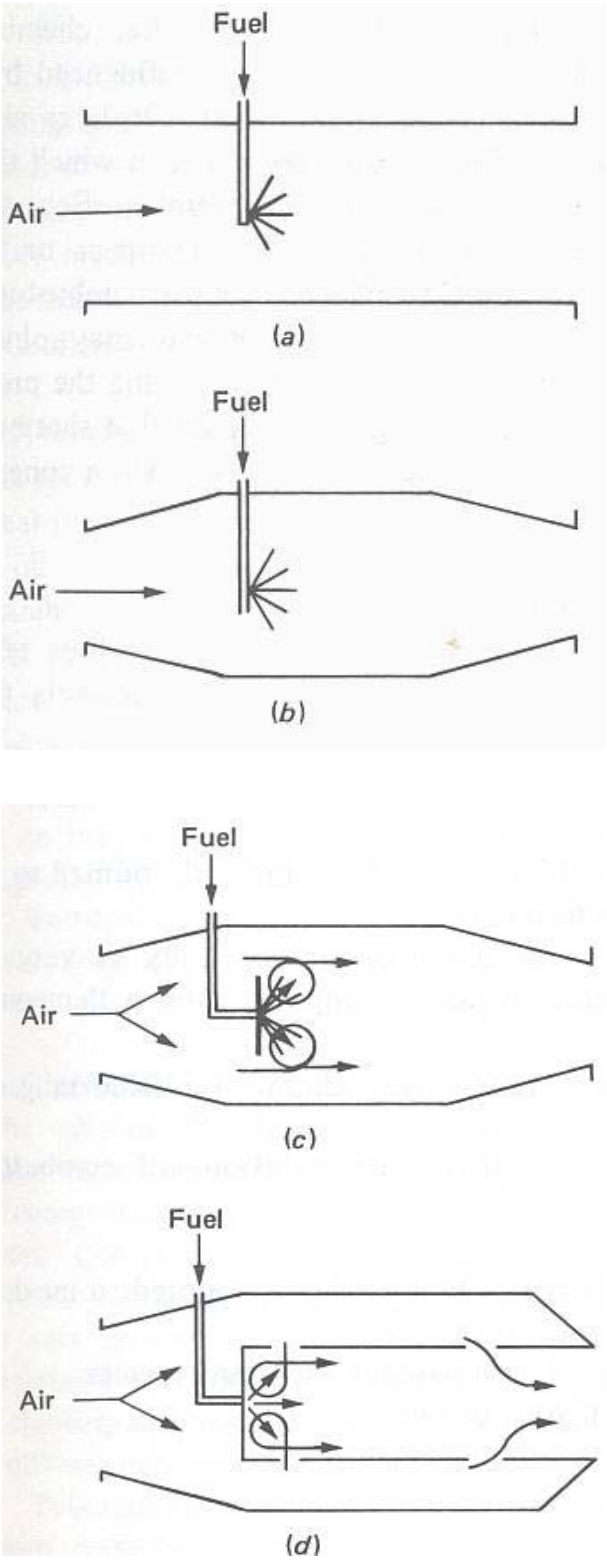

Figure 2.1 The development stages of the modern gas turbine combustor [23]

Today, there are three main types of combustors in use, namely, tubular-, annular- and tubo-annular or can-annular combustors. These names refer to the shape of the combustor chamber.

The tubular chamber comprises a cylindrical liner mounted concentrically inside a cylindrical casing. In annular chambers, however, an annular liner is mounted concentrically in an annular casing. In the case of tubo-annular or can-annular chambers, a group of cylindrical liners is placed in the desired arrangement in an annular casing. Table 2.1 sums up some of the advantages and disadvantages of the different chamber types.

Table 2.1 Some advantages and disadvantages of different combustor chamber types [23]

Chamber type	Advantages	Disadvantages
Tubular	• Very robust • Fuel and airflow patterns are easily matched	• High pressure losses • Weight: too heavy • Geometry: too long • Interconnectors required
Annular	• Weight: small • Geometry: short • Minimum frontal area	• Buckling problems • Unstable outlet temperature traverse • Fuel and airflow patterns not easily matched
Tubo-annular	• Very robust • Low pressure loss • Fuel and airflow patterns easily matched • Geometric and weight characteristics better than tubular chambers	• Geometric and weight characteristics poorer than with annular chambers • Connectors required

The combustion chamber is also divided into three separate regions, namely, the primary zone, intermediate or secondary zone, and the dilution zone, as shown in Figure 2.2. The purposes of the primary zone are to provide adequate time temperature and turbulence and to secure the flame to attain essentially complete combustion of the fuel. By the use of a small number of large jets, large-scale recirculation is obtained. The maximum volumetric heat-release rate tends to be low due to the relatively slow mixing of fresh mixture and combustion products. However, burning can be maintained over a wide range of fuel flows and at low pressures. Small-scale recirculation is obtained by the use of a large number of small jets [23]. The aggressive mixing results in high volumetric heat-release rates for stoichiometric mixtures. The difficulty with this system is that the burning range is narrow and the performance at low-pressures is poor, although the potential for low emissions is high in combination with changeable geometry.

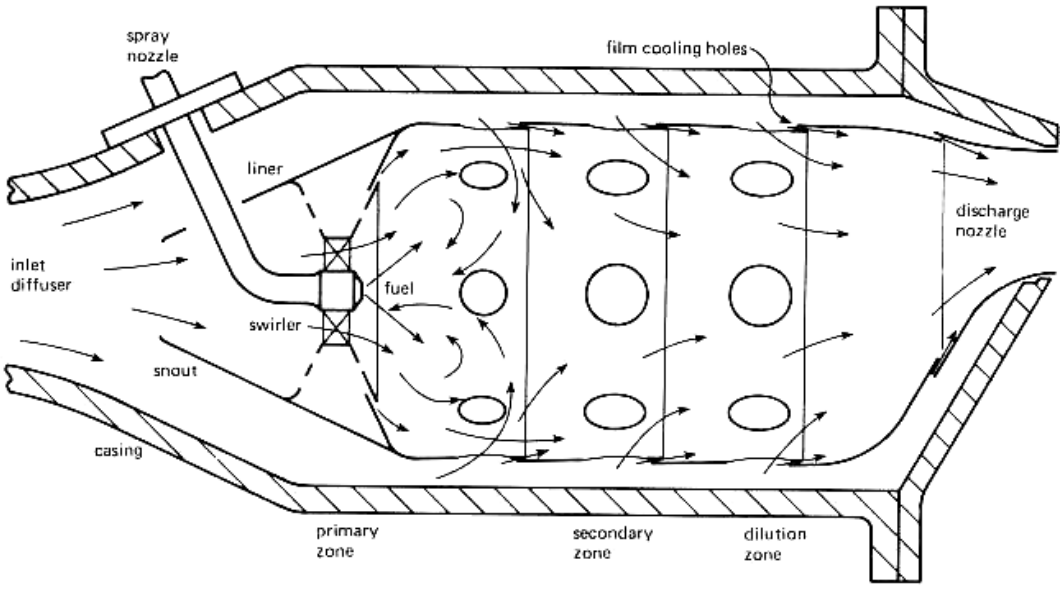

Figure 2.2 Different regions and components of a can-annular gas turbine combustor [22]

After the primary zone comes the intermediate or secondary zone. The function of the intermediate zone is twofold. During low altitude operation it serves as a region in

which the losses due to dissociation in the gas flow can be recovered while imperfectly mixed mixture pockets are burned completely. During high altitude operation, i.e., low pressure, the reaction rate in the primary zone is slower and combustion is far from complete as the entrance of the intermediate zone is reached. The intermediate zone can therefore be viewed as an extension of the primary zone in these circumstances, providing more time for combustion at high temperatures. The length of the intermediate zone is thus a trade-off between chamber length and combustor efficiency, the values of which range from 0.5 to 0.7 of the liner diameter [23].

The dilution zone comes prior to the turbine inlet. The objective of the dilution zone is to admit the remaining air not used in the combustion and wall-cooling processes through a set of holes in the liner walls and thereby create an outlet stream with a mean temperature and a temperature distribution which is suitable for the turbine. The size and shape of these dilution holes are selected to optimise the penetration of these jets, i.e. the air streams through the liner holes, and the subsequent mixing with the main stream. The maximum possible penetration with the available liner pressure drop is approximately five jet diameters. Because the jets penetrate across the liner, the minimum jet diameter is related to the width of the liner. The air available for dilution amounts to between 20 and 40 percent of the total combustor airflow [23].

The performance of a gas turbine combustor is greatly affected by its aerodynamic properties. In order to ensure complete combustion, minimum soot deposits and a satisfactory temperature distribution in the exhaust gases, proper mixing is of paramount importance. Unfortunately, thorough mixing can be achieved only at the expense of combustor length and pressure loss. Therefore, one of the main objectives in combustor design is to minimize the length and the pressure drop while achieving adequate mixing within the liner and a stable flow pattern with no parasitic losses. Because of the complex nature of aerodynamic design, only three aspects of combustor aerodynamics are presented briefly. Other aspects may be found in texts with more extensive discussions [22-24]. The three aspects of importance to this study

include the flow in the *annulus*, the flow *through the liner* and the flow *within the liner*.

Before discussing these three aspects, it would be appropriate to review some important parameters in combustor design. In order to facilitate combustor design, a reference velocity U_{ref} has been defined as the mean velocity across a plane of maximum cross-section in the absence of a liner. Subsequent relations for reference dynamic pressure p^d_{ref} and Mach number M_{ref} follow from the velocity, as follows

$$U_{ref} = \frac{\dot{m}_3}{\rho_3 A_{ref}}$$

$$p^d_{ref} = \frac{\rho_3 U^2_{ref}}{2}$$

$$M_{ref} = \frac{U_{ref}}{\sqrt{\gamma R T_3}}$$

Two important dimensionless pressure-loss parameters in combustor design are the *overall pressure loss* and the *pressure loss factor*. The two equations are related, and the relation can be found in advanced texts [23, 24]. The overall pressure loss is the ratio of the total pressure drop across the combustor to the total inlet pressure $\left(\frac{\Delta P_{3-4}}{P_3}\right)$, with values between 4 and 10 percent, excluding the *hot loss,* i.e., the fundamental loss in pressure due to combustion. The overall pressure loss is furthermore dependant on the operating conditions of the combustor.

The pressure loss factor is the ratio of the total pressure drop across the combustor to the reference dynamic pressure ratio $\left(\frac{\Delta P_{3-4}}{p^d_{ref}}\right)$ and is a fixed property of the combustor chamber. It is of importance because it denotes the flow resistance between the compressor outlet (i.e., subscript 3 or combustor inlet) and the turbine inlet (i.e., subscript 4 or combustor outlet). Aerodynamically, it may be regarded as equivalent to a ‘drag coefficient’ [23]. The pressure loss factor represents the sum of the diffuser

pressure loss factor $\left(\frac{\Delta P_{diff}}{p^{d}_{ref}}\right)$ and the liner pressure loss factor $\left(\frac{\Delta P_{L}}{p^{d}_{ref}}\right)$, both of which are to be kept at a minimum. In practice, there is little that can be done to minimize diffuser losses [23]. The liner pressure loss factor is essentially determined by the total effective hole area in the liner. All these losses account for the cold loss. The hot loss is determined through

$$\frac{\Delta P_{hot}}{p^{d}_{ref}} = K_1\left(\frac{T_4}{T_3} - K_2\right)$$

where K_1 and K_2 are determined experimentally and lies between 0.5 and 1.0 percent of P_3.

The airflow pattern within the liner and the distribution of liner wall temperatures are strongly influences by the flow conditions in the *annulus*. The reference velocity of the combustor and the liner-to-casing cross-sectional area ratio largely govern the mean velocity in the annulus. Even though convective cooling on the liner walls is augmented by high annulus velocities, low velocities are preferred due to lower skin-friction losses, lower expansion losses, steeper jet penetration angles, higher hole discharge coefficients and minimum variations in annulus velocity and static pressure. Critical areas are found in the vicinity of the dilution holes where the use of static pressure-fed cooling slots is prohibited because of the formation of a thick boundary layer. Measurements should then be taken to control the flow in the dilution-hole region to ensure a proper air feed through the dilution holes [23].

Flow *through the liner* holes depends strongly on the geometry and the flow conditions in the vicinity of the hole, which influence its effective flow area as well as the size of the hole and the pressure drop across it.

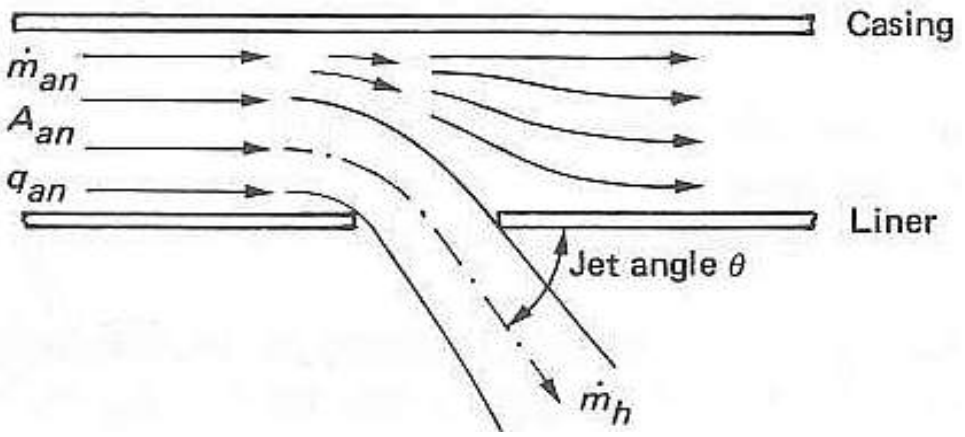

Figure 2.3 Flow representation through a liner wall [23]

The basic equation for liner hole mass flow may be expressed as

$$\dot{m}_h = C_D A_h \left[2\rho_3 \left(p_{0i} - p_j\right)\right]^{0.5}$$

where p_{0i} = stagnation pressure before the hole

p_j = static pressure after the hole

C_D = discharge coefficient

A_h = geometric hole area

By rewriting and rearranging the basic equation [23], an equation for the discharge coefficient may be obtained as

$$C_D = \frac{\alpha}{A_r K^{0.5}}$$

where α = hole-to-annulus mass flow fraction $= \dfrac{\dot{m}_h}{\dot{m}_{an}}$

A_r = hole-to-annulus area ratio $= \dfrac{A_h}{A_{an}}$

K = jet-to-annulus dynamic pressure $= 1 + \dfrac{\Delta p_L}{q_{an}}$

The liner hole discharge coefficients are strongly influenced by hole-shape, hole-type, hole-spacing to annulus height, liner pressure drop, static pressure distribution around the hole, swirl and local annulus air velocity. The jet angle, θ, will reduce the effective hole diameter when reduced. Correlations from experimental data for C_D and θ have been established and published [23-25]. The cooling slots are treated in the same manner as the liner holes [41] or may be treated as a sudden expansion element. Note that only incompressible flow is generally prevalent here.

It is evident from the equation describing the mass flow through the liner holes that the effective flow resistance is a non-linear function of pressure drop. This non-linearity is to be properly accounted for in the numerical scheme which was stipulated in the study objectives (Chapter 1). Further, flow Mach numbers downstream of the opening can reach up to Mach 0.7 [23] while flow in the annulus is often at Mach numbers below 0.3. The pipe network flow methodology should therefore be capable of simulating both fully compressible as well as incompressible flow. This was also pointed out in the study objectives (Chapter 1).

The airflow pattern *within the liner* is an important aspect because it must guarantee efficient and stable combustion, easy light-up, sufficient wall cooling, and must deliver a suitable gas temperature profile to the turbine. The number, size, shape and nature of the liner holes determine this airflow pattern. For the sake of completeness, the airflow pattern will be discussed as it passes through the primary, intermediate and dilution zones of the combustor.

As mentioned earlier, the airflow pattern in the primary zone must provide the conditions for achieving high heat-release rates, as well as good stability. However, the actual quantity of air supplied is also very important. Although the fuel flow rate is determined by the combustor fuel-air ratio, the nature of the combustion process is primarily dependent on the primary zone fuel-air ratio. For a *lean* primary zone (i.e., a fuel-weak primary zone), the heat release is low and the liner wall temperature is therefore cooler, no exhaust smoke and carbon deposits are present, and an intermediate zone is unnecessary. However, a high recirculation velocity hampers

ignition performance. For a *stoichiometric* primary zone the maximum heat release is obtained and the primary zone can be made small, while little or no smoke and carbon deposits are present. Unfortunately the liner walls receive a lot of heat. Lastly, for a *fuel-rich* primary zone, the ignition performance is good, and good combustion efficiency is achieved at low power conditions. However, the drawbacks to this type of operation include the presence of copious exhaust smoke, a low volumetric heat-release rate and the need for a longer intermediate zone [23].

The intermediate zone does not receive high precedence when the airflows through the combustor are estimated. Usually, the remaining available airflow (after the needs of the primary and dilution zone have been calculated) is used for the intermediate zone. The length of the intermediate zone usually depends on the application of the gas turbine engine (i.e., for cruising at high altitudes for long time periods high combustor efficiency is of paramount importance). Thus, the intermediate zone enhances the efficiency of the combustion process and is a remarkable benefit during start-up, acceleration and low-power conditions while lowering the temperature of predilution gasses and preventing hot regions from reaching the nozzle guide vanes.

Estimating and placing the flow patterns in the dilution zone to provide a satisfactory temperature profile is where the so-called ‘black art’ comes in. It is very difficult to achieve a consistent and satisfactory temperature profile, and trial-and-error methods have primarily been used. Today, it is accepted that a satisfactory temperature profile depends on both adequate jet penetration and the use of the correct number of dilution jets to form enough localized mixing regions, but establishment thereof remains largely a matter of experience. Further design considerations are quite extensive and can be obtained in advance texts [23, 24].

2.3 Closure

This chapter provided a basic overview of the operation of gas turbine combustion chambers in the vast topic of combustion. Elements that are relevant to the understanding of this study were discussed. The reader is also introduced to the complexity of flows and flow splits within the combustor as well as the pressure drop flow equation that governs the flow through a liner hole. The main features of the combustor, which will be modelled in this work, were discussed.

CHAPTER 3

Governing Equations and Pipe Network Discretization Strategies

Chapter 3describes the derivation of the strong form of 1-D general governing equations as well as the discretization strategy for a pipe network.

3.1 Preamble

In this chapter, a theoretical investigation takes place to derive a model suitable to handling passage flows in general. The difficulty in modelling these passages is that they have an influence upon one another due to their interconnectivity. Due to this characteristic of these passages, a flow network may be created and needs to be solved subsequently in a simultaneous manner.

An understanding how the governing fluid flow equations represent the physical flow phenomenon are necessary to be able to derive such a model effectively. The three-dimensional equations governing fluid flow are therefore presented. Because an efficient solution is of interest and the equations are subsequently reduced to one-dimensional form.

3.2 The governing equations

The analysis of fluid flow is based on determining the relationships between the physical laws for a particular situation at hand (Table 3.1).

Table 3.1 The physical laws governing general fluid flow

Physical Law	Description
THE CONTINUITY EQUATION	The law of the conservation of mass
THE MOMENTUM EQUATION	Newton's second law of motion
THE ENERGY EQUATION	The fist law of thermodynamics, which is the principle of the conservation of energy
THE ENTROPY EQUATION	The second law of thermodynamics
THE EQUATION OF STATE	The thermodynamic properties of the fluid in question from either the equation of state for a perfect gas, empirical equations or an idealized model

The mathematical expressions corresponding to these principles are combined to obtain the equations describing the fluid flow problem at hand [26].

3.2.1 General compressible flow equations

The derivations of the governing equations, both in integral form or in differential form, can be found in several texts [9, 26-31] and will be presented briefly in the following paragraphs. A full derivation can be found in Appendix A.

The continuity equation

In the absence of nuclear and relativity effects, the mass of a system is a constant according to the law of the conservation of mass.

$$(Mass)_{System} = const \tag{3.1}$$

Applied to a control volume, the integral form for the continuity equation becomes,

$$\int_{\upsilon} \frac{\partial \rho}{\partial t} d\upsilon + \int_{A} \rho \mathbf{V} \cdot (dA) = 0 \tag{3.2}$$

which states that the rate at which mass accumulates within the control volume υ is equal to the rate at which mass leaves the control volume through a control surface. The first term is omitted when working with steady flows. The differential form for the continuity equation, valid for control volumes, is more useful in describing multidimensional flows. The derivation of the continuity equation into its differential form may be conducted through two approaches. The first approach uses the divergence theorem while the second applies the integral equation on a control volume of differential size. The result of both approaches yield the differential equation for continuity as

$$\frac{\partial \rho}{\partial t} + \nabla \cdot (\rho \mathbf{V}) = 0 \tag{3.3}$$

The momentum equations

The momentum equations are the equations obtained when Newton's second law of motion is applied to fluid flow through a control volume as

$$\mathbf{F}_{external} = \int_{\upsilon} \frac{\partial \rho \mathbf{V}}{\partial t} d\upsilon + \int_{A} \mathbf{V}\left(\rho \mathbf{V} \cdot d\,\mathbf{A}\right) \tag{3.4}$$

and can be expressed as

$$\mathbf{F}_{external} = \int_{\upsilon} \mathbf{B}\,\rho d\upsilon - \int_{A} p d\mathbf{A} + \mathbf{F}_{\mathbf{shear}} \tag{3.5}$$

The external force $\mathbf{F}_{external}$ is due to the sum of a body force and a surface force. The body force **B**, is a force that acts upon the entire mass of the fluid (e.g., gravity, electrical and magnetic forces on a charged fluid). The surface force is a force that acts on the boundaries of the system through their contact with the surroundings. It consists of a normal component and a tangential component where the latter is referred to as the shear force which equals zero when working with an inviscid fluid. The normal force is caused by pressure for an inviscid fluid but also contains the effects of shear when working with a viscous fluid.

Therefore, by equating the Equations (3.4) and (3.5) and retaining the surface forces in the form of $\mathbf{F}_{\mathbf{surface}}$, one arrives at the integral form of the momentum equations

$$\int_{\upsilon} \mathbf{B}\,\rho d\upsilon + \mathbf{F}_{\mathbf{surface}} = \int_{\upsilon} \frac{\partial \rho \mathbf{V}}{\partial t} d\upsilon + \int_{A} \mathbf{V}\left(\rho \mathbf{V} \cdot d\,\mathbf{A}\right) \tag{3.6}$$

In its differential form, the momentum equations are also known as the Navier-Stokes equations. By yet again employing either one of the two transformation approaches mentioned, the differential form of the momentum equations results in

$$\rho \frac{D\mathbf{V}}{Dt} + \nabla p - \rho \mathbf{B} - d\mathbf{F}_{\mathbf{shear}} = 0 \tag{3.7}$$

for a viscous fluid in a state of uniform motion. In general, the substantial derivative is $\frac{D(\ )}{Dt}$ and may be expressed in vector notation as

$$\frac{D(\ )}{Dt} = \frac{\partial(\ )}{\partial t} + (\mathbf{V}\cdot\nabla)(\ ) \tag{3.8}$$

However, it would be appropriate to note that arriving at Equation (3.7) is not as straightforward as it seems to be and may also be simplified for flows with a constant average viscosity and/or for incompressible flows.

The energy equation

The energy equation is derived from the first law of thermodynamics, which is also referred to as the law of energy conservation. In essence, it is the change in the stored energy in a system that is equal to the amount of heat energy transferred into the system less the amount of work energy done by the system.

$$dE = \delta Q - \delta W \tag{3.9}$$

Employing the substantial derivative for the stored energy, the rate of change in stored energy for a control volume may be expressed as [26]

$$\frac{DE}{Dt} = \int_{\upsilon}\frac{\partial}{\partial t}\left[\rho\left(u + \frac{V^2}{2} + gz\right)\right]d\upsilon + \int_A\left[u + \frac{V^2}{2} + gz\right](\rho\mathbf{V}\cdot d\mathbf{A}) \tag{3.10}$$

The heat transported to the control volume occurs by means of the three main heat transport modes (conduction, convection and radiation) and is regarded as positive. Usually, the application determines the transport mode or modes. Furthermore, the work done by the control volume consists of shaft work $\mathbf{W_{shaft}}$ (work done by a rotary shaft crossing the system boundary, e.g., compressors) and flow work $\mathbf{W_{shear}}$ (work done by shear stress within the fluid) and pressure work given by

$$\dot{W}_n = \int_A pv(\rho\mathbf{V}\cdot d\mathbf{A}) \tag{3.11}$$

where p is the pressure and v the specific volume. Combining Equations (3.10) and (3.11) establishes the integral form of the energy equation for a control volume

$$\dot{W}_{shaft} + \dot{W}_{shear} - \dot{Q} + \int_{\upsilon} \frac{\partial}{\partial t}\left[\rho\left(u + \frac{V^2}{2} + gz\right)\right] d\upsilon + \int_A \left[h + \frac{V^2}{2} + gz\right](\rho \mathbf{V} \cdot d\mathbf{A}) = 0 \qquad (3.12)$$

This integral form may be converted to the differential form by the use of the two approaches mentioned, which results in

$$\delta\dot{W}_{shaft} + \delta\dot{W}_{shear} - \delta\dot{Q} + \rho\frac{D}{Dt}\left[h + \frac{V^2}{2} + gz\right] - \frac{\partial p}{\partial t} = 0 \qquad (3.13)$$

The derivation of the energy equation concludes an overview of the derivation of the governing equations for compressible fluid flow needed in this research. The derivation of the remaining equations may be found in the texts mentioned in the beginning of this section. The governing equations of compressible fluid flow are highly non-linear, and general analytical solutions thereof are, for all practical purposes, non-existent.

3.3 The one dimensional general compressible flow equations

In this section the general compressible flow equations are reduced to their repective one-dimensional form. Assumptions made regarding the reduction of these equations in the light of this work will be stated. Refer to Figure 3.1 for the appropriate flow directions.

Continuity equation

Equation (3.3) can be expanded as follows:

$$\frac{\partial}{\partial t}(\rho) + \frac{\partial}{\partial x}(\rho u) + \frac{\partial}{\partial y}(\rho v) + \frac{\partial}{\partial z}(\rho w) = 0 \qquad (3.14)$$

where x,y,z is the Cartesian directions and u,v,w denotes the flow velocity in each of the directions.

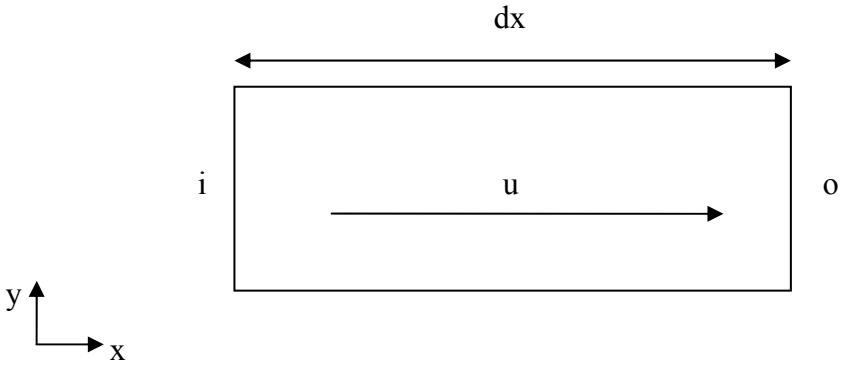

Figure 3.1 Flow element for one-dimensional flow

For a one-dimensional analysis, the flow in only one direction is important, in the x-direction for this case. Therefore v=w=0 and Equation (3.14) reduces to

$$\frac{\partial}{\partial t}(\rho)+\frac{\partial}{\partial x}(\rho u)=0 \tag{3.15}$$

where u denotes the average velocity at a point in the direction of the pipe[1]. Throughout the course of this study, steady one-dimensional flow was considered. Therefore $\partial/\partial t=0$ and the continuity equation concequently becomes

$$\frac{\partial}{\partial x}(\rho u)=0 \tag{3.16}$$

Momentum equation

Equation (3.7) is the basic differetial form of the momentum equation for an infinitesimal element. Through reordering and rewriting some symbols, the common three-dimensional form of the equation becomes:

$$\rho\frac{D\mathbf{V}}{Dt}=\rho\mathbf{g}-\overline{\nabla}p+\overline{\nabla}\cdot\tau_{ij} \tag{3.17}$$

[1] Matters pertaining to the validity of the governing equations, kindly refer to the Appendix F: "Validity of the Governing Equations".

where τ_{ij} is the stress tensor which is rewritten to a single deformation law for a newtonian viscous fluid as [29]

$$\tau_{ij} = -p\delta_{i,j} + \mu\left(\frac{\partial u_i}{\partial x_j} + \frac{\partial u_j}{\partial x_i}\right) + \delta_{i,j}\lambda \mathrm{div}\boldsymbol{V}$$

Note that tensor notation is used here where i and j denote Cartesian coordinate directions. As previously, Equation (3.17) can now be reduced to the following equation for one-dimensional steady state flow in the x-direction.

$$\frac{\partial}{\partial x}(\rho u^2) = \rho g_x - \frac{\partial p}{\partial x} + \frac{\partial}{\partial y}\left(\mu \frac{\partial u}{\partial y}\right) \tag{3.18}$$

3.4 The one dimensional network model

This work focuses on the modelling of flow through pipe networks. From the literature study in Chapter 1, it is evident that the method with the best convergence characteristics would be a loop-nodal method. Using this method, the loop pressures are calculated prior to the branch flows. The problem with this type of method is that defining "loops" in complex networks are quite difficult because of the different combinations that are possible. This is of significance, as the loop definition will most definitely have a huge influence on the convergence characteristics of the scheme [7]. Certain loop definitions will result in a sparse solution matrix with a broad bandwidth, which will slow down convergence considerably especially when working with large matrices, while other definitions would not, especially when the solution matrix is well posed.

With the nodal method, large networks may be simulated with relative ease. No loop definitions are necessary, and each and every node 'knows' to how many elements it is connected to and who its neighbours are. The problem, however, is that the convergence characteristic of this method is poor. This poor characteristic result from

an inappropriate choice of the convergence criteria formulation as well as from solving the branch flows prior to the nodal pressures according to Greyvenstein and Laurie [8].

In the following paragraphs, a method is described that uses the nodal formulation but solves the nodal pressures instead of the branch flows as proposed by Greyvenstein and Laurie [8]. After the nodal pressures are solved, the branch flows are calculated. Since the nodal pressures are solved initially, the good convergence characteristics of the loop methods are inherited.

Flow network

Figure 3.2 shows an arbitrary node and the branches connecting to the node. By employing Kirchoff's first law and the continuity equation on the node, the mass flow into the node must equal the mass flow out of the node. The sign convention for the node will be that the mass flow into the node will be regarded as positive, while the mass flow leaving the node will be regarded as negative.

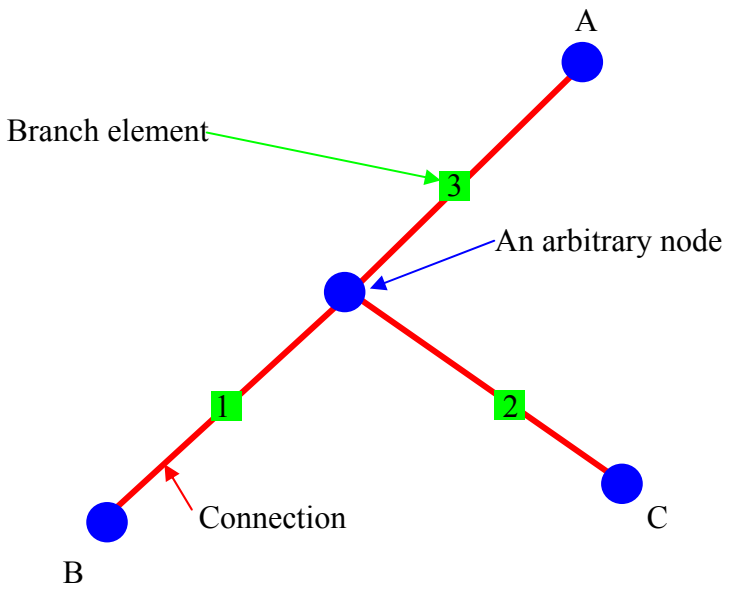

Figure 3.2 An arbitrary node with connecting branches

Therefore, the sum of the mass flows equals zero in the absence of an external mass addition or extraction to the node. In the case of an external mass flow to or from the node, the sum of the mass flows will equal the external mass flow. This is mathematically described as follows:

$$\sum_{j=1}^{J} \rho_{i,j} Q_{i,j} = -d_i \tag{3.19}$$

where $Q_{i,j}$ is the element flow, $\rho_{i,j}$ the element density and d_i the external mass flow into the node.

We consider the momentum equations next. Noting that the equation is only valid for a point in the flow field and omitting the gravity term in the x-direction, Equation (3.18) becomes

$$\frac{\partial}{\partial x}\left(\rho u^2\right) = -\frac{\partial}{\partial x}\left(p\right) + Fr \tag{3.20}$$

where $Fr = u^2 c_f$ denotes a product between the average pipe velocity u and the coefficient c_f, which describes the effect of flow frictional losses. Equation (3.20) can be used to calculate the pressure drop flow relation for any given variable area duct. However, in a duct or pipe *network* simulation, Equation (3.20) cannot be used in the current form because the static pressure across a branch connection with minimal frictional losses (assumed in this work) is not constant. Different static pressures for each element connecting to a particular node will consequently be calculated. The number of different static pressures calculated at a node will depend on the number of elements connected to that particular node. This problem can be corrected by using the total pressure in the simulation instead of the static pressure, as this is constant across a branch connection by virtue of Bernoulli's equation. The total pressure is the sum of the dynamic pressure and the static pressure and is given in the following equation

$$p_0 = p_{dyn} + p_s \tag{3.21}$$

where the dynamic pressure is $p_{dyn} = \frac{1}{2}\rho u^2$. Rearranging Equation (3.21) and substituting the dynamic pressure terms into Equation (3.21), an expression for the static pressure in terms of the total and the dynamic pressure can be found. This expression for static pressure is subsequently substituted into Equation (3.20) giving

$$\frac{\partial}{\partial x}\left(\rho u^2\right) + \frac{\partial}{\partial x}\left(p_0 - \frac{1}{2}\rho u^2\right) = Fr \tag{3.22}$$

Rearranging Equation (3.22) we obtain the strong form of the momentum equation (describing 1-D pipe flow at a point along the pipe) for both steady compressible and incompressible flow.

$$\frac{1}{2}\frac{\partial}{\partial x}\left(\rho u^2\right) + \frac{\partial p_0}{\partial x} = Fr \tag{3.23}$$

The density of a compressible fluid in an element may be calculated using an equation of state for the fluid. In the case of a perfect gas,

$$\rho = \frac{p}{R \cdot T} \tag{3.24}$$

where p is the static pressure, R the ideal gas constant and T the temperature. The element temperatures may be obtained by employing the energy equation in the case of non-isothermal flow.

3.5 Computational representation and storage of a duct network

The storage scheme to be employed originates from the work of George and Liu [33]. Although there are better storage schemes in terms of space and memory usage, this scheme is the simplest to implement. Figure 3.3 depicts the computational stencil, or mesh, for a certain node and shows the branches/elements, connecting to the node. The global indices are i and $n_{i,j}$ while $b_{i,j}$, and j is a local index with respect to node i. The adjacent nodes to node i are the upstream or downstream nodes j, depending on the flow direction of the branches/elements connected to this node. Therefore, node i is connected to adjacent nodes $n_{i,j}$ via branches $b_{i,j}$ where $j=1,2,\ldots,J$. The number J then represents a number of branches/elements connected to node i.

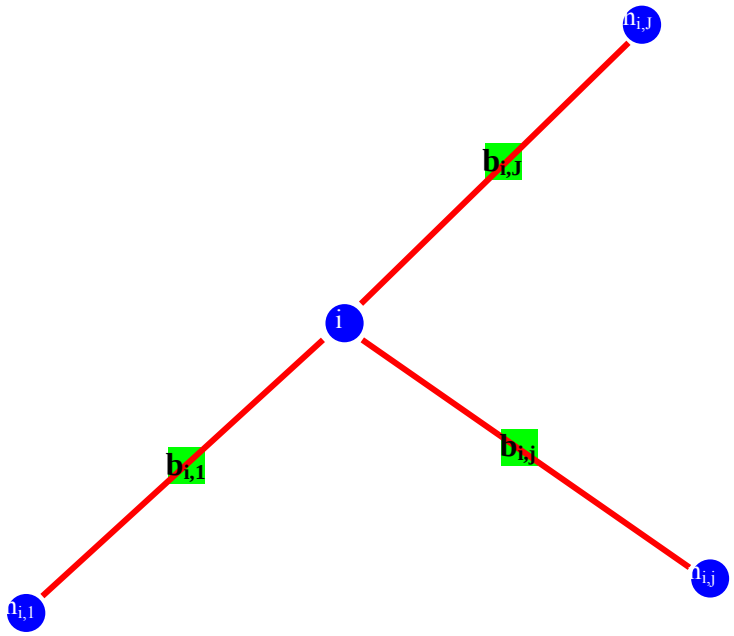

Figure 3.3 Computational stencil for a node in the network

For a network, two connectivity matrices are defined, namely, the element connectivity matrix and the nodal connectivity matrix. The element connectivity matrix represents the branches connected to a node, while the nodal connectivity matrix represents the neighbouring nodes to the node in question. Figure 3.4 shows a schematic representation of an actual network.

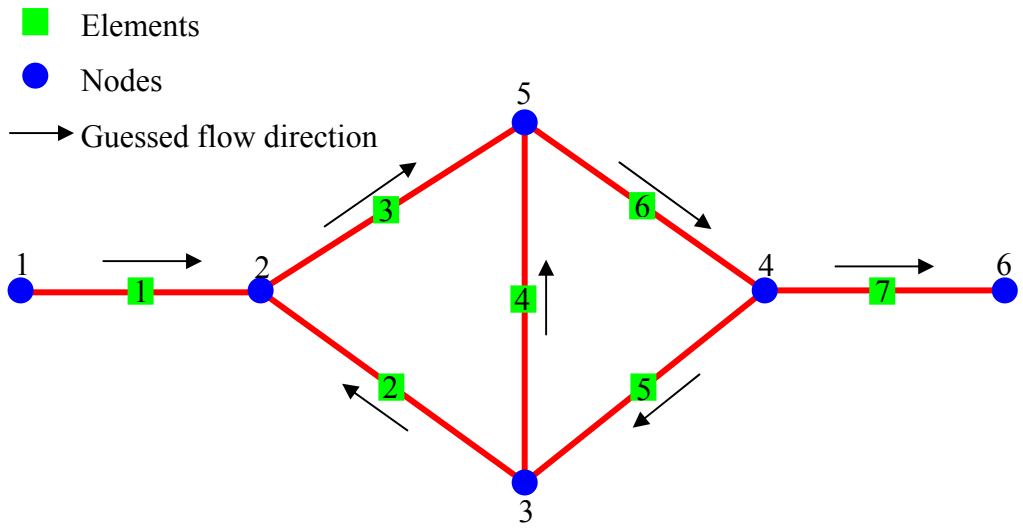

Figure 3.4 Schematic representation of an example pipe network

Mathematically, the structure of the network is described uniquely as follows using connectivity matrices **B** and **N**. For the network example under consideration, **B** is as follows:

$$\mathbf{B} = [b_{i,j}] = \begin{bmatrix} -1 & 0 & 0 \\ 1 & 2 & -3 \\ -2 & -4 & 5 \\ 3 & 4 & -6 \\ -5 & 6 & -7 \\ 7 & 0 & 0 \end{bmatrix}$$

where the rows depict the global node number and the columns depicts the local branch/element number. The matrix **N** is calculated as:

$$\mathbf{N} = [n_{i,j}] = \begin{bmatrix} 2 & 0 & 0 \\ 1 & 3 & 5 \\ 2 & 4 & 5 \\ 3 & 5 & 6 \\ 2 & 3 & 4 \\ 4 & 0 & 0 \end{bmatrix}$$

where the rows depict the global node number and the columns depict the adjacent node number.

3.6 Heat transfer network

Isothermal flow is considered throughout this thesis as this work represents the first step in the development of gas turbine combustor modelling. The following paragraphs describes the heat transfer network, which was implemented in the simulation package, however, no tests were conducted to verify the results. The heat transfer network represents, in essence, the energy equation that has to be solved for a given duct network. Hence, the energy equation is an energy balance that has to be satisfied at each and every node within the duct network. When working with incompressible flows, the link between the flow and the energy equations is weak and it is therefore sufficient to solve the energy equation only once after the flow equations have been solved to obtain the temperature field in the network [8]. However, when working with compressible flows, this link is very strong, and the energy equation needs to be solved during every iteration of the solution process. Pending the application, this energy equation may be formulated in such a manner that it would satisfy the particular needs of the application.

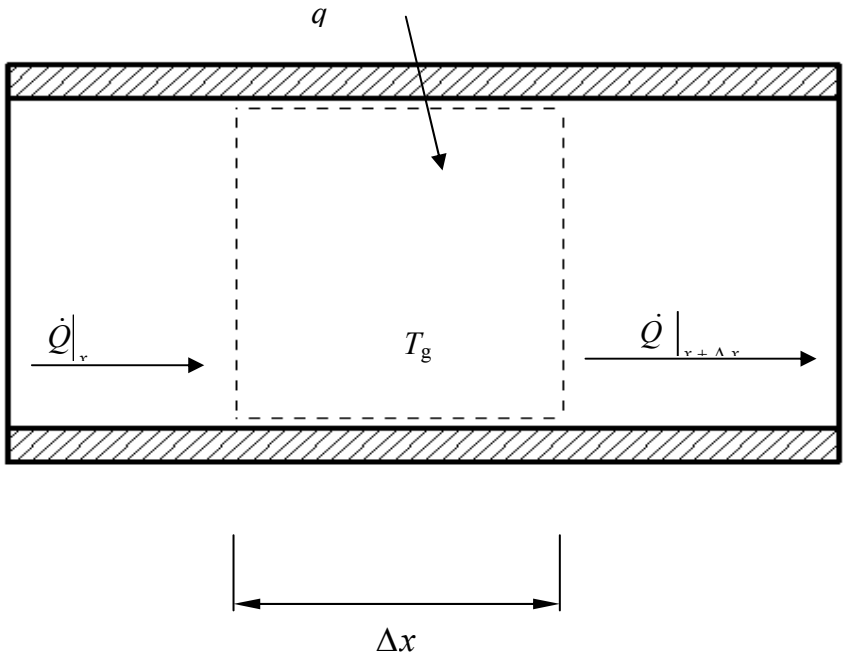

Figure 3.5 The energy balance for a control volume within a duct segment

Figure 3.5 represents the control volume for a duct segment which includes heat transfer and is used to derive expressions for the heat transfer in a single duct segment, which will then be applied to the whole network and for the average gas temperature within the duct segment.

Using the steady flow energy equation [32], the heat transfer across the duct wall must equal the gas flow rate times its enthalpy increase as follows

$$Q = \dot{Q}\Big|_{x+\Delta x} - \dot{Q}\Big|_{x} \tag{3.25}$$

Assuming that the gas specific heat (c_p) remains constant over the length of the duct, Equation (3.25) can be rewritten as

$$Q = \dot{m}c_p\left(T\Big|_{x+\Delta x} - T\Big|_{x}\right) \tag{3.26}$$

Therefore the exit temperature $T\Big|_{x+\Delta x}$ of the segment duct can be calculated by rearranging Equation (3.26) as

$$T\Big|_{x+\Delta x} = \frac{qP_r\Delta x}{\dot{m}c_p} + T\Big|_{x} \tag{3.27}$$

where q = heat flux into the duct segment
P_r = perimeter of the duct segment
Δx = length of the duct segment
$\dot{m}$ = the mass flow through the duct segment

Equation (3.27) may now be expanded to obtain the nodal temperatures in the gas network by applying the energy balance once again at a node. Utilizing Kirchoff's law, only the heat coming into the node, because of inflows from the adjacent duct segment with heat transfer, are regarded as significant, and all the duct segments with flows leaving the node are disregarded. Therefore, heat flows into the node must equal

the heat added to the connecting branches. Assuming that there is no heat generation within the node,

$$\sum \dot{Q}_{\text{inflows}} - \sum \dot{Q}_{\text{outflows}} = \sum Q_{\text{external}} \tag{3.28}$$

By substituting the equations for heat flux, (i.e., Equation 3.26) and rearranging, the temperature at a node in the network is given by

$$T_{node} = \frac{\left(\sum Q_{\text{external}} + \sum \dot{m} c_p T_{\text{adjacent\_nodes}}\right)_{\text{inflows}}}{\left(\sum \dot{m} c_p\right)_{\text{inflows}}} \tag{3.29}$$

This equation can now be used readily to calculate the nodal temperatures.

3.7 Closure

In this chapter, the general governing equations of fluid flow were presented, as well as the derivation thereof for three dimensions. These equations were subsequently reduced to their one-dimensional strong form to describe both steady compressible and incompressible flow. A flow network discretization strategy was also discussed and a flow network example using the nodal technique considered. A heat transfer network using the one-dimensional energy formulation was described and applicable formulations were derived.

CHAPTER 4

Numerical Implementation

*Chapter 4 discusses the **Numerical Implementation** of the theoretical network model derived in Chapter 3. Different applicable numerical schemes are reviewed, and a proposed numerical scheme is explained in detail and compared to the other numerical methods in terms of complexity and applicability.*

4.1 Preamble

Chapter 3 provided the derivation of the governing equations in strong form as well as an outline of the basic discretization strategy which will be used to simulate fluid flow in a pipe network. Two basic equations governing the steady compressible and incompressible flow in the network branches were derived viz. mass and momentum conservation.

In this chapter solution strategies are discussed and a solution algorithm developed. The solution algorithm furnishes a so-called pressure correction matrix, which is to be solved in order to calculate pressures at nodes within the network. Steady state flows are calculated from the discretized momentum equation.

Two methodologies to construct the solution matrix were implemented. The first method is the one published by Greyvenstein and Laurie [8] and the second method is a hybrid pipe network method based on the work of latter. It, however, employs a single equation set to describe both steady incompressible liquid and gas and fully compressible gas flows where the dynamic pressure component is fully taken into consideration. In addition, the model has the capability to compute flows through variable area ducts with discontinuous changes in cross-sectional area in the case of incompressible flow. The differentiation of flow related non-linearities such as flow friction are further dealt with in a straightforward manner when constructing the pressure correction equation. The inclusion of the latter will be shown in the next chapter to furnish notably improved convergence characteristics. The above developments are viewed as contributions to the pipe-network flow modelling research fraternity.

The pressure correction matrix is solved by a direct solution method for linear systems and some of these methods are investigated, together with matrix reordering techniques. The choice of a particular solution method and matrix-ordering technique will have an influence on the efficiency of the solver. In this study the LU factorization method was used due to its proven track record in pipe network analysis problems [8] and ease of implementation.

4.2 Implementation of the Greivenstein and Laurie method

This is a constant cross-section pipe, variable density hybrid pipe flow simulation scheme which is based on the SIMPLE pressure correction methodology developed by Patankar and Spalding [18, 34]. When first published, this was a ground breaking scheme which allowed for the solution of both compressible and incompressible flow provided that the dynamic pressure component is small [8]. This basic methodology was selected for this work as it is viewed as a most proficient steady-state hybrid pipe network scheme.

For compressible flow, the initial temperature field is usually guessed. The continuity, pressure drop and density equations are then solved simultaneously to yield the flow rate, pressures and densities. The energy equations are subsequently solved for and the temperature field is updated. The continuity, pressure drop and density equations are then solved again, and the process repeats itself until convergence is reached. For incompressible flow, it would be sufficient to solve the energy equation once after the flows, pressures and densities have been solved because of the ineffectual link between the flow and the energy equations [8].

As mentioned, the pressures, flows and densities are solved simultaneously via the pressure-correction method. The corrected values are calculated adding a correction value to the guessed or predicted values using the following relationships [18]:

$$p_i = p^*_i + p'_i \tag{4.1}$$

$$Q_{i,j} = Q^*_{i,j} + Q'_{i,j} \tag{4.2}$$

$$\rho_{i,j} = \rho^*_{i,j} + \rho'_{i,j} \tag{4.3}$$

where p_i is the nodal pressure at node i, $Q_{i,j}$ is the flow at element i,j and $\rho_{i,j}$ the density at element i,j. Note that, as pointed out above, this method is only valid for cases where the dynamic pressure is much smaller than the static pressure viz. $p_i \approx p_{oi}$, and hence no distinction is made between the two pressures. The nodal temperatures and pressures are initially guessed. The initial values are denoted with a star (*). The initial density is then calculated using either the equations of state for the fluid, or any other table or formulation giving the fluid's density for a specified pressure and temperature. With these initial values, the initial flows may be calculated by employing the flow equations. The values tagged with an accent (′) are the correction values that have to be obtained through the pressure drop-flow equation. The corrected values are then calculated via Equations (4.1) to (4.3). During the iterative solution procedure, the initial or guessed values are then set equal to the corrected values, and the whole process is repeated.

4.2.1 Flow Equations

From Chapter 3, the continuity equation, the pressure drop equation and the density equation are applied to the computational stencil given in Figure 3.3, as follows:

For continuity at a node,

$$\sum_{j=1}^{J} s_{i,j}\rho_{i,j}Q_{i,j} = -d_i \tag{4.4}$$

where $i = 1,2,\ldots,I$ at a node

$$s_{i,j} = \begin{bmatrix} 1 & \text{if} & \text{flow enters the node} \\ -1 & \text{if} & \text{the flow exits the node} \end{bmatrix}$$

d_i = external mass flow into the node.

For the pressure drop-flow rate relationship across a constant cross-sectional area element [8],

$$\Delta p_{i,j} = p_{n_{i,j}} - p_i = s_{i,j} H_{i,j} g_{i,j} f_{i,j} \tag{4.5}$$

where,

$$H_{i,j} = \frac{Q_{i,j}}{|Q_{i,j}|}$$
$$g_{i,j} = g_{i,j}(\rho_{i,j})$$
$$f_{i,j} = f_{i,j}(|Q_{i,j}|)$$

For the ideal gas density at a node *i*,

$$\rho_i = \frac{p_i}{RT_i} \tag{4.6a}$$

or for a branch / element

$$\rho_{i,j} = \frac{p_i + p_{n_{i,j}}}{2RT_{i,j}} \tag{4.6b}$$

where

$T_{i,j}$ = temperature of the element (the average gas temperature in the case of a duct.)

4.2.2 Pressure Correction Equation

As mentioned previously, the discretization strategy involves calculating pressure correction values and then updating the latest pressure accordingly. A relation for the pressure-correction is obtained by differentiation of the pressure drop-flow equation (Equation (4.5)) with respect to the element flow [8]:

$$\frac{p'_{n_{i,j}}}{Q'_{i,j}} - \frac{p'_i}{Q'_{i,j}} = s_{i,j} H_{i,j} f_{i,j} G_{i,j} \frac{\rho'}{Q'_{i,j}} + s_{i,j} g_{i,j} F_{i,j} \tag{4.7}$$

where

$$G_{i,j} = \frac{\partial g_{i,j}}{\partial \rho_{i,j}}$$

$$F_{i,j} = \frac{\partial f_{i,j}}{\partial |Q_{i,j}|}$$

Through substituting the density equation (Equation (4.6)) into Equation (4.7) above, and rearranging the terms, an equation for the flow correction is established as

$$Q'_{i,j} = p'_{n_{i,j}} \left[\frac{1}{s_{i,j} g^*_{i,j} F^*_{i,j}} - \frac{a_{i,j} H_{i,j} f^*_{i,j} G^*_{i,j}}{g^*_{i,j} F^*_{i,j}} \right] - p'_i \left[\frac{1}{s_{i,j} g^*_{i,j} F^*_{i,j}} + \frac{a_{i,j} H_{i,j} f^*_{i,j} G^*_{i,j}}{g^*_{i,j} F^*_{i,j}} \right] \tag{4.8}$$

where $a_{i,j} = \frac{1}{2RT_{i,j}}$ and where the superscript '*' indicates the guessed values of $Q_{i,j}$ and $\rho_{i,j}$ to evaluate the expression [8]. To arrive at an equation for the pressure correction, the corrected flow (Equation (4.2)) and the corrected density values (Equation (4.3)) are substituted in the continuity equation (Equation (4.4)), resulting in

$$\sum_{j=1}^{J} s_{i,j}\left(\rho^*_{i,j}Q^*_{i,j} + \rho'_{i,j}Q^*_{i,j} + \rho^*_{i,j}Q'_{i,j}\right) = -d_i \qquad (4.9)$$

where the density and flow correction term, $\rho'_{i,j}Q'_{i,j}$, has been omitted. This term is insignificant as the solution approaches convergence [8]. The pressure correction equation, the equations for flow corrections (Equation (4.8)) and density corrections obtained from (Equation (4.6)) are now substituted into Equation (4.9), resulting in

$$p'_i = \frac{\left(\sum_{j=1}^{J}\left(c_{i,j}p'_{n_{i,j}}\right) + b_i\right)}{c_{i,i}} \qquad (4.10)$$

where,

$$c_{i,i} = \sum_{j=1}^{J}\left(\frac{\rho^*_{i,j}}{g^*_{i,j}F^*_{i,j}} + s_{i,j}H_{i,j}a_{i,j}\left(\frac{\rho^*_{i,j}f^*_{i,j}G^*_{i,j}}{g^*_{i,j}F^*_{i,j}} - \left|Q^*_{i,j}\right|\right)\right)$$

$$c_{i,j} = \frac{\rho^*_{i,j}}{g^*_{i,j}F^*_{i,j}} - s_{i,j}H_{i,j}a_{i,j}\left(\frac{\rho^*_{i,j}f^*_{i,j}G^*_{i,j}}{g^*_{i,j}F^*_{i,j}} - \left|Q^*_{i,j}\right|\right)$$

$$b_i = d_i + \sum_{j=1}^{J}\left(\rho_{i,j}Q_{i,j}s_{i,j}\right)$$

$$with \quad i = 1,2,\ldots,I$$

This pressure correction equation (Equation 4.10) is now solved for every node of the network simultaneously, and the corrected values for pressure, flow and density are calculated by means of Equations (4.1) to (4.3) and (4.8). The density correction used in Equation (4.3) is merely calculated through Equation (4.6) using the pressure correction values of Equation (4.10) instead of the nodal static pressure. A more thorough derivation of the pressure correction equation may be found in Appendix B and reference [8].

4.3 A proposed compressible and incompressible flow method

Greyvenstein and Laurie's model was implemented and applied to a number of test cases (see Chapter 5). Although this model is able to solve steady state compressible fluid flow, it does not in general furnish an accurate solution for mach numbers higher than 0.3. This is particularly due to the dynamic pressure component not being fully taken into consideration when significant, which was noted by the authors. It may therefore be viewed as an incompressible flow model where the density is allowed to change during the solution. Due to the volatile nature of airflow within a combustor chamber (jet mach numbers have been tested up to speeds of 240m/s or M≈0.7, Levebre [23]) we believe that the dynamic pressures do play an important part in a gas turbine combustor, and that a numerical model must be able to accurately describe such flow. Using the general fluid flow equations as derived in Chapter 3, an alternative solution strategy, able to handle fully compressible as well as incompressible flows with a significant dynamic pressure was developed. This should be applicable to variable area ducts in the case of incompressible flow. Note that this set of governing equations employed differs from Greyvenstein's [20] transient compressible work. This will be detailed in the following paragraphs.

As per Greyvenstein and Laurie [8], the pressure correction methodology of Patankar and Spalding [18,34] is once again applied in the improved method. As before, the corrected values are calculated adding a correction value to the guessed or predicted values using the following relationships [18]:

$$p_{0i} = p_{0i}^{*} + p_{0i}' \tag{4.1}$$

$$Q_{i,j} = Q_{i,j}^{*} + Q_{i,j}' \tag{4.2}$$

$$\rho_{i,j} = \rho_{i,j}^{*} + \rho_{i,j}' \tag{4.3}$$

where $p_{0i,j}$ denotes the total nodal pressure, $Q_{i,j}$ the element flow and $\rho_{i,j}$ the element density.

4.3.1 Flow Equations

The discretization strategy in Chapter 3 again refers. For mass-continuity at a node,

$$\sum_{j=1}^{J} s_{i,j}\rho_{i,j}Q_{i,j} = -d_i \tag{4.4}$$

where $i = 1,2,\ldots,I$

$$s_{i,j} = \begin{bmatrix} 1 & \text{if} & \text{flow enters the node} \\ -1 & \text{if} & \text{the flow exits the node} \end{bmatrix}$$

d_i = external mass flow into the node.

Next, the momentum equation for 1-D compressible and incompressible flows at a point along the general pipe element derived in Chapter 3 is discretized over the one-dimensional element shown schematically in Figure 4.1. The equation is repeated for convenience.

$$\frac{\partial p}{\partial x} + \frac{\partial}{\partial x}\left(\rho u^2\right) = Fr \tag{3.20}$$

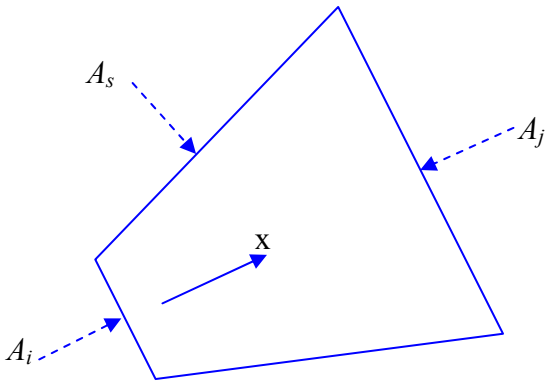

Figure 4.1 Element over which the discretization takes place

Equation (3.20) is now integrated over the control volume in Figure 4.1

$$\int_V \frac{\partial}{\partial x}(p)dV + \int_V \frac{\partial}{\partial x}\left(\rho u^2\right)dV = Fr_v \tag{4.11}$$

where V denotes the total volume of the element and $Fr_v = s_{i,j} H_{i,j} c_{f_{i,j}} u_{i,j}^2$. Applying the Divergence Theorithm to the volume integrals, the following surface integrals in the x-direction are obtained:

$$\oint_A p n_x dA + \oint_A \rho u^2 n_x dA = Fr \tag{4.12}$$

where $A = A_i \cup A_j \cup A_s$ and $Fr = s_{i,j} H_{i,j} c_{f_{i,j}} u_{i,j}^2 A_j$. Here n_x is the component of the surface normal vector in the direction of the pipe. For convenience, the two terms on the left-hand-side of Equation (4.12) will be evaluated separately. The first term may be expanded as follows:

$$\oint_A p n_x dA = \oint_{A_j} p n_x dA + \oint_{A_i} p n_x dA + \oint_{A_s} p n_x dA \tag{4.13}$$

The third term of Equation (4.13), $\oint_{A_s} p n_x dA$, will be expanded separately later and is now referred to as β. Removing p from the integral and substituting the applicable value for n_x for the remaining terms, Equation (4.13) becomes

$$\oint_A p n_x dA = p_j \oint_{A_j} dA + p_i \oint_{A_i} (-1) dA + \beta \tag{4.14}$$

where, in line with the 1-D approach, p_j and p_i denotes the average static pressures over the cross section normal to the flow.

Evaluating the integrals, Equation (4.14) becomes

$$\oint_A p n_x dA = p_j A_j - p_i A_i + \beta \tag{4.15}$$

The second term of Equation (4.12) is now evaluated and may be expanded as follows:

$$\oint_A \rho u^2 n_x dA = \oint_{A_j} \rho u^2 n_x dA + \oint_{A_i} \rho u^2 n_x dA + \oint_{A_s} \rho u^2 n_x dA \tag{4.16}$$

Because there is no flow through the surface A_s, the third term on the right-hand-side of Equation 4.16 becomes zero. Density and velocity is not functions of the area and may therefore be moved from the integral viz.

$$\oint_A \rho u^2 n_x dA = \rho_j u_j^2 \oint_{A_j} n_x dA + \rho_i u_i^2 \oint_{A_i} n_x dA \tag{4.17}$$

Applying the value for n_x and evaluating the integral, Equation (4.17) becomes

$$\oint_A \rho u^2 n_x dA = \rho_j u_j^2 A_j - \rho_i u_i^2 A_i \tag{4.18}$$

Substituting Equations (4.15) and (4.18) into (4.12) an expression for the momentum equations is obtained.

$$p_j A_j - p_i A_i + \beta + \rho_j u_j^2 A_j - \rho_i u_i^2 A_i = Fr \tag{4.19}$$

Rearranging the expression for static pressure (Equation (3.21)), substituting the expression for static pressure into Equation (4.19) and assuming negligible change in fluid density over a branch connection, Equation (4.19) is written in terms of the total pressure as

$$p_{0j} A_j - p_{0i} A_i + \beta + \frac{1}{2}\left(\rho_j u_j^2 A_j - \rho_i u_i^2 A_i\right) = Fr \tag{4.20}$$

The β-term in Equation (4.14) accounts for the change in static pressure due to changes in pipe flow area. As per the study objectives an expression will be developed for β for incompressible flow. From Figure 4.1 and Bernoulli we may obtain the following expression for the pressure from the definition of total pressure.

$$p(x) = p_{0i} - \frac{1}{2}\rho_j \frac{Q^2(x)}{A^2(x)} \tag{4.21}$$

In terms of Q_i, Equation (4.21) becomes

$$p(x) = p_{0i} - \frac{1}{2}\frac{\rho_i^2}{\rho_j}\frac{Q_i^2}{A^2(x)} \tag{4.22}$$

Substituting Equation (4.22) into the expression for β and evaluating the integral over the element, the following results

$$\beta = -1\left(p_{0i}\left(A_j - A_i\right) + \frac{1}{2}\frac{\rho_i^2}{\rho_j}Q_i^2\left(\frac{1}{A_j} - \frac{1}{A_i}\right)\right) \tag{4.23}$$

which is applicable to a generic axisymmetric duct with varying cross-sectional area. The latter includes geometrically complex pipes such as sudden expansions, as no simplifying assumption has been made in the derivation with regards to the element-wise static pressure distribution. Note that the effect of flow frictional loss is already accounted for via the *Fr* term. Substituting Equation (4.23) and the expression for Fr into Equation (4.20) the following expression for the momentum is obtained.

$$\Delta p_{0i,j} = p_{0j} - p_{0i} = s_{i,j}c_{f_{i,j}}u_{i,j}^2 + \frac{\rho_i^2 Q_i^2}{2\rho_j A_j}\left(\frac{1}{A_j} - \frac{1}{A_i}\right) - \frac{1}{2A_j}\left(\rho_j A_j u_j^2 - \rho_i A_i u_i^2\right) \tag{4.24}$$

The subscript i,j refers to the element properties which is evaluated at the centre of an element whereas the subscript *i* and *j* refer to the nodal properties. In comparison with the previous pressure drop-flow equation (Equation (4.5)), this relationship is a function of the elemental-flow, the elemental-density, the nodal densities, the element in and out flows and a loss coefficient of the particular element. Therefore it is necessary to obtain relationships or equations for each of these in terms of the variables solved for i.e. p_{0i}, $Q_{i,j}$, and $\rho_{i,j}$.

As the objective is to solve for the elemental flow $Q_{i,j}$ and not the elemental flow velocity $u_{i,j}$, we need to obtain an expression for the element and element in and out flow velocities $u_{i,j}$, u_i and u_j in terms of the variables solve for. The elemental velocity $u_{i,j}$ is merely the elemental flow divided by the mean elemental cross sectional area.

$$u_{i,j} = Q_{i,j} / A_{i,j} \tag{4.25}$$

The velocity u_a is calculated from Q_a in a similar manner where a = {i,j}. Unfortunately Q_a is not explicitly solved for and must be calculated as a function of $Q_{i,j}$ which may be obtained through the conservation of mass-flow. This implies that the nodal densities ρ_i and ρ_j need to be solved simultaneously with Q_a. This is detailed next.

From continuity, the nodal velocities are calculated as

$$u_a = \frac{\rho_{i,j} Q_{i,j}}{\rho_a A_a} \tag{4.26}$$

where a = {i,j}

However, ρ_a is a function of u_a, which is in turn a function of the static pressure at node a. The relation for ρ_a in terms of u_a and p_{0a} is given by:

$$\rho_a = \delta_{ac}\frac{p_a}{RT_a} + \delta_{ai}\rho_{ai}(T_a) \tag{4.27}$$

where

$$\delta_{ac} = \begin{cases} 0 & \text{for incompressible fluids} \\ 1 & \text{for ideal gasses} \end{cases},$$

$$\delta_{ai} = \begin{cases} 1 & \text{for pressure incompressible fluids and liquids} \\ 0 & \text{for ideal gasses} \end{cases},$$

Here $a=c$ denotes compressible gas and $a=i$ denotes incompressible gas and liquid, R is the ideal gas constant and T the temperature. The elemental density is taken as the linear average of the nodal densities:

$$\rho_{i,j} = \frac{1}{2}(\rho_j + \rho_i) \tag{4.28}$$

The above density interpolation expression is second order accurate. Equations (4.26) and (4.27) need to be solved simultaneously via numerical iteration to obtain ρ_a and u_a for a given p_{0a}. After implementing the above, Equation (4.24) becomes

$$\Delta p_{0i,j} = s_{i,j}H_{i,j}c_{fi,j}Q_{i,j}^2 + \frac{\rho_{i,j}^2}{2\rho_j A_j}\left(\frac{1}{A_j} - \frac{1}{A_i}\right)Q_{i,j}^2 - \frac{\rho_{i,j}^2}{2A_j}\left(\frac{1}{\rho_j A_j} - \frac{1}{\rho_i A_i}\right)Q_{i,j}^2 \tag{4.29}$$

The above equation constitutes the weak form of the momentum equation which is to be solved for over each element and describes compressible and incompressible steady flows in constant area ducts as well as incompressible flow in variable area ducts[2].

4.3.2 Pressure Correction Equation

As previously, to determine the relationship between the pressure correction and the flow correction, the pressure drop-flow equation (Equation (4.29)) is differentiated

[2] Matters pertaining to the validity of Equation (4.29), kindly refer to the Appendix G: "Validity of Equation (4.29)".

with respect to the element flow. Before the equation is differentiated, it is advantageous to rewrite it in the following form

$$p_{0j} - p_{0i} = Q_{i,j}^2 \cdot \varphi_{i,j} \tag{4.30}$$

where

$$\varphi_{i,j} = s_{i,j} H_{i,j} c_{fi,j} + \frac{\rho_{i,j}^2}{2\rho_j A_j}\left(\frac{1}{A_j} - \frac{1}{A_i}\right) - \frac{\rho_{i,j}^2}{2A_j}\left(\frac{1}{\rho_j A_j} - \frac{1}{\rho_i A_i}\right)$$

Equation (4.30) is now differentiated with respect to the element flow:

$$\frac{\partial p_{0j}}{\partial Q_{i,j}} - \frac{\partial p_{0i}}{\partial Q_{i,j}} = s_{i,j} H_{i,j} 2Q_{i,j}\varphi + s_{i,j} H_{i,j} Q_{i,j}^2 \frac{\partial \varphi_{i,j}}{\partial Q_{i,j}} \tag{4.31}$$

Because the partial differential terms $\partial()$ on the left-hand-side will become zero as convergence is reached, they may be replaced by the correction term $()'$ [8]. Equation (4.31) therefore becomes

$$\frac{p'_{0j}}{Q'_{i,j}} - \frac{p'_{0i}}{Q'_{i,j}} = s_{i,j} H_{i,j}\left(2Q_{i,j}\varphi + Q_{i,j}^2 \frac{\partial \varphi}{\partial Q_{i,j}}\right) \tag{4.32}$$

Provided that the Jacobian term $\frac{\partial \varphi}{\partial Q_{i,j}}$ is known, this expression for the flow-correction in terms of the pressure-correction, which is applicable to both compressible gas and incompressible gas and liquid flow, is viewed as straightforward to implement. A further advantage of this approach is that the non-linearities introduced in the c_f

coefficient such as friction is automatically taken in consideration in $\frac{\partial \varphi}{\partial Q_{i,j}}$ which may have a significant effect on convergence (See Chapter 5). To complete the proposed algorithm, $\frac{\partial \varphi}{\partial Q_{i,j}}$ is computed numerically to first order accuracy as follows:

$$\frac{\partial \varphi}{\partial Q_{i,j}} = \frac{\varphi\left(Q_{i,j} + dQ_{i,j}\right) - \varphi\left(Q_{i,j}\right)}{dQ_{i,j}} \tag{4.33}$$

where $dQ_{i,j} = \max(10^{-3}Q_{i,j},\ 10^{-5}Q^{max}{}_{i,j})$. The latter value keeps $dQ_{i,j}$ from becoming zero. The effect of the order of accuracy of Equation (4.33) on solution accuracy and convergence characteristics was found to be negligible. The cost of computing the above Jacobian term was also found to be insignificant in terms of the scheme's overall CPU cost, as the bulk of the computational effort is expended on inverting the pressure correction matrix.

Through rearranging the terms of Equation (4.32), an equation for the flow correction is now established as

$$Q'_{i,j} = \frac{p'_{0j} - p'_{0i}}{s_{i,j} H_{i,j} \left(2Q_{i,j}\varphi + Q^2_{i,j} \frac{\partial \varphi}{\partial Q_{i,j}} \right)} \tag{4.34}$$

The density correction may be obtained via Equation (4.28) as follows

$$\rho'_{i,j} = \frac{1}{2}\left(\rho'_j + \rho'_i\right) \tag{4.35}$$

The expression for the pressure correction in terms of the flows and the densities may now be derived by substituting Equations (4.1) to (4.3), (4.34) and (4.35) into Equation (4.9), which results in

$$p'_{0i} = \frac{\left(\sum_{j=1}^{J} \left(c_{i,j} p'_{0j} \right) + b_i \right)}{c_{i,i}} \tag{4.36}$$

where,

$$c_{i,i} = \sum_{j=1}^{J} \left(\frac{\rho^*_{i,j}}{\eta} - \frac{1}{2} \alpha_j Q^*_{i,j} \right) s_{i,j}$$

$$c_{i,j} = \left(\frac{\rho^*_{i,j}}{\eta} + \frac{1}{2} \alpha_i Q^*_{i,j} \right) s_{i,j}$$

$$b_i = d_i + \sum_{j=1}^{J} \left(\rho^*_{i,j} Q^*_{i,j} s_{i,j} \right)$$

$$\eta = H_{i,j} \left(2 Q^*_{i,j} \varphi + Q^{*2}_{i,j} \frac{\partial \varphi}{\partial Q^*_{i,j}} \right)$$

$$\alpha_a = 1 \Bigg/ \left(RT_{i,j} + \frac{1}{2} \left(\frac{\rho^*_{i,j} Q^*_{i,j}}{\rho^*_a A_a} \right)^2 \right)$$

$$with \quad a = i \; or \; j \quad and \quad i = 1,2,\ldots,I$$

This pressure correction equation is now solved, at all nodes in the network simultaneously, and the corrected values for pressure, flow and density are calculated by means of Equations (4.1), (4.34), (4.2), (4.35) and (4.3).

4.4 Flow Elements

Three types of flow elements are used in this work and will be discussed next. These three elements are a pipe element, a sudden expansion element and a liner hole element. Using the Darcy-Weisbach equation, an expression for the flow coefficient c_f may be derived.

$$c_f = \frac{1}{2} K_{i,j} \rho_{i,j} \tag{4.37}$$

where $K_{i,j}$ is the element loss factor. Different expressions for $K_{i,j}$ for the flow elements used are given in Table 4.1.

Table 4.1 Loss factors for flow elements

	Element Type	Loss factor expression
1	Pipe element	$K_{i,j} = \frac{L_{i,j} f_{i,j}}{d_{i,j}}$
2	Sudden expansion element	$K_{i,j} = \left(1 - \frac{d_i^2}{d_j^2}\right)^2$
3	Liner hole element	$K_{i,j} = \left(\frac{\rho_{i,j}}{\rho_i}\frac{1}{Cd^2} - \frac{\rho_{i,j}}{\rho_j}\right)$

Note that the loss factors for the first two elements may be found in a fluid mechanics textbook [28] and that the loss factor of the last element is derived from the expression for liner hole flow in Chapter 2.

4.5 Friction Factor

Many equations to determine the friction factor are available in the literature. Two of the equations apply for laminar flow conditions, and the remaining three equations are used for turbulent flow conditions. The equations for laminar flow conditions for circular and rectangular duct are

$$f = \frac{64}{\mathrm{Re}} \tag{4.38}$$

and

$$f = \frac{96}{\mathrm{Re}} \tag{4.39}$$

respectively. The equations for turbulent flow conditions all fit the well-known Moody diagram. These equations are also known as Chen's equation, Churchill's equation and Swamee-Jain's equation, and are as follows

Chen's equation [54]: (4.40)

$$\frac{1}{\sqrt{f}} = -2.0\log\left\{\frac{1}{3.7065}\left(\frac{\varepsilon}{\mathrm{D}}\right) - \frac{5.0452}{\mathrm{Re}} \times \log\left[\frac{1}{2.8257}\left(\frac{\varepsilon}{\mathrm{D}}\right)^{1.1098} + \frac{5.8506}{\mathrm{Re}^{0.8981}}\right]\right\}$$

Haaland's equation [28]:

$$\frac{1}{f^{1/2}} \approx 1.8 \log\left[\frac{6.9}{\mathrm{Re}_d} + \left(\frac{\varepsilon/d}{3.7}\right)^{1.11}\right] \tag{4.41}$$

Swamee and Jain's equation [33]:

$$f = 1.325\left\{\ln\left[0.27\left(\frac{\varepsilon}{D}\right) + 5.74\left(\frac{1}{\mathrm{Re}}\right)^{0.9}\right]\right\}^{-2} \tag{4.42}$$

Equation (4.41) is an accurate representation of the Colebrook relation, which fits the Moody diagram for transitional and turbulent flows. In all the equations above, f is the friction factor, Re is the Reynolds number and ε is the surface roughness.

4.6 Numerical solution strategies

In Chapter 1, one noticed that amid the advantages of nodal methods in the simulation of gas networks, the most troubling disadvantage has traditionally been the poor convergence characteristic, which renders the method impractical for simulation

purposes. It is also very sensitive to initial values. Using the SIMPLE method, related difficulties are encountered, especially when the pressure correction coefficients differ significantly between elements [18]. A remedy to these difficulties is to properly solve the pressure correction matrix before one moves on to the next iteration of the overall solution algorithm [8].

The pressure correction equation can be written in matrix form as

$$\boldsymbol{A}\boldsymbol{p}' = \boldsymbol{b} \tag{4.43}$$

with

$$a_{i,i} = c_{i,i} \tag{4.44}$$

$$a_{i,n_{ij}} = -c_{i,j} \tag{4.45}$$

and the other elements of $\boldsymbol{A}$ equal to zero. If the pressure correction equation is solved exactly, by definition, the continuity equation will also be satisfied exactly, and the reliability of the nodal method would subsequently be improved.

4.6.1 Solution methods

The system of equations to be solved (i.e., the pressure equations), were developed in such a way that they form a linear system of equations. The advantage inherited by this means of development is that the linear system may be solved through direct methods. These direct methods consist of the notorious Gauss elimination method, the LU factorization method, the LDL^t factorisation method, the Coleski method, Crout factorisation for tridiagonal linear systems and the Envelope method [36].

Apart from the direct methods for solving linear systems, there are also indirect methods. These methods are often used to solve large sparse matrices and include the Jacobi iterative method, the Gauss-Seidel iterative method and the SOR method [36]. The penalty paid for utilizing indirect methods is that of longer computational times in the case of small systems. Also it is not always possible to solve sparse matrices with

indirect methods. When a matrix is singular, an indirect method will converge to a solution, namely, the absolute value of which is decided by the initial guess [18]. However, a direct method would refuse to furnish a solution.

Three of these methods have been considered in this study, two of which fall into the direct method category and the remaining one into the indirect method category. The direct methods considered were Gauss elimination method and LU factorisation. The indirect method considered was the Gauss-Seidel iterative method. The LU factorization method was found to offer comparable or improved performance as compared to the other methods, while being relatively simple to implement. It was therefore chosen for the purposes of this study. Further information may be found in Appendix C.

4.6.2 Matrix reordering

Matrix-reordering methods are often considered when being tasked with inverting a matrix due to the potential savings in both storage space and computational time [37]. Numerous matrix forms have been proposed as objectives for ordering strategies. Extensive research has been done on banded and variable-band matrices such as shown in Figure 4.3. Variable-band forms are commonly referred to as skyline, profile or envelope forms.

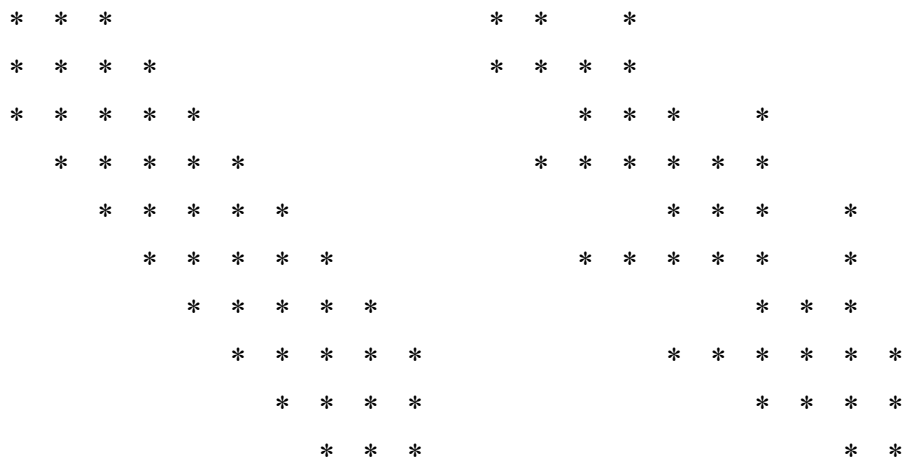

Figure 4.3 Band and variable-band forms

To obtain these matrix forms, numerous methods and algorithms have been developed by various authors and a discussion of these methods may be found in the references [33, 37–38]. Some of these methods include block tridiagonal methods, the reversed Cuthill-McKee (RCM) method, one-way dissection and nested dissection methods. The reversed Cuthill-McKee method (A detailed description of the working of the reversed Cuthill-McKee method is found in Appendix D) was chosen for utilization in this study because of its success, as elaborated by many authors [37]. Trail runs of the Cuthill-McKee method revealed that, for small networks, no substantial improvement in solution time was obtainable. Therefore the computing effort incurred using the reversed Cuthill-McKee does not warrant the use thereof at this stage, however, it may be important to apply this method when large networks are examined.

4.7 Convergence

As described in Chapter 1, various authors [7,9,10,11,28,39] use the variation in computed nodal or element flow between successive iterations as a convergence criterion in a network that, more often than not, yields inaccurate results when applied to nodal methods if the solution converges. This criteria is usually in the form of

$$\varepsilon \geq \frac{\sum\left(Q^{n} - Q^{n-1}\right)}{Q^{n}} \tag{4.46}$$

where ε = convergence criteria / tolerance

Q^{n} = flow rate obtained from the current iteration

Q^{n-1} = flow rate obtained from the previous iteration

Greyvensteyn and Laurie [8] discovered that these accuracy problems do not originate from an inherent flaw in the methods, but from an inappropriate choice of the convergence parameter. They propose a convergence criterion for pressure-based

nodal methods that consists of two convergence parameters, namely, a continuity convergence parameter and a pressure drop convergence parameter. The continuity parameter checks if the continuity equation is satisfied, while the pressure drop parameter checks if the pressure drop-flow equation has been satisfied.

The continuity convergence parameter, ε_m, is defined as

$$\varepsilon_m = \frac{|h_i|_{\max}}{|\dot{m}|_{mean}} \tag{4.47}$$

where $|\dot{m}|_{mean}$ is the mean of the absolute values of all the mass element flows and $|h_i|_{\max}$ is the maximum of the absolute residual nodal mass flow. The mean mass element flow and is given as

$$|\dot{m}|_{mean} = \frac{1}{b}\sum_{i=1}^{b}|\dot{m}_i| \tag{4.48}$$

where b is the number of branches/elements

and the residual nodal mass flow by

$$h_i = \sum_{j=1}^{J}\left(s_{i,j}\rho_{i,j}Q_{i,j}\right) + d_i \tag{4.49}$$

The pressure drop convergence parameter, ε_p, is defined as

$$\varepsilon_p = \sum_{n=1}^{b}\left|\frac{\Delta p_1 - \Delta p_2}{\Delta p_1}\right| \tag{4.50}$$

where b = number of elements.

Δp_1 = pressure drop across an element as calculated from flows via the momentum equation.

Δp_2 = pressure difference between the two nodes associated with an element as calculated from the pressure-correction matrix.

To ensure an accurate solution, both ε_m and ε_p should become sufficiently small (e.g., $\varepsilon_m, \varepsilon_p \leq 10^{-3}$). Finally for stability, all the pressure drop-flow rate coefficients must be positive [8,18].

4.8 Closure

In this chapter, a network numerical solution methodology was developed. The proposed method is capable of dealing with both compressible flow in constant area ducts as well as incompressible flows in variable area ducts. It is further simpler to implement than existing hybrid pipe-network methods *and* naturally takes into account all flow related non-linearities when constructing the pressure correction matrix. The latter will be shown to result in significantly improved convergence characteristics. By deriving the appropriate pressure drop-flow relationships, elements for any type of axi-symmetric flow device may be created.

CHAPTER 5

Simulation Package and Validation

Chapter 5 considers the Simulation Package and the Validation thereof. A brief description of the package is given as well as the simulations of published networks to validate the accuracy of the proposed method.

5.1 Preamble

This chapter deals with the incorporation of the proposed numerical routine into a simulation package. The simulation package allows the user to design the network visually, specify the boundary conditions at certain locations and adjust fluid parameters, flow characteristics and solver options. In the subsequent paragraphs a visual discussion of the simulation package, with figures of the relevant windows, will be provided.

During the development of the simulation package, the network model was tested on published and textbook networks. These test networks not only established a basis of accuracy for the network model, but also tested the characteristics of the proposed numerical scheme in terms of stability and efficiency. The networks used for verification purposes are an air gas network published by Greyvenstein and Laurie [8], a compressible helium pipeline network published by Greyvenstein [20], a sudden expansion test case from the textbook of White [28] and a liner hole.

5.2 The Simulation Package

THE OPERATING ENVIRONMENT

The simulation package was designed and developed for the Microsoft® Windows™ environment. The program is an interactive simulation package with user and graphics capabilities. The programming language used for this project was Borland C++ Builder 5. A modular program structure was used in the development of the simulation package. The first module allows the user to design and to define a network using a graphical interface. The other modules are utilised automatically by the simulation package as soon as the user wishes to solve the network. The second module sets up the connectivity matrices for the particular network. The third module calculates the initial values for pressures and flows whereafter the solution coefficients are calculated and placed in the solution matrix. A solver module is activated and the pressure correction is calculated. The correction module sets the corrected values for the pressures, flows and densities. The results are subsequently shown after convergence or once the maximum number of iterations, as specified by the user, is reached.

THE DESIGN WINDOW

The design window shows an arbitrary network (Figure 5.1), which may be modified by adding branches (elements) or nodes by selecting the relevant drawing mode in the upper left-hand corner of the design window. Branch or nodal data are entered on the right-hand side before the node or branch is placed. Choosing the select option can also change branch or nodal data accordingly. Standard *Windows* operations (such as *New*, *Open*, *Save*, and *Save As*) can be found in the 'File' menu.

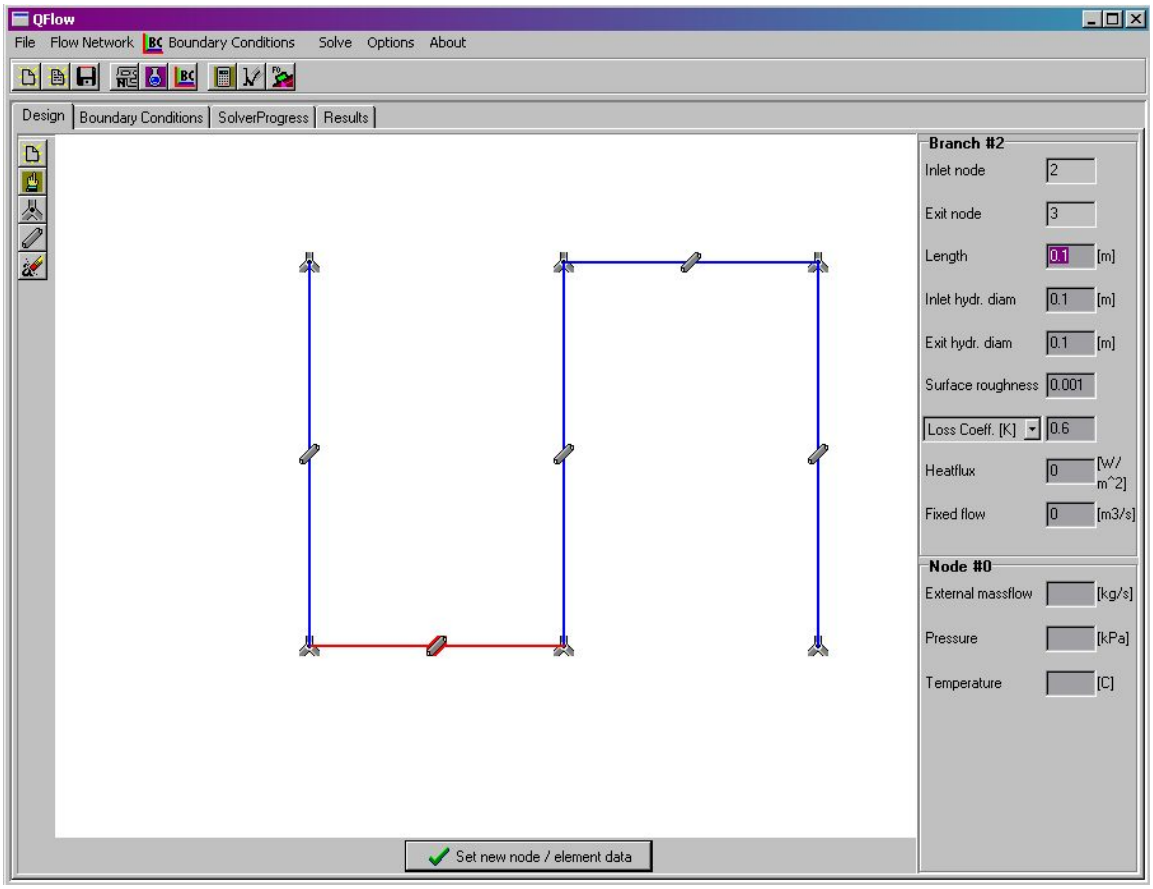

Figure 5.1 The main program interface including the design window

BOUNDARY CONDITIONS

Some of the necessary boundaries are set in the boundary conditions window (Figure 5.2). This enables the user, for instance, to specify constant duct parameters to facilitate the design of the network. Outlets and inlets are boundary conditions that have to be designed along with the network, (i.e., a branch connected to a remote node with a specific pressure will be regarded as a boundary condition). This will be either an input or an output boundary, depending on the particular network.

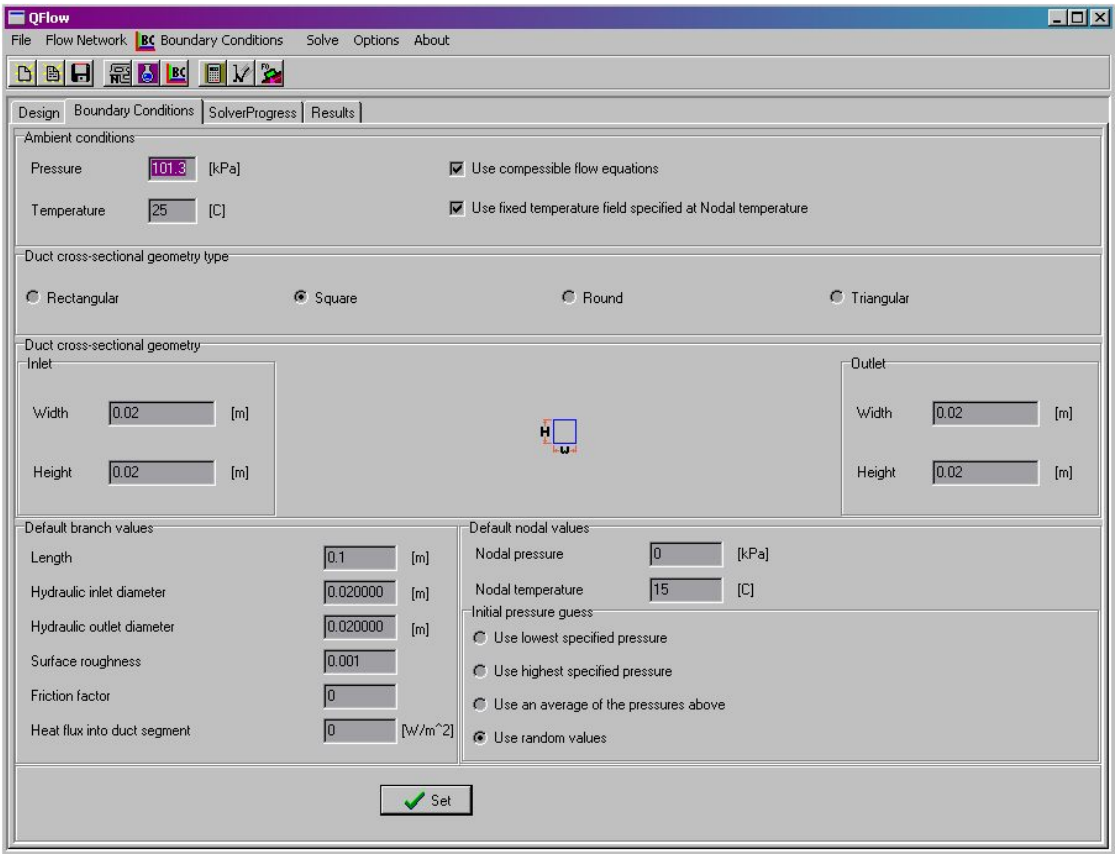

Figure 5.2 Boundary conditions window

FLUID PROPERTIES

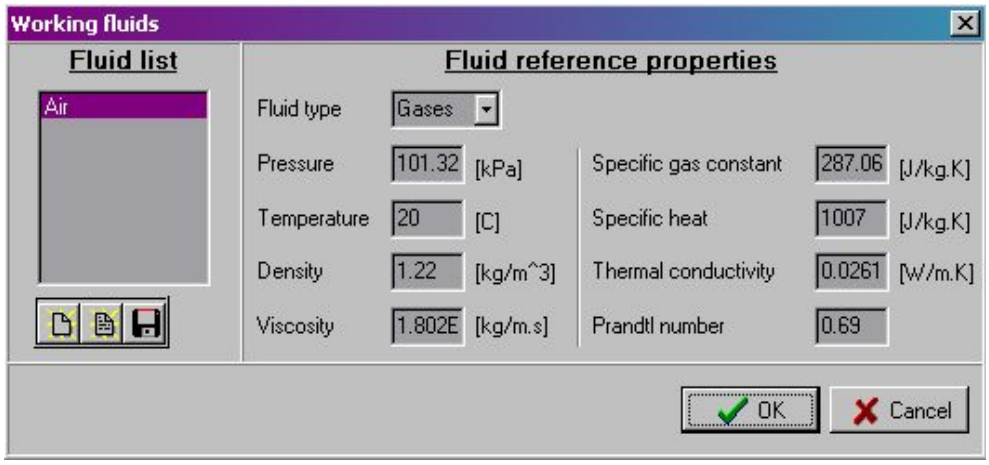

Figure 5.3 Fluid properties window

Different working fluids, as well as their reference properties, may be added by using the fluid properties window (Figure 5.3). From the working fluid list, a fluid may be selected for a particular network. The solver will then use the properties of the chosen fluid in the solution of the network.

FRICTION OPTIONS

Figure 5.4 shows the friction options box. The user may use either a constant value for the friction factor as specified in the design window at every branch, or may select a friction factor formula for a particular case. Provided within the simulation package are two laminar flow friction factors and three turbulent flow friction factor formulations. If any of these friction factor relations are chosen, the previously specified friction factor will be omitted and a friction factor using the chosen relationship will be calculated.

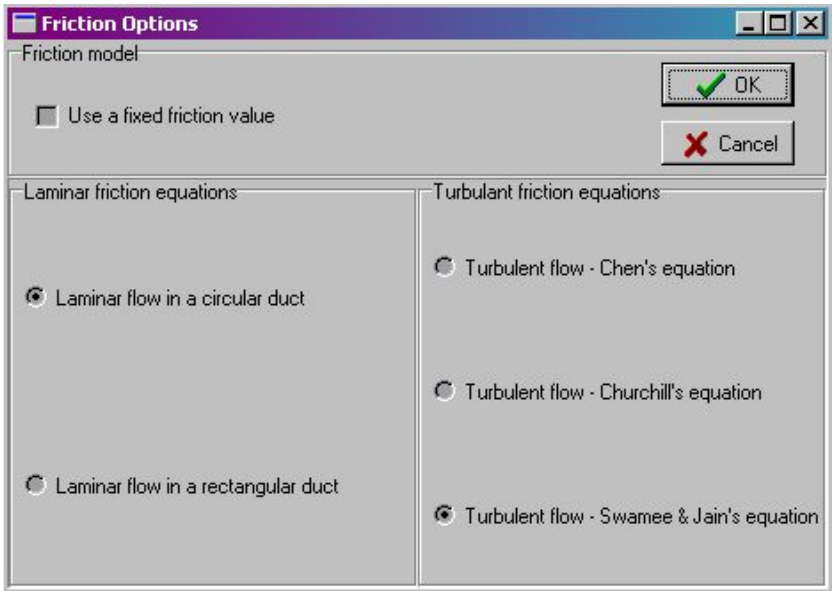

Figure 5.4 Friction options window

SOLVER PROGRESS AND SOLVER OPTIONS

In Figure 5.5 the solver options dialog box and the solver progress window are displayed. The solver progress window shows the number of iterations that are completed as well as the level of convergence of the solution and the convergence criteria (horizontal line on graph). The convergence of the solution is a logarithmic value and is plotted against the number of iterations. The convergence of the solution is calculated from the nodal pressure difference as explained in Chapter 4.

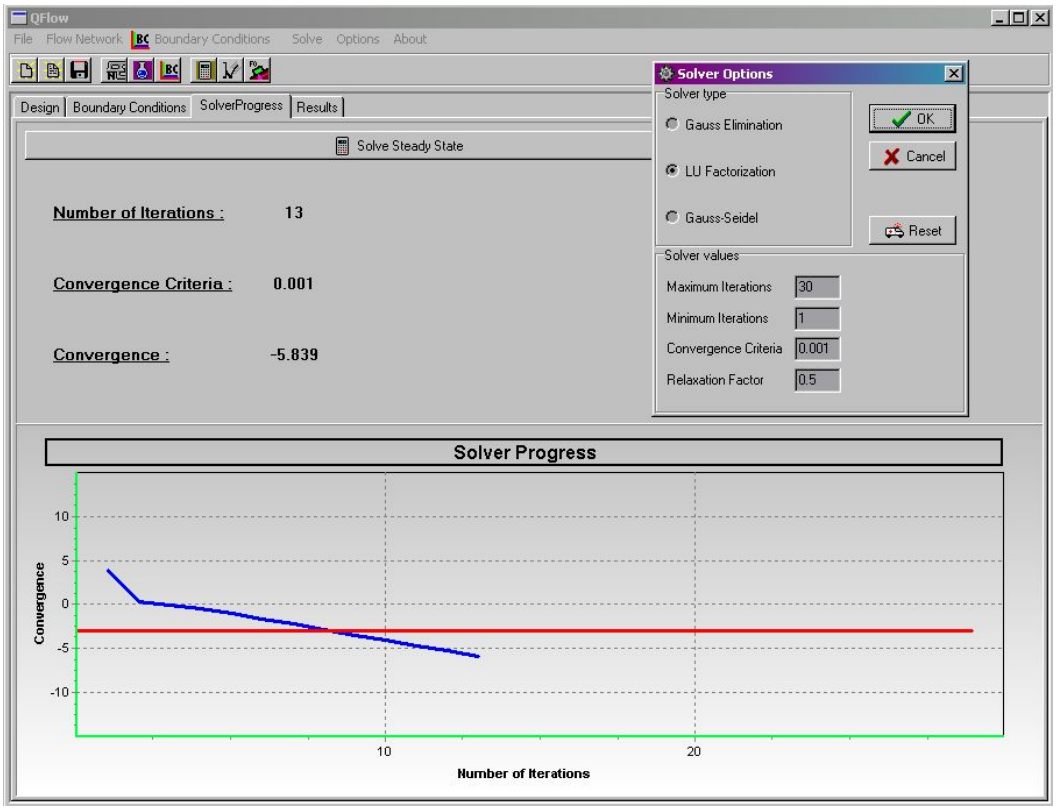

Figure 5.5 Solver progress and solver options window

The solver options dialog box enables the user to specify different solver types as well as some solver values. The solver type refers to the type of direct or indirect solution method to be used. Because these methods originate from linear algebra, they should eventually all yield the same results although their solution times may differ. The solver values to be specified include the minimum and the maximum number of

iterations as well as the convergence criteria. Because of the pressure-based method used, the pressure corrections may have to be under-relaxated in order to obtain a converged solution [18].

RESULTS WINDOW

Figure 5.6 depicts the results window, which contains the solved flows, densities, pressures and temperatures. In this network a constant temperature field and a constant pipe friction factor were used.

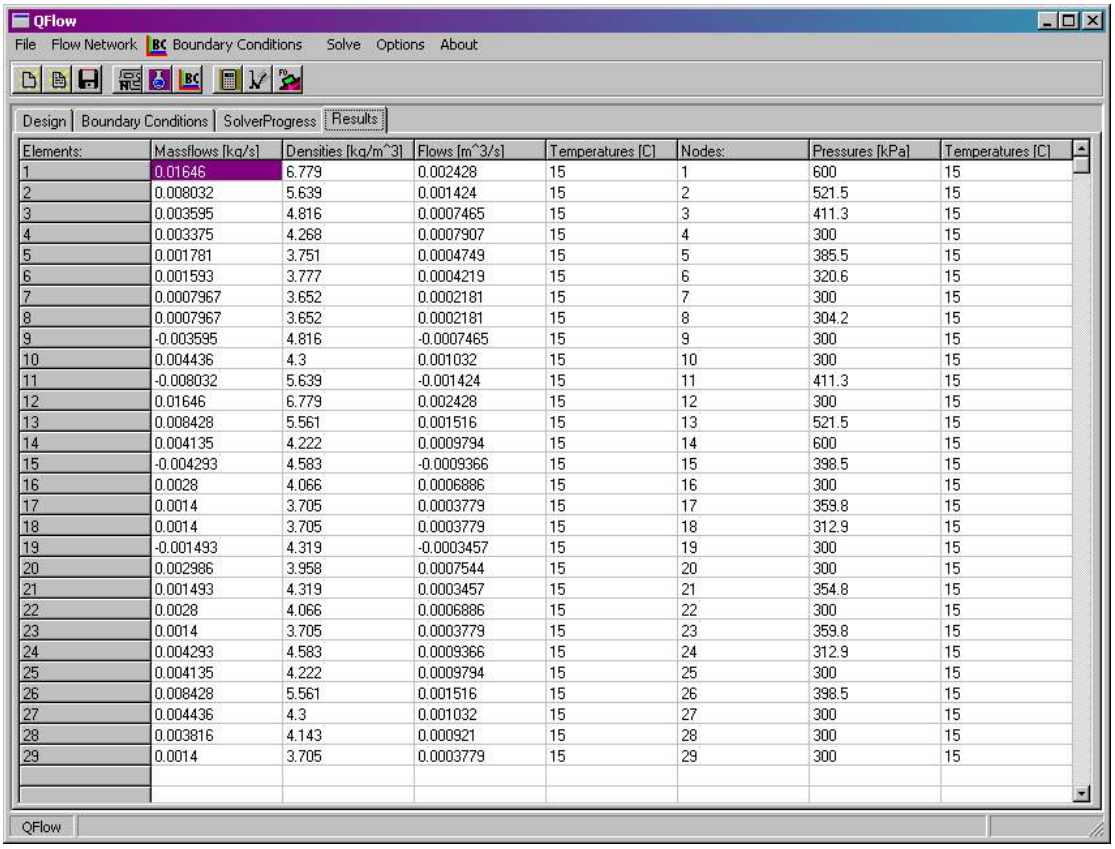

Elements:	Massflows [kg/s]	Densities [kg/m^3]	Flows [m^3/s]	Temperatures [C]	Nodes:	Pressures [kPa]	Temperatures [C]
1	0.01646	6.779	0.002428	15	1	600	15
2	0.008032	5.639	0.001424	15	2	521.5	15
3	0.003595	4.816	0.0007465	15	3	411.3	15
4	0.003375	4.268	0.0007907	15	4	300	15
5	0.001781	3.751	0.0004749	15	5	385.5	15
6	0.001593	3.777	0.0004219	15	6	320.6	15
7	0.0007967	3.652	0.0002181	15	7	300	15
8	0.0007967	3.652	0.0002181	15	8	304.2	15
9	-0.003595	4.816	-0.0007465	15	9	300	15
10	0.004436	4.3	0.001032	15	10	300	15
11	-0.008032	5.639	-0.001424	15	11	411.3	15
12	0.01646	6.779	0.002428	15	12	300	15
13	0.008428	5.561	0.001516	15	13	521.5	15
14	0.004135	4.222	0.0009794	15	14	600	15
15	-0.004293	4.583	-0.0009366	15	15	398.5	15
16	0.0028	4.066	0.0006886	15	16	300	15
17	0.0014	3.705	0.0003779	15	17	359.8	15
18	0.0014	3.705	0.0003779	15	18	312.9	15
19	-0.001493	4.319	-0.0003457	15	19	300	15
20	0.002986	3.958	0.0007544	15	20	300	15
21	0.001493	4.319	0.0003457	15	21	354.8	15
22	0.0028	4.066	0.0006886	15	22	300	15
23	0.0014	3.705	0.0003779	15	23	359.8	15
24	0.004293	4.583	0.0009366	15	24	312.9	15
25	0.004135	4.222	0.0009794	15	25	300	15
26	0.008428	5.561	0.001516	15	26	398.5	15
27	0.004436	4.3	0.001032	15	27	300	15
28	0.003816	4.143	0.000921	15	28	300	15
29	0.0014	3.705	0.0003779	15	29	300	15

Figure 5.6 Results window

5.3 Verification of the numerical scheme

COMPRESSED AIR NETWORK

Greyvenstein and Laurie [8] published a compressed air network example in their paper to demonstrate the performance of their method. The developed algorithm will now be used to analyse this network in order to verify accuracy. Figure 5.7 shows the layout of the network with boundary conditions. The element related data is available in the paper of Greyvenstein and Laurie [8]and is included for convenience in Table 5.1.

Table 5.1 Element (pipe) data for the compressed air network

Element no	Inlet node	Exit node	Diameter [m]	Length [m]
1	1	2	200	0.019
2	2	3	400	0.01588
3	3	5	400	0.01588
4	5	6	100	0.01
5	6	7	100	0.01
6	6	8	100	0.01
7	8	9	100	0.01
8	8	10	100	0.01
9	5	11	400	0.01588
10	11	12	100	0.01
11	11	13	400	0.01588
12	14	13	200	0.019
13	13	15	400	0.01588
14	15	16	100	0.01
15	17	15	400	0.01588
16	17	18	100	0.01
17	18	19	100	0.01
18	18	20	100	0.01
19	21	17	400	0.01588
20	21	22	100	0.01
21	23	21	400	0.01588
22	23	24	100	0.01
23	24	25	100	0.01
24	26	23	400	0.01588
25	26	27	100	0.01
26	2	26	400	0.01588
27	3	4	100	0.01
28	5	28	100	0.01
29	24	29	100	0.01

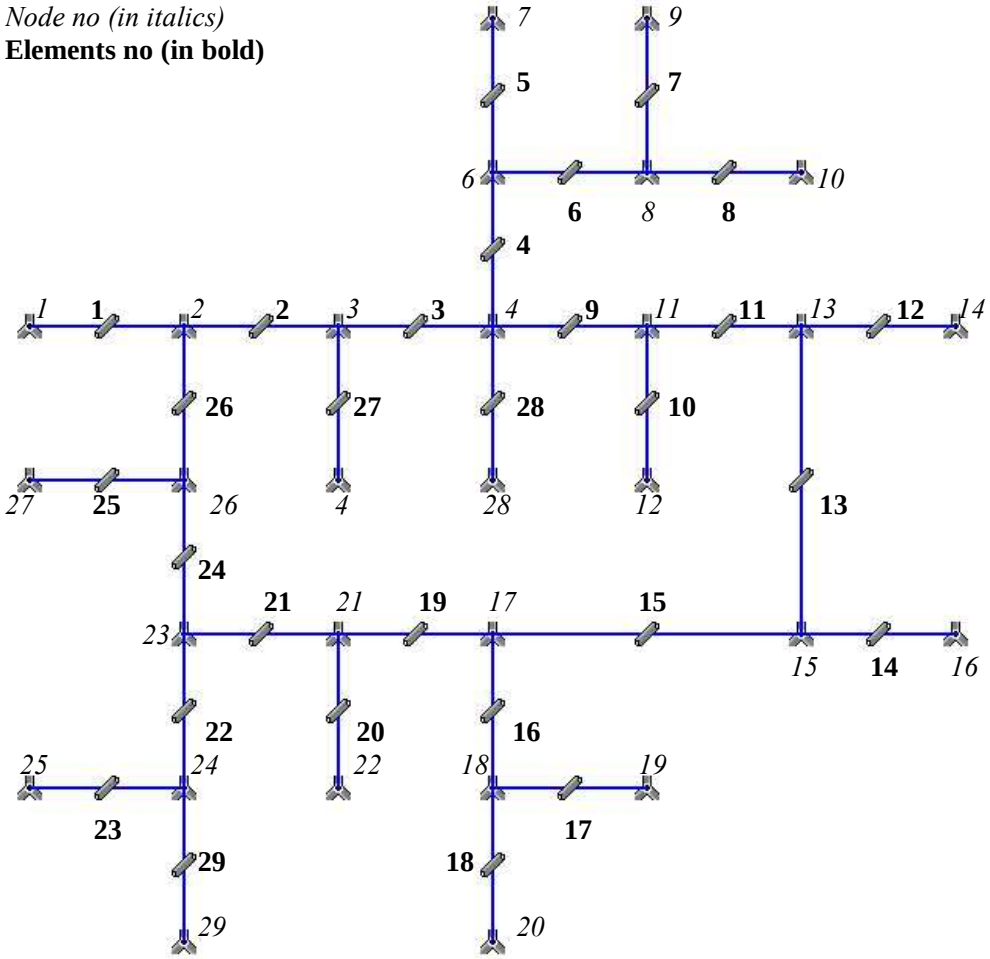

Figure 5.7 Compressed air network

The boundary conditions to this network are inlet or supply pressures of 600 kPa, while the outlet or discharge pressures are set equal to 300 kPa. The supply pressures are applied to nodes one and fourteen, and the discharge pressures are applied to all nodes with only one connecting element. The friction factor is initially fixed to f=0.03 as per the aforementioned paper. The temperature field has been kept constant at 15^{o}C with no heat addition or subtraction. The relaxation factor was set to 1.0.

Table 5.2 Results of the simulation package for the compressed air network.

Results							
	Constant friction network (f=0.03)				Variable friction network		
	Published[8]		This work		This work		
no	Mass flow [kg/s]	Pressure [kPa]	Mass flow [kg/s]	Pressure [kPa]	Mass flow [kg/s]	Pressure [kPa]	f
1	0.01646	600.00	0.01645	600.00	0.03109	600.00	0.008
2	0.00803	521.51	0.00803	521.51	0.01517	529.37	0.009
3	0.00360	411.34	0.00360	411.37	0.00663	419.93	0.010
4	0.00338	300.00	0.00337	300.00	0.00610	300.00	0.009
5	0.00178	385.50	0.00178	385.53	0.00328	390.66	0.011
6	0.00159	320.57	0.00159	320.58	0.00282	324.93	0.011
7	0.00080	300.00	0.00080	300.00	0.00141	300.00	0.013
8	0.00080	304.23	0.00080	304.23	0.00141	305.91	0.013
9	-0.00360	300.00	-0.00360	300.00	-0.00663	300.00	0.010
10	0.00444	300.00	0.00443	300.00	0.00855	300.00	0.009
11	-0.00803	411.34	-0.00803	411.37	-0.01517	419.93	0.009
12	0.01646	300.00	0.01645	300.00	0.03109	300.00	0.008
13	0.00843	521.51	0.00842	521.51	0.01592	529.37	0.008
14	0.00413	600.00	0.00413	600.00	0.00802	600.00	0.009
15	-0.00429	398.49	-0.00429	398.51	-0.00790	408.65	0.010
16	0.00280	300.00	0.00280	300.00	0.00513	300.00	0.010
17	0.00140	359.77	0.00140	359.78	0.00256	366.92	0.012
18	0.00140	312.86	0.00140	312.87	0.00256	316.43	0.012
19	-0.00149	300.00	-0.00149	300.00	-0.00277	300.00	0.013
20	0.00299	300.00	0.00299	300.00	0.00553	300.00	0.010
21	0.00149	354.80	0.00149	354.82	0.00277	359.86	0.013
22	0.00280	300.00	0.00280	300.00	0.00513	300.00	0.010
23	0.00140	359.77	0.00140	359.78	0.00256	366.92	0.012
24	0.00429	312.86	0.00429	312.87	0.00790	316.43	0.010
25	0.00413	300.00	0.00413	300.00	0.00802	300.00	0.009
26	0.00843	398.49	0.00842	398.51	0.01592	408.65	0.008
27	0.00444	300.00	0.00443	300.00	0.00855	300.00	0.009
28	0.00382	300.00	0.00382	300.00	0.00715	300.00	0.009
29	0.00140	300.00	0.00140	300.00	0.00256	300.00	0.012

The solved pressures and flows are shown in Table 5.2 (Constant friction network) and compare well with the results of Greyvenstein and Laurie. The convergence history of the solution process is depicted in Figure 5.8. The initial residual is different from that of the other authors which is suspected to be due to different initial guessed values employed. In this work guessed nodal pressures were used as initial values. These were chosen just below the highest specified pressure in the network and are automatically calculated by the solver. Convergence to engineering accuracy

($\log(\varepsilon_p)$=-4) was however reached within 8 iterations, which is similar to that of the other authors. The proposed formulation therefore offers similar accuracy and performance to the methodology of Greyvenstein and Laurie.

In real life pipe networks, friction is a function of the flow through the network and not fixed as previously simulated. Therefore the analysis for the same compressed air pipe network was repeated with friction values as a function of the flow ($f(Q)$) through the network via the described method. This analysis was also used to evaluate the effect on convergence of taking the friction factor as a function of the flow ($f(Q)$) when constructing the pressure correction matrix. The surface roughness was set to e = 0.001mm for all the pipes, which corresponds to that of drawn tubing. All the other properties and conditions were as per the previous analysis.

For the first simulation, the friction f was kept constant when constructing the pressure correction equation ($df/dQ = 0$), the relaxation factor was kept at 1.0 and convergence to engineering accuracy was reached in 11 iterations as shown in Figure 5.8. The simulation was repeated, and this time the friction factor was taken as a function of the flow when constructing the pressure correction matrix ($df/dQ \neq 0$). Convergence was now reached in 7 iterations. Note that the solved pressures and flows for both construction methodologies were identical and is given in Table 5.2.

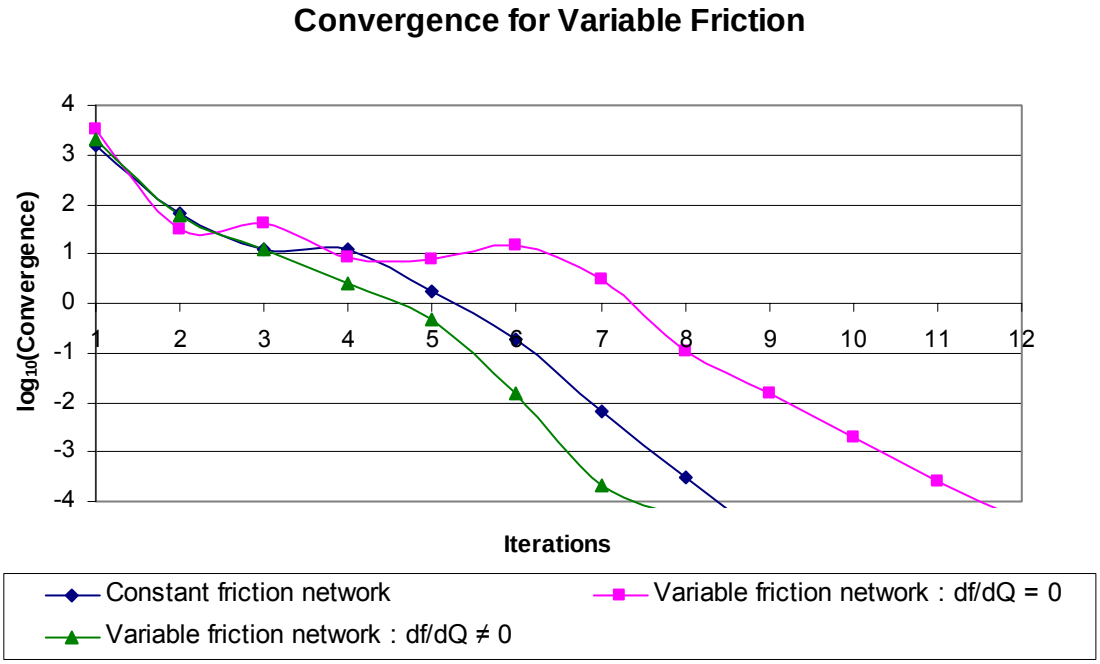

Figure 5.8 Convergence plots for the compressed air network simulation

Therefore, from this test case it can be concluded that the proposed methodology offers similar performance compared to that of the other hybrid formulation in terms of both accuracy and convergence characteristics. It is also demonstrated that all types of flow related non-linearities should be taken into consideration when constructing the pressure correction matrix as this may have a significant effect on convergence. The proposed methodology facilitates this in a natural manner.

ISOTHERMAL STEADY-STATE COMPRESSIBLE FLOW THROUGH A 100M LONG PIPELINE

The steady-state compressible flow benchmark example recently published by Greyvenstein [20] refers. The test case involves a 100m long pipeline with a diameter of 0.5m. Helium flows through the pipeline with a total outlet pressure of 200kPa and an inlet temperature of 300K. The friction factor is assumed to be constant at $f = 0.02$. The results of Greyvenstein as well as an "analytical" solution obtained via a fourth

order Runga Kutta numerical integration procedure of the following equation set [26], will be used for validation purposes.

$$\frac{dM}{M} = \frac{\left(1+0.5(\gamma-1)M^2\right)}{1-M^2}\left\{\frac{\gamma M^2}{2}\left(\frac{fdx}{D}\right)+\frac{\left(1+\gamma M^2\right)}{2}\frac{dT}{T}\right\} \qquad (5.1)$$

The additional flow properties may be obtained from the following formulations [26]:

$$\dot{m} = ApM\sqrt{\frac{\gamma}{RT}\left(1+\frac{\gamma-1}{2}M^2\right)} \qquad (5.2)$$

$$\frac{P}{p} = \left(1+\frac{\gamma-1}{2}M^2\right)^{\gamma/(\gamma-1)} \qquad (5.3)$$

$$\frac{T}{t} = \left(1+\frac{\gamma-1}{2}M^2\right) \qquad (5.4)$$

where the properties in uppercase refers to the stagnation condition and in lowercase to the static condition. M denotes the Mach number.

In order to analyse this example, the mass flow through the pipeline needs to be calculated so that it can be used as an input at the inflow boundary. The mass flow is calculated through Equation (5.2) for the outlet conditions by utilizing the total temperature as a function of the outlet Mach number. The values for the properties of Helium are supplied, in brackets, where appropriate.

$$\dot{m}_2 = Ap_2M_2\sqrt{\frac{\gamma}{RT_2}\left(1+\frac{\gamma-1}{2}M_2^2\right)}$$

where A = cross sectional area

p_2 = static outlet pressure

M_2 = outlet Mach number

T_2 = total outlet temperature

R = gas constant (2077.1 J/kgK)

γ = specific heat ratio (1.667)

The static outlet pressure in terms of the total outlet pressure and the outlet Mach number can be calculated by means of Equation (5.3). Table 5.3 show the results.

Table 5.3 Calculated mass flows at the respective outlet Mach numbers.

M_2	T_2 (K)	p_2 (kPa)	mdot$_2$ (kg/s)
0.0	300.000	200.00	0.00
0.1	301.001	198.34	6.37
0.2	304.002	193.48	12.43
0.3	309.005	185.75	17.90
0.4	316.008	175.63	22.56
0.5	325.013	163.72	26.29
0.6	336.018	150.65	29.03
0.7	349.025	137.01	30.80

The pipeline problem was analysed using the Greyvenstein and Laurie method and the proposed method. The simulation package solved for the total inlet pressures and the total pressure ratios for the pipeline were subsequently calculated for the respective outlet Mach numbers. The results are plotted on the same graph as the benchmark problem as well as the solution of Greyvenstein [20] (Figure 5.9). The proposed method agrees well with the benchmark solution but the Greyvenstein and Laurie method deviates from the benchmark solution at Mach numbers exceeding Mach 0.3. This deviation is due to the dynamic pressure term being neglected or very small, as the latter was assumed by Greyvenstein and Laurie [8].

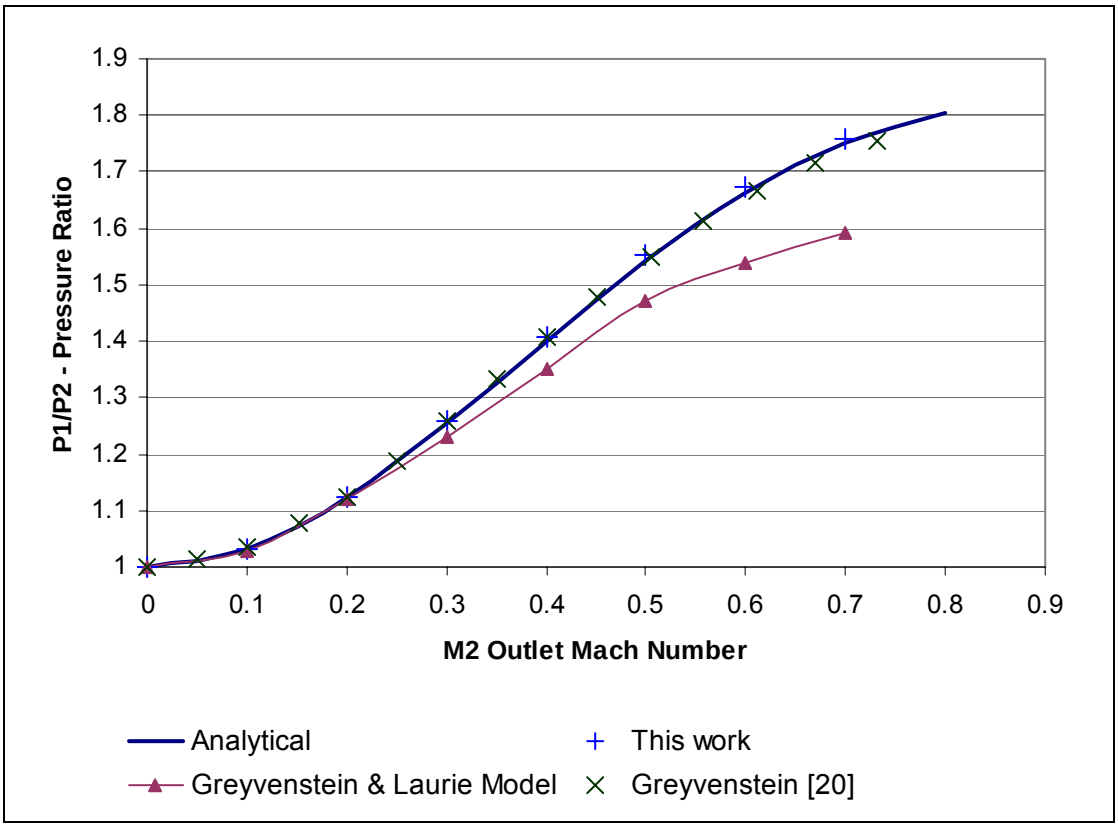

Figure 5.9 The pressure ratio as a function of outlet Mach number for steady isothermal flow in a 100m long pipe line.

In this work we employ 10 elements to discretize the pipeline, as opposed to the 20 elements used by the other author. As similarly accurate simulation values were obtained, this deems the equation set employed in this work as more accurate. The trade-off is that it is limited to networks where the change in density over a branch connection is small, which is not the case with the other author's work.

Table 5.4 documents the convergence statistics for different relaxation factor values and outlet Mach numbers for this test case. It is clear that in general, the lower the relaxation factor the more stable the method, however, the number of required iterations increases dramatically (more than twice that of the highest relaxation factor in almost all the cases). A reasonable trade-off between stability of the method and the cost of computation was found to be a relaxation factor of 1.0.

Table 5.4 Convergence data for different Mach numbers and relaxation factors for the isothermal pipeline.

M2	Relaxation Factor			
	0.5	0.8	1	1.2
0.1	16	9	7	unstable
0.2	18	10	7	7
0.3	20	12	9	6
0.4	22	13	10	8
0.5	23	14	11	9
0.6	28	18	13	11
0.7	32	19	14	12

SUDDEN EXPANSION ELEMENT

This test case is aimed at demonstrating the algorithm's capability to, in addition to accurately describing compressible flow, model incompressible flow with the added complexity of a discontinuously varying duct cross section. For this purpose, the sudden expansion incompressible flow problem described by White [28] was modelled. A schematic of the test case is shown in Figure 5.10.

As shown, two reservoirs are connected by cast-iron pipes of varying diameters, which are joined abruptly, with sharp-edged entrance and exit. Including minor losses, the water flow rate is to be calculated if the surface of reservoir 1 is 13.716m higher than that of reservoir 2, which results in a pressure difference of 134.5 kPa.

The following properties for water at 20^{o}C are used:

Density = 999.8 kg/m^3

Viscosity = 0.001 kg/m.s

Using White [28], the following data for the pipes, entrance and exit is obtained.

Surface Roughness = 0.04572mm

Entrance Loss coefficient = 0.5

Exit loss coefficient	= 1
Lengths both	= 6.096m
Pipe diameters	= da = 0.0254m and db = 0.0508m

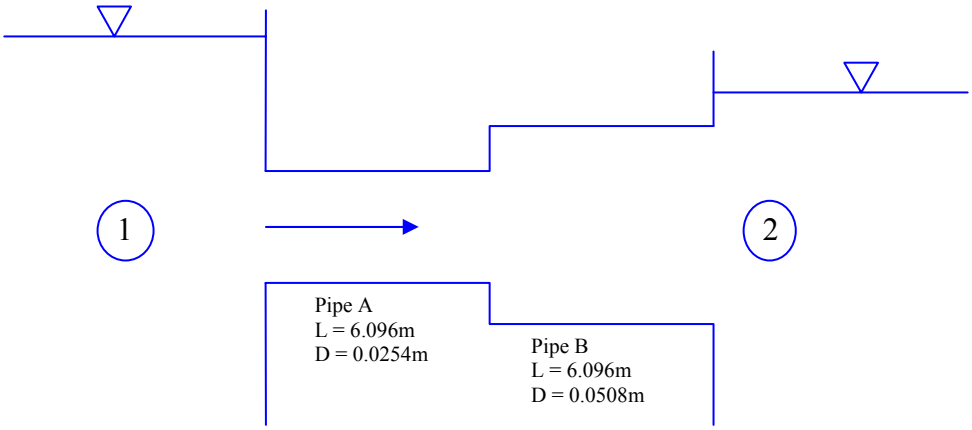

Figure 5.10 Textbook problem schematic

Figure 5.11 shows how the problem was modelled via the simulation package where element 1 = entrance, element 2 = pipe a, element 3 = sudden expansion, element 4 = pipe and element 5 = exit.

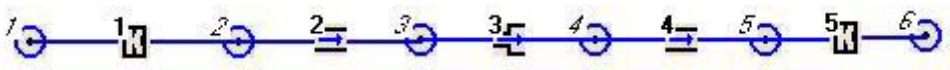

Figure 5.11 Sudden expansion model

The relaxation factor was set to 0.5 and the simulation package was set to use the density as a constant. The predicted flow was calculated as 0.003262 m^3/s, which is within three percent of the value published by White [28]. This result was obtained within 15 iterations as shown in the convergence plot (Figure 5.12). The capability of the proposed scheme to model incompressible flow over a sudden expansion is therefore demonstrated.

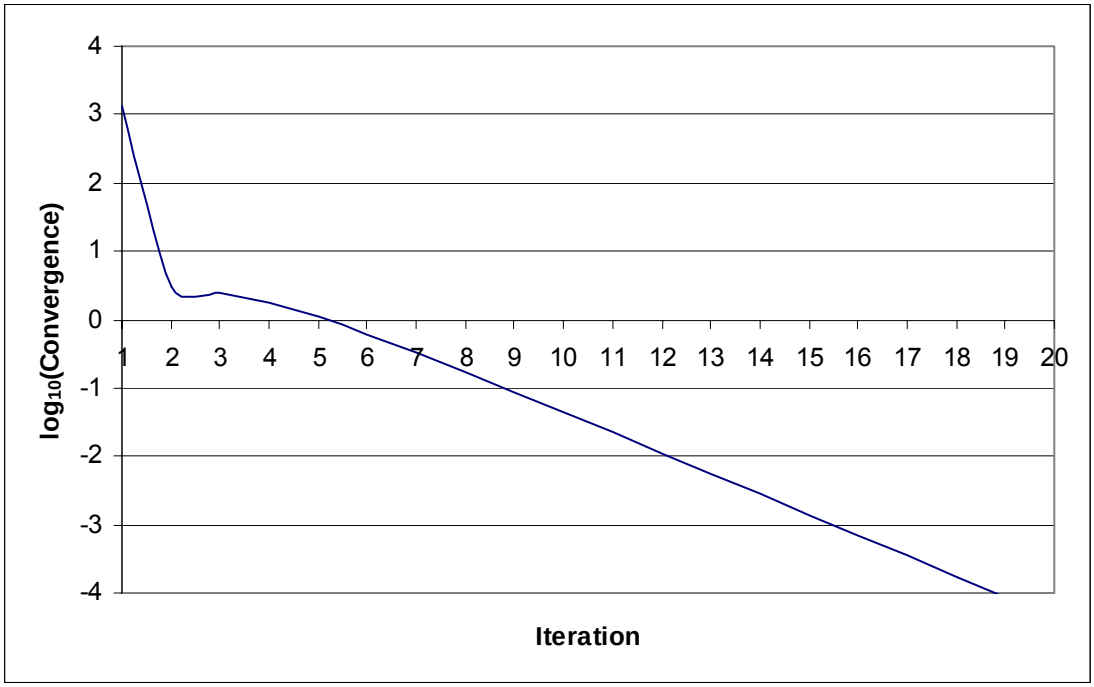

Figure 5.12 Convergence plot for the sudden expansion

LINER HOLE ELEMENT

The following test case was created to verify the network model's capability to simulate airflow through a liner hole element. The expression for a liner hole from Chapter 4 and the following data was used:

Mass flow = 0.05 kg/s

Density (air) = 1.22 kg/m^3

Diameter of the liner hole = 0.024495 m^2

Cd (plain holes) = 0.62

Substituting these values into the liner hole expression, a total pressure drop of

Δp_0 = 7.3889 kPa

was calculated, which will be used to validate the simulated pressure drop.

Figure 5.13 shows how the problem was modelled via the simulation package where element 1 = pipe, element 2 = liner hole and element 3 = pipe. The liner hole element is automatically handled by the simulation package. The pipe elements were made short ($L_1 = L_2 = 0.1$m) and a fixed friction of 0.01 to limit their influence on the final result.

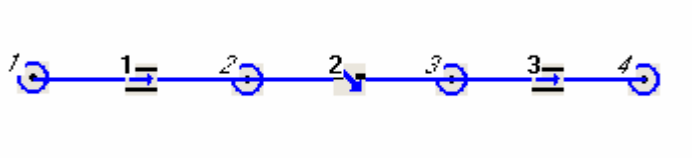

Figure 5.13 Liner hole model

The relaxation factor was set to 0.8. The problem converged and the pressure drop calculated in the simulation matched that of the above calculation very well. The pressure drop obtained from the simulation was

$$\Delta p_0 = 7.5781 - 0.18841 = 7.3896 \text{ kPa}$$

This result was obtained within 8 iterations as shown in the convergence plot (Figure 5.14). The capability of the simulation package to calculate flow over a liner hole is therefore demonstrated

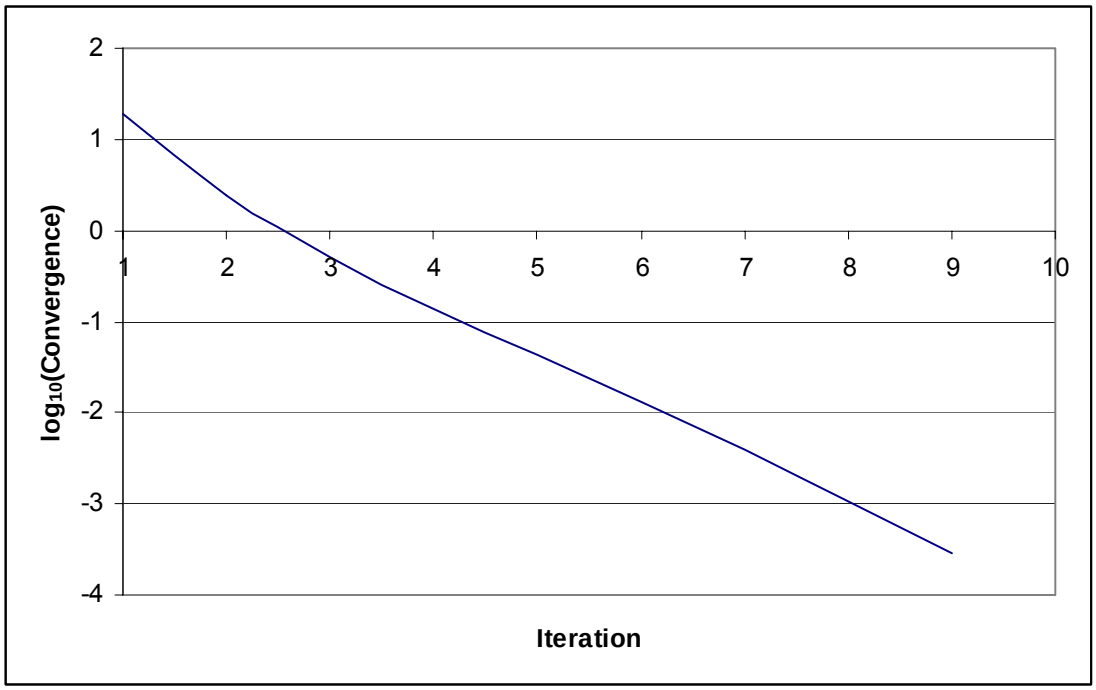

Figure 5.14 Convergence plot for the liner hole

5.4 Closure

The modular user-interface of a developed pipe-network flow simulation package was detailed. The accuracy and performance of the simulation package was validated through several benchmark problems. The proposed methodology's ability to accurately model both fully compressible and incompressible flow was demonstrated. In the case of the latter, a variable area element was also successfully dealt with. This methodology was also found to yield similar or improved results as compared to that of other methods. Convergence performance was also found to be similar to other techniques.

Chapter 6

Applications

*Chapter 6 describes the a**pplication** of the network model to a gas turbine combustor and a turbine blade, and discusses the results that were obtained.*

6.1 Preamble

The literature survey shown that in the preliminary design phase, there is a need to simulate flows in gas turbine combustors in a more efficient and simplified manner. A pipe network model therefore may prove to be helpful in addressing this need because the network model is able to link the different flow paths to one another easily. In the previous chapters a network methodology has been proposed which is able to solve a range of flow problems including flow through liner holes. The proposed model was validated against published networks and a basis for accuracy was established. In this chapter the proposed network model is used to simulate the flow splits through a research combustor.

6.2 Research combustor

Figure 6.1 shows a single can research combustor with a reference length (L_{ref}) and diameter (D_{ref}) of 174.8 mm and 88.4 mm respectively. This combustor has been analysed in various research studies, and details may be found in the references [39-42]. The combustor is made of stainless steel and coated with thermal barrier coating on the inside of the liner. There are three distinct zones into which the combustor can be divided namely, the primary, secondary and dilution zones. Six jets are located in the primary zone, twelve jets in the secondary zone and ten jets in the dilution zone. Film-cooling air is injected into the secondary and dilution zones by means of stacked rings with 40 entry holes.

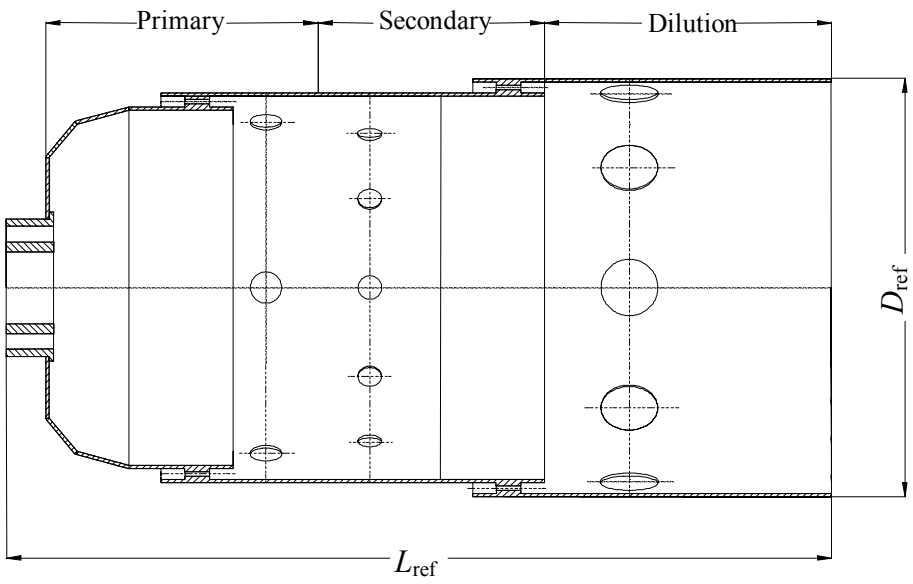

Figure 6.1 The single can research combustor

The research combustor is geometrically representative of practical combustors, and was designed to operate with a mass flow rate of 0.1 kg/s. The combustor was tested at atmospheric conditions, and an overall pressure drop of 1.94 kPa across the combustor was measured [40].

Table 6.1 The experimental isothermal mass flow splits of a research combustor [41]

Hole type	Ag [mm^2]	% Mass flow
Swirler	184.19	8.35
Primary	205.27	12.50
Secondary	235.62	15.26
Dilution	1084.34	60.52
Cooling 1	25.45	1.73
Cooling 2	25.45	1.74

This pressure drop represents a pressure change of 2.45 percent, which is well within the 5 percent range of practical combustors. The various flow splits in the combustor, i.e. the swirler, primary, secondary, dilution jets and cooling air flows, are obtained experimentally during isothermal conditions and are summarised with the geometrical areas in Table 6.1

The combustor chamber is modelled in 2D due to the current interface of the simulation package. Note that every flow path may be simulated individually which will require a more advanced program interface. The holes for the air jets in the primary, secondary and dilution zones therefore have to be reduced to two inlet holes in each zone (Figure 6.2). The appropriate hole area in 2D for a specific zone is then calculated by dividing the sum of the areas of all the holes by two. The same strategy is used to take the cooling airflow into account.

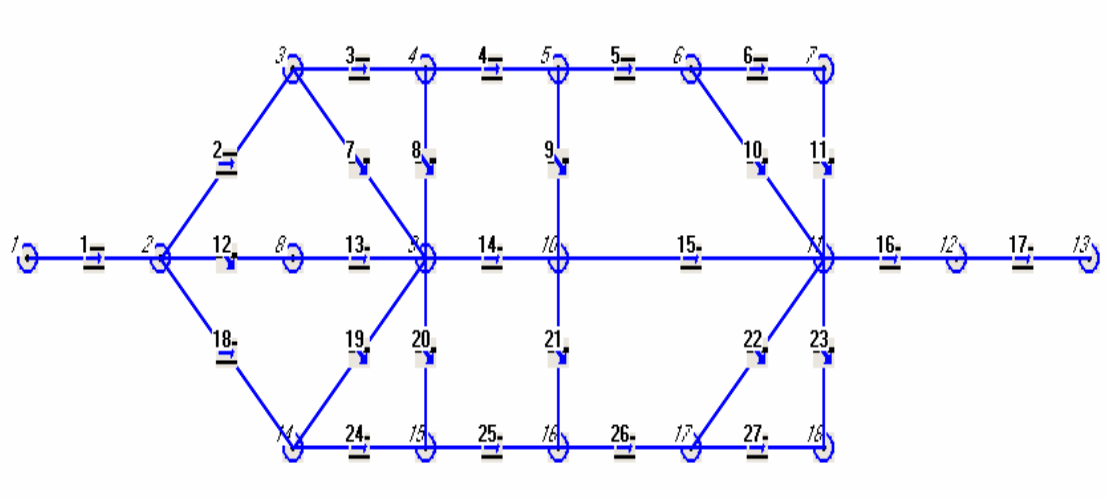

Figure 6.2 The 2D network representation of the research combustor

Each flow path in the combustor chamber is represented by an element with specific properties, and these elements are connected via nodes placed on specific points. The properties related to each element include flow, density, and friction as in normal duct segments. Table 6.2 explains the different elements and supplies the elemental data. The nodes contain the massflow, pressure and temperature information.

Table 6.2 The elemental data table

Element(s)	Representation	Total area [mm^2]	Effective area/ element [mm^2]	Effective diameter/ element [m]	Loss type	Loss value	Length [m]
1	Inlet annulus	31415.93	31415.93	0.200000	Friction	-	0.1000
2, 18	Contracting section	27878.00	13939.00	0.133200	Friction	-	0.0237
3, 24	Annulus C1	26275.64	13137.82	0.129300	Friction	-	0.0220
4, 25	Annulus P	26275.64	13137.82	0.129300	Friction	-	0.0220
5, 26	Annulus S	26275.64	13137.82	0.129300	Friction	-	0.0220
6, 27	Annulus C2	25566.52	12783.26	0.127600	Friction	-	0.0338
7, 19	Cooling ring 1	25.45	12.725	0.004025	Cd	0.80	-
8, 20	Primary holes	205.27	102.64	0.011430	Cd	0.73	-
9, 21	Secondary holes	235.62	117.81	0.012250	Cd	0.76	-
10, 22	Cooling ring 2	25.45	12.725	0.004025	Cd	0.80	-
11, 23	Dilution holes	1130.97	565.49	0.026830	Cd	0.68	-
12	Swirler	184.19	184.19	0.015310	Cd	0.54	-
13	Swirl chamber	4476.97	4476.97	0.075500	Friction	-	0.0457
14	Primary zone	5140.28	5140.28	0.080900	Friction	-	0.0220
15	Secondary zone	5140.28	5140.28	0.080900	Friction	-	0.0558
16	Dilution zone	5849.40	5849.40	0.086300	Friction	-	0.0437
17	Outlet	9852.03	9852.03	0.11200	Friction	-	0.3000

In this cold flow simulation of the combustor the air was allowed to flow freely through the combustor. This is necessary to see how the network model picks up the flow splits. The annulus area around the liner wall was modelled as a series of elements connected to one another. Nodes were placed at positions where air had to go through the different zones and cooling channels.

An inlet mass-flow of 0.1 kg/s and an outlet pressure of 101.32 kPa were specified at node 1 and node 14 respectively. A fixed temperature field of 288 K at all nodes was specified. Every element was constructed with the data found in Table 6.2. The discharge coefficients that were used originate from the experimental data compiled by Turck and Van Niekerk [40 - 42].

The results from the network model were compiled as percentages of the total mass flow (See Table 6.3), enabling a comparison to the measurements in Table 6.1. The network simulation converged in 18 iterations using a relaxation factor of 0.5. The pressure drop over the combustor chamber was calculated as 3.2 kPa.

A 3-D CFD model of the research combustor was obtained from a previous study [40]. The CFD analysis is conducted to obtain a second set of data for verification purposes. The inputs to this analysis are an inlet mass-flow boundary of 0.1 kg/s and an outlet pressure boundary of 101.3 kPa. The results obtained by the CFD model were converted to the same format as Table 6.1. The mass-flows through the holes in the various zones were all added together to give the total mass-flow in each zone. Because the total mass-flow is known, these mass-flows can be expressed as a percentage of the total mass-flow. The CFD analysis is now readily comparable with that of the network analysis and the experimental data.

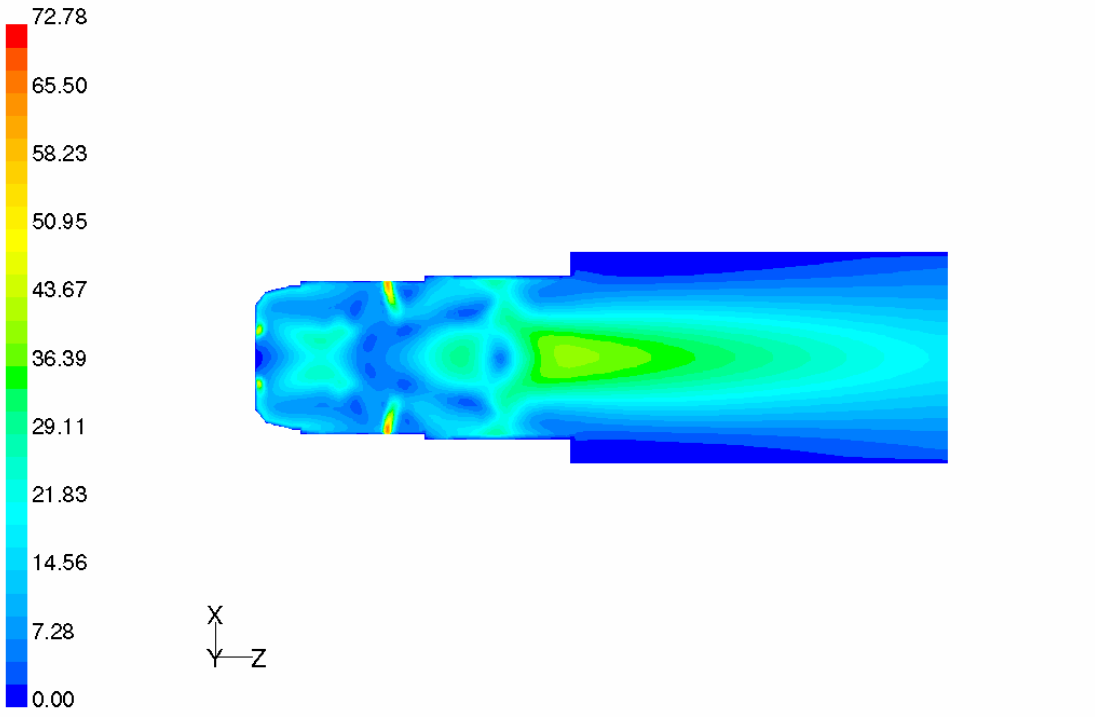

Figure 6.3 A plane view of cold air velocity [m/s] through the combustor

The results obtained with the CFD model are shown in table 6.3 and compares acceptably with experimental data [41 (Table 6.1), although differences in the flow as a percentage of the total mass-flow were observed. A pressure drop of 2.8 kPa is calculated from this analysis. Figure 6.3 shows the results of the CFD simulation of the combustor during cold flow operation. Table 6.3 gives the results obtained by the simulations.

Table 6.3 Numerical results of the network model and CFD simulations for cold flow operation

	Mass flow [kg/s]	Area [mm^2]	% Mass flow
Network model:			
Swirler	0.00803	184.19	7.96
Primary	0.01300	205.27	12.88
Secondary	0.01447	235.62	14.34
Dilution	0.06212	1130.97	61.56
Cooling 1	0.001644	25.45	1.63
Cooling 2	0.001644	25.45	1.63
CFD model:			
Swirler	0.00744	184.19	7.44
Primary	0.01086	205.27	10.86
Secondary	0.01274	235.62	12.74
Dilution	0.06549	1130.97	65.5
Cooling 1	0.00173	25.45	1.73
Cooling 2	0.00173	25.45	1.73

Evaluation

From the results it is evident that the network model solves the flows and the flow splits in the combustor adequately. The pressure drop over the combustor of 3.2 kPa is calculated with the network model, which is 10% higher than that of the CFD results. Both these values are higher than the experimental pressure drop of 1.94 kPa and may be explained by the fact that the pressure measurement was not taken at sea level while the simulations were conducted at sea level. In comparison to the experimental data given in Table 6.1, the network model yielded results quite close to the measured isothermal mass-flow values. In comparison to the CFD data, the network model calculated the flow split adequately, although differences in the primary, secondary zones are more significant compared to the experimental data. Reasons for these deviations may result from an incorrect specification of the surface roughness coefficient, which leads to an incorrectly calculated frictional loss coefficient. This may result in an decreased loss coefficient that will decrease the flow resistance in a particular element, allowing more flow through the element. Therefore the accurate specification and use of the friction factor is of importance in the numerical model.

In another observation of the primary and secondary zones, the network model predicted approximately 2 percent more mass-flow than the CFD model, while the mass-flow in the dilution zone was under-predicted by approximately 4 percent. This raises questions about the accuracy of the discharge coefficients as supplied by the references [41, 42]. It may be concluded that the results of the network model are bound to agree with the experimental measurements because the values used for the discharge coefficients (C_D) in the network model are the same as those determined experimentally. Using the mass flow splits from the CFD analysis one may estimate the value for the discharge coefficient which was found to be approximately 0.64 which is close to the limit value of 0.62 as explained by Levebre [23]. One may therefore conclude that the discharge values for the liner holes supplied by Turck [41] are erroneous. This explains the difference in mass flow between the CFD analysis and the measured mass flows. The discharge coefficient should therefore be applied with caution. A better remedy would be to calculate the discharge coefficients

empirically, if possible, to avoid inaccuracies as a result of inaccurate C_D values. In conclusion, the network model showed remarkable promise in adequately simulating difficult geometries, such as gas turbine combustors.

6.3 Closure

Gas flow and gas flow-splits in a gas turbine combustor were simulated. The combustion chamber of a research combustor was simulated using the proposed network methodology derived previously and also with a commercial CFD solver. The network simulation gave comparable results in comparison to the measured data and the CFD results. The promise of the gas network approach as a very useful preliminary design tool was illustrated.

CHAPTER 7

Conclusions and Recommendations

The ***conclusion*** *summarises the achievements and limitations of the proposed pipe network methodology. Recommendations are made for further work.*

7.1 Summary

The preliminary design of a gas turbine combustor is a tedious task and normally requires the use of simplified semi-empirical models during the initial design phase. When different configurations and new technological designs are required that differ significantly from proven concepts, these empirical procedures prove to be extremely limited. The requirement therefore, was identified for an improved empirical model that can be used for the initial overall geometrical design of gas turbine combustors account for the effect that the different zone layouts will have on each another.

The general governing equations of fluid flow were presented, as well as the derivation thereof for three dimensions. These equations were subsequently reduced to their one-dimensional strong form to describe both steady compressible and incompressible flow. A flow network discretization strategy was discussed and a flow network example using the nodal technique considered. A network simulation methodology, which solves a single set of equations for both compressible and incompressible flows or flows with significant dynamic pressure fluctuations across the elements, was constructed. The resulting set of governing equations are further applicable to pipe elements with large area changes in the case of incompressible flow. The formulation allowed for combustor type components to be modelled as an element in the network. This work constituted the first phase in the development of a network simulation technology for application to gas-turbine combustors, and was therefore limited to isothermal flow.

The proposed network method is implemented into a *Windows* based simulation package with a user interface. The ability of the proposed method to accurately model both compressible and incompressible flow is demonstrated through the analysis of a number of benchmark problems. It was shown that the proposed methodology yields similar or improved results as compared to that of others. The proposed method is applied to a research combustor to solve for isothermal flows and flow splits.

7.2 Contributions and conclusions

The following contributions were made in this study:

- A single equation set network simulation model able to describe both steady incompressible and compressible flow where the dynamic pressure component is fully taken in consideration was developed.

- The model was shown to be able to compute compressible flows at Mach numbers up to 0.7 for constant area cross sectional pipe accurately with an analysis time of a few seconds.

- The proposed model was further able to compute flows through geometrically complex variable cross-sectional area elements, such as sudden expansions, for incompressible flows as well as flows through liner holes

- For validation purposes, the proposed methodology was applied to a number of benchmark problems. It was found to yield similar or improved solutions as compared to that of other work. Convergence performance was found to be similar.

- Elements where the friction factor is highly flow dependant was solved efficiently due to the fact that such flow related non-linearities was properly treated in the methodology. When the friction factor was taken as a function of the flow when constructing the pressure correction matrix (i.e. $df/dQ \neq 0$) a notable improved convergence characteristic in terms of the number of iterations was observed while retaining the accuracy of the solution. Only 7 iterations were needed to reach convergence in comparison to the 11 iterations where the friction was kept constant.

- The developed methodology was applied to model flow trough a research combustor. Isothermal flow and flow splits were successfully calculated and the

predicted flows were in relative close agreement to measured data as well as detailed CFD analysis.

Finally, following is a summary of non-numerical technology related insights gained from this study:

- The developed user interface of the simulation package makes it possible for the user to set up a problem with ease, and the solution methodology furnishes a solution in a few seconds.
- Use of the network approach to solve physical problems one-dimensionally proved to be a very helpful tool indeed. Difficult and complex geometries can be modelled with ease. It takes very little time to obtain a converged solution; therefore computing costs are reduced and numerous design iterations may be performed quickly.
- The accuracy of the solution to a particular problem using the network approach depends on various factors. Firstly, accuracy depends on how well the initial problem is represented geometrically by the network approach (i.e., typically, the more elements used the more accurate the solution). Secondly, the accuracy of the solution is influenced by empirical relationships such as flow friction factors.

7.3 Recommendations for further work

A methodology for the simulation of combustor flow problems, which may be represented by a pipe network, has been developed successfully. The following recommendations for further work are made to further this design tool:

- The ability of the network methodology can be greatly enhanced by deriving a simulation network model for compressible flow in pipes with variable flow cross sectional area.
- The ability of the network methodology may be extended by adding the energy equation to the methodology. The three methods of heat transfer which are prevalent in gas turbine combustors are conduction, convection and radiation. In

the simulation of the hot flows in combustors, all three modes of heat transfer will have to be considered.

- The development of new elements that describes other flow processes (e.g. pumps) will enhance the functionality of the network approach making it a more general and versatile as a design tool. However, the accuracy of the network method will depend on how accurate the derived formulation describes the physical process of that particular element.

- During the course of this study, a program that solves the combustor flows one-dimensionally was encountered. The program, HoleFlow, developed by Dr. J.E. van Niekerk [42], uses the flow split loss coefficients of the combustor as inputs, among others, to calculate the performance, flows and temperatures of the combustor. This program and the network model may be integrated in such a way that the network model provides the flow splits while HoleFlow acts as the energy equation to the network model.

- The program created in this study is limited to a few hundred nodes and branches. Possible code improvements include dynamic allocation of memory so that any number of nodes and elements may be used. An extended database for different fluids or gases is also advisable, as well as a database for the different element types if the program is to be commercially viable.

Nomenclature

Symbols

A	Flow coefficient matrix
$A_{i,j}$	$1/(2 R T_{i,j})$
$b_{i,j}$	Element associated with node i and branch j
B	Element connectivity matrix
c_f	Friction coefficient
d_i	External mass flow into the node i
D	Hydraulic diameter
E	Total number of elements
$f(Q)$	Function in terms of the flow (used in the pressure drop eq.)
F	First order derivative of f in terms of the flow
$g(\rho)$	Function in terms of the density (used in the pressure drop eq.)
G	First order derivative of g in terms of the density
h_c	Heat transfer coefficient
h_i	Mass flow error in node i
$H_{i,j}$	Flow direction correction factor
i	Node number
I	Total number of nodes
j	Element number
J	Total number of elements connecting to a node
L	Element length
$\dot{m}$	Mass flow rate
$n_{i,j}$	Node associated with node i and branch j
N	Node connectivity matrix
p	Static pressure

p_0	Total pressure
Q	Flow or heat transfer
R	Gas constant
$s_{i,j}$	Flow direction factor
T_a	Nodal temperature
$T_{i,j}$	Elemental temperature
T_g	Average gas temperature

Greek Symbols

∂	Partial differential operator
Δ	Delta, a difference
ε	Convergence parameter
Σ	Summation of specific terms
λ	Effectiveness

Subscripts

i,j	Quantities that apply to $e_{i,j}$
a	a = { i or j }

References

[1] Holdeman, J.D., Mongia, H.C., Mularz, E.J., *Assesment, development and application of combustor aerothermal models,* 33rd Int. Gas Turbine and Aeroengine Congress and Exposition, Amsterdam, 1988.

[2] Mongia, H.C., Reynolds, R.S., Srinivasan, R., *Multidimensional gas turbine combustion modelling: Applications and limitations,* AIAA Journal, Vol. 24, No.6, pp. 890-904, 1986.

[3] Hammond D.C., Mellor, A.M., *A prelimary investigation of gas turbine combustor modelling,* Combustion Science and Technology, Vol. 2, pp 67-80, 1970.

[4] Mellor, A.M., Fritsky, K.J., *Turbine combustor preliminary design approach,* Journal of Propulsion and Power, Vol. 6, no. 3, pp. 334-343, 1990.

[5] Burrus, D.L., Shyy, W., Braaten, M.E., *Numerical model for analytical predictions of combustor aerothermal performance characteristics*, APGARD CP 422, USA, 1987.

[6] Mellor, A.M., *Design of modern turbine combustors*, Academic Press, USA, 1990.

[7] Osiadacz, A.J., *Simulation and analysis of gas networks*, J.W. Arrowsmith Ltd., Bristol, 1987.

[8] Greyvenstein, G.P., Laurie, D.P., *A segregated CFD approach to pipe network analysis*, Int. J for Numerical Methods in Engineering, Vol. 37, pp. 3685-3705, 1994.

[9] Potter. M.C., Wiggert, D.C., *Mechanics of fluids*, Prentice-Hall International Editions, New Jersey, 1991.

[10] Osiadacz, A.J., Pienkosz, K., *Methods of steady-state simulation for gas networks*, Int. J. Systems SCI, Vol. 19, No. 7, pp. 1311-1321, 1988.

[11] Osiadacz, A.J., *Methods of steady state simulation of a gas network*, Int. J. Systems SCI, Vol. 19, No. 11, pp. 2395-2405, 1988.

[12] Osiadacz, A.J., Bell, D.J., *Dynamic simulation of gas networks by decomposistion and coordination*, Math. Engng. Ind., Vol. 5, No. 3, pp. 235-254, 1995.

[13] Goldfinch, M.C., *Microcomputers simulate natural gas networks*, Oil and Gas Journal, pp. 180-184, Sept. 1984.

[14] Thorley, A.R.D., Tiley, C.H., *Unsteady and Transient flow of compressible fluids in pipelines – a review of theoretical and some experimental studies*, Int. J. of Heat and Fluid Flow, Vol. 8, Issue 1, pp. 3 – 15, March 1987.

[15] Pretorius, J.J., *Gas network analysis including heat transfer*, Presentation at the Armscor RIMC Meeting, Durban, August 2001.

[16] Osiadacz, A.J., Pienkosz, K., *Analysis of loop methods for simulating gas networks*, Computer methods in applied mechanics and engineering, Vol. 65, pp. 201 - 213, 1987.

[17] Logan, D.L., *A first course in the finite element method - Second edition*, PWS Publishing Company, Boston, 1993.

[18] Patankar, S.V., *Numerical heat transfer and fluid flow*, Hemisphere Publishing Co., Washington D.C., 1980.

[19] Greyvenstein, G.P., Meyer, J.P., *Differencing of density in a compressible flow for a pressure-based approach*, AIAA Journal, Vol. 32, No. 3, pp. 659-661, 1993.

[20] Greyvenstein, G.P., *An implicit method for the analysis of transient flows in pipe networks*, Int. J for Numerical Methods in Engineering, Vol. 53, pp. 1127-1143, 2002.

[21] Stuttaford, P.J., Rubini, P.A., *Prelimanary gas turbine combustor design using a network approach,* Transactions of ASME, Paper no. 96-GT-135, 1996.

[22] Harman, R.T.C., *Gas turbine engineering*, MacMillan Press Ltd., London, 1981.

[23] Lefebvre, A.H., *Gas turbine combustion*, Hemisphere Publishing Corporation, New York, 1983.

[24] Northern Research and Engineering Corporation (NREC), *The design and development of gas turbine combustors*, Vol. 2, Woburn, MA,USA, 1980.

[25] Adkins, R.C., Gueroui, D., *An improved method for accurate prediction od mass flow through combustor liner holes*, ASME paper 86-GT-149, Jnl. of Engineering for Gas Turbines and Power, Vol. 108, pp. 491-497, July 1986.

[26] Zuchrow, M.J., Hoffman, J.D., *Gas Dynamics*, Vol. 1, John Wiley & Sons, New York, 1991.

[27] Emanuel, G., *Gas dynamics: Theory and Applications*, AIAA, New York, 1986.

[28] White, F.M., *Fluid Mechanics -Second Edition*, McGraw-Hill Inc., New York, 1986.

[29] White, F.M., *Viscous Fluid Flow - Second Edition*, McGraw-Hill, Inc., New York, 1991.

[30] Janna, W.S., *Introduction to Fluid Mechanics – Third Edition*, PWS Publishing Company, Boston, 1993.

[31] Saad, M.A., *Compressible fluid flow*, Prentice Hall Inc., New Jersey, 1985.

[32] Mills, A.F., *Basic Heat and Mass Transfer*, Richard D. Irwin, Inc., 1995.

[33] George, A., Liu, J.W., *Computer solution of Large Sparse Positive Definite Systems*, Prentice-Hall Inc., New Jersey, 1981.

[34] Patankar, S.V., Spalding, D.B., *A calculation procedure for heat mass and momentum transfer in three dimensional parabolic flows*, Int. J. Heat and Mass Transfer, Vol. 15, pp. 1787-1806, 1970.

[35] Osiadacz, A.J., *Comparison of numerical methods for steady-state simulation for gas networks*, Civ. Eng. Syst., Vol. 5, pp. 25-30, March 1988.

[36] Burden, R.L., Faires, J.D., *Numerical Analysis, Sixth Edition*, Brooks/Cole Publishing Company, California, 1997.

[37] Duff, I.S., Erisman, A.M., Reid, J.K., *Direct Methods for Sparse Matrices*, Oxford, 1986.

[38] Kraus, A.D., *Matrices for Engineers*, Hemisphere Publishing Corporation, Washington, 1987.

[39] Rahman, F., *The numerical simulation of turbine blade cooling*, Bachelors Dissertation, University of Pretoria, 2000.

[40] Morris, R.M., *An experimental and numerical investigation of a gas turbine research combustor*, Masters Dissertation, University of Pretoria, March 2000.

[41] Turck, W.A., *BVM verbrandingstegnologie ontwikkeling: Isotermiese meetings*, 94TFD087, 1995.

[42] Van Niekerk, J.E., *Extended one-dimensional computer flow distribution model: HOLEFLOW V2.0*, PTE/00/018, 2000.

[43] Hicks, R.A., Wilson, C.W., *Comparison between measured and predicted wall temperatures in a gas turbine combustor,* Transactions of ASME, Paper no. 99-GT-59, 1999.

Appendices

Appendix A.

A DETAILED DERIVATION OF THE GENERAL FLOW EQUATIONS.

The derivations of the governing equations, both in integral form or in differential form, can be found in several texts [33, 50-55] and will be conveniently presented here.

The continuity equation

In the absence of nuclear and relativity effects, the mass of a system is a constant according to the law of the conservation of mass.

$$(Mass)_{System} = const \tag{A.1}$$

Applied to a control volume in the absence of nuclear and relativity effects, the integral form for the continuity equation becomes,

$$\int_{\upsilon} \frac{\partial \rho}{\partial t} d\upsilon + \int_{A} \rho \mathbf{V} \cdot (dA) = 0 \tag{A.2}$$

which describes the rate at which mass accumulates within the control volume υ is equal to the rate at which mass is leaving the control volume υ through a control surface A. The first term is omitted when working with steady flows. When multidimentional flows are considered, the differential form for the continuity equation, valid for control volumes, is needed. The derivation of the continuity equation into its differential form may be conducted through two approaches. The first approach uses the divergence theorem while the second applies the integral equation on a control volume of differential size. The result of both approaches yield the differential equation for continuity as

$$\frac{\partial \rho}{\partial t} + \nabla \cdot (\rho \mathbf{V}) = 0 \tag{A.3}$$

The momentum equations

The momentum equations are the equations obtained when Newton's second law of motion is applied to fluid flow through a control volume. For a system of fluid particles, Newton's second law of motion is

$$\mathbf{F}_{external} = \frac{d\mathbf{M}}{dt} \tag{A.4}$$

which results in

$$\mathbf{F}_{external} = \int_{\upsilon} \frac{\partial \rho \mathbf{V}}{\partial t} d\upsilon + \int_{A} \mathbf{V} (\rho \mathbf{V} \cdot d\mathbf{A}) \tag{A.5}$$

The external force $\mathbf{F}_{external}$ is the sum of a body force and a surface force. The body force **B**, is a force that acts upon the entire mass of the fluid, e.g., gravity, electrical and magnetic forces on a charged fluid. The surface force is a force that acts on the boundaries of the system through their contact with the surroundings. It consists of a normal component and a tangential component where the latter is referred to as the shear force which equals zero when working with an inviscid fluid. The normal force is caused by pressure for an inviscid fluid but also contains the effects of shear when working with a viscous fluid. Mathematically it becomes

$$\mathbf{F}_{external} = \int_{\upsilon} \mathbf{B} \rho d\upsilon - \int_{A} p d\mathbf{A} + \mathbf{F}_{\mathbf{shear}} \tag{A.6}$$

Therefore, by equating the equations A.5 and A.6 and retaining the surface forces in the form of $\mathbf{F}_{\mathbf{surface}}$, one arrive at the integral form of the momentum equations

$$\int_{\upsilon} \mathbf{B}\rho d\upsilon + \mathbf{F}_{\text{surface}} = \int_{\upsilon} \frac{\partial \rho \mathbf{V}}{\partial t} d\upsilon + \int_{A} \mathbf{V}(\rho \mathbf{V} \cdot d\mathbf{A}) \qquad \text{(A.7)}$$

In its differential form, the momentum equations are also known as the Navier-Stokes equations. By yet again employing either one of the two transformation approaches mentioned, the differential form of the momentum equations results in

$$\rho \frac{D\mathbf{V}}{Dt} + \nabla p - \rho \mathbf{B} - d\mathbf{F}_{\text{shear}} = 0 \qquad \text{(A.7)}$$

for an inviscid or viscous fluid in a state of uniform motion. However, it would be appropriate to note that arriving at this equation is not as straightforward as it seems to be. Equation A.7 may also be simplified for flows with a constant average viscosity and/or for incompressible flows.

The energy equation

The energy equation is derived from the first law of thermodynamics, which is also referred to as the law of energy conservation. In essence, it is the change in the stored energy in a system that is equal to the amount of heat energy transferred into the system less the amount of work energy done by the system.

$$dE = \delta Q - \delta W \qquad \text{(A.8)}$$

In terms of rate and employing the substantial derivative for the stored energy, the stored energy for a control volume may be expressed as

$$\frac{DE}{Dt} = \int_{\upsilon} \frac{\partial}{\partial t}\left[\rho\left(u + \frac{V^2}{2} + gz\right)\right] d\upsilon + \int_{A}\left[u + \frac{V^2}{2} + gz\right](\rho \mathbf{V} \cdot d\mathbf{A}) \qquad \text{(A.9)}$$

The heat transported to the control volume occurs by means of the three main heat transport modes: conduction, convection and radiation, and is regarded as positive. Usually the application determines the transport mode or modes. Furthermore, the

work done by the control volume consists out of shaft work $\mathbf{W_{shaft}}$ (work done by a rotary shaft crossing the system boundary, e.g., compressors),
flow work $\mathbf{W_{shear}}$ (work done by shear stress within the fluid) and pressure work given by

$$\dot{W}_n = \int_A pv(\rho \mathbf{V} \cdot d\mathbf{A}) \qquad \text{(A.10)}$$

By combining equations A.9 and A.10, establishes the integral form of the energy equation for a control volume

$$\dot{W}_{shaft} + \dot{W}_{shear} - \dot{Q} + \int_{\upsilon} \frac{\partial}{\partial t}\left[\rho\left(u + \frac{V^2}{2} + gz\right)\right] d\upsilon + \int_A \left[h + \frac{V^2}{2} + gz\right](\rho \mathbf{V} \cdot d\mathbf{A}) = 0 \qquad \text{(A.11)}$$

This integral form may be converted to the differential form by the use of the two approaches mentioned, which results in

$$\delta\dot{W}_{shaft} + \delta\dot{W}_{shear} - \delta\dot{Q} + \rho\frac{D}{Dt}\left[h + \frac{V^2}{2} + gz\right] - \frac{\partial p}{\partial t} = 0 \qquad \text{(A.12)}$$

The derivation of the energy equation concludes the derivation of the governing equations for compressible fluid flow needed in this research. The derivation of the remaining equations may be found in the texts mentioned in the beginning of this section. The governing equations of compressible fluid flow are highly non-linear and general solutions thereof are, for all practical circumstances, nonexistent.

Appendix B.

FULL DERIVATION OF THE PRESSURE EQUATION.

Following Patankar, the corrected values are calculated adding a correction value to the guessed or predicted values using the following relationships:

$$p = p^* + p' \tag{C.1}$$

$$Q = Q^* + Q' \tag{C.2}$$

$$\rho = \rho^* + \rho' \tag{C.3}$$

Form continuity,

$$\sum_{j=1}^{J} s_{i,j}\rho_{i,j}Q_{i,j} = -d_i \tag{C.4}$$

where, $i = 1,2,\ldots,i$

$$s_{i,j} = \begin{bmatrix} 1 & \text{if} \quad b_{i,j} > 0 \\ -1 & \text{if} \quad b_{i,j} < 0 \end{bmatrix}$$

d_i = external mass flow into the node.

Substituting eq. 1,2,3 into eq. 4 yields,

$$\sum_{j=1}^{J} s_{i,j}\left(\rho^*_{i,j} + \rho'_{i,j}\right)\left(Q^*_{i,j} + Q'_{i,j}\right) = -d_i$$

and rewriting results in

$$\sum_{j=1}^{J}\left(\rho^*_{i,j}Q^*_{i,j} + \rho^*_{i,j}Q'_{i,j} + \rho'_{i,j}Q^*_{i,j} + \rho'_{i,j}Q'_{i,j}\right)s_{i,j} = -d_i \tag{C.5}$$

The term $\rho'_{i,j}Q'_{i,j}$ may be omitted because of the fact that both ρ' and Q' becomes zero near convergence. Therefore the accuracy will also not be affected. To continue the derivation of the pressure correction, the relationship between the pressure correction and the flow correction must be determined using the pressure drop – flow rate relationship.

The general form of the pressure drop – flow rate relationship is,

$$\Delta p_{i,j} = p_{n_{i,j}} - p_i = s_{i,j}H_{i,j}g_{i,j}f_{i,j} \tag{C.6}$$

where,

$$H_{i,j} = \frac{Q_{i,j}}{|Q_{i,j}|}$$
$$g_{i,j} = g_{i,j}(\rho_{i,j})$$
$$f_{i,j} = f_{i,j}(|Q_{i,j}|)$$

To determine the relationship between the pressure correction and the flow correction, the pressure and flow terms is replaced with the correction terms (accented terms) and the pressure drop–flow equation (C.6) is differentiated with respect to the flow, which results in

$$\frac{\partial p'_{n_{i,j}}}{\partial Q'_{i,j}} - \frac{\partial p'_i}{\partial Q'_{i,j}} = s_{i,j} H_{i,j} f_{i,j} G_{i,j} \frac{\partial \rho'}{\partial Q'_{i,j}} + s_{i,j} g_{i,j} F_{i,j} \qquad \text{(C.7)}$$

where,

$$G_{i,j} = \frac{\partial g_{i,j}}{\partial \rho_{i,j}}$$
$$F_{i,j} = \frac{\partial f_{i,j}}{\partial |Q_{i,j}|}$$

Replacing the $\frac{\partial y'}{\partial X'}$ terms with $\frac{y'}{X'}$ terms (y and X is arbitary parameters) results in

$$\frac{p'_{n_{i,j}}}{Q'_{i,j}} - \frac{p'_i}{Q'_{i,j}} = s_{i,j} H_{i,j} f_{i,j} G_{i,j} \frac{\rho'}{Q'_{i,j}} + s_{i,j} g_{i,j} F_{i,j} \qquad \text{(C.8)}$$

Form the density,

$$\rho_{i,j} = \frac{p_i + p_{n_{i,j}}}{2RT_{i,j}} \qquad \text{(C.9)}$$

the density correction becomes

$$\rho'_{i,j} = \frac{p'_i + p'_{n_{i,j}}}{2RT_{i,j}} \qquad \text{(C.10)}$$

where, $T_{i,j}$ = temperature of the element.

Substituting eq. C.10 into eq. C.8 results in an expression for the flow correction in terms of the pressure correction

$$Q'_{i,j} = p'_{n_{i,j}}\left[\frac{1}{s_{i,j}g^*_{i,j}F^*_{i,j}} - \frac{a_{i,j}H_{i,j}f^*_{i,j}G^*_{i,j}}{g^*_{i,j}F^*_{i,j}}\right] - p'_i\left[\frac{1}{s_{i,j}g^*_{i,j}F^*_{i,j}} + \frac{a_{i,j}H_{i,j}f^*_{i,j}G^*_{i,j}}{g^*_{i,j}F^*_{i,j}}\right] \tag{C.11}$$

where,

$$a_{i,j} = \frac{1}{2RT_{i,j}}$$

Now one can continue to derive the pressure correction. Substituting eq. C.11, C.10 into eq. C.5 results in eq. C.12

$$\sum_{j=1}^{J} s_{i,j}\left(\begin{array}{l}\rho^*_{i,j}Q^*_{i,j} + a_{i,j}\left(p'_i + p'_{n_{i,j}}\right)Q^*_{i,j} + \\ \rho^*_{i,j}\left(\begin{array}{l}p'_{n_{i,j}}\left[\dfrac{1}{s_{i,j}g^*_{i,j}F^*_{i,j}} - \dfrac{a_{i,j}H_{i,j}f^*_{i,j}G^*_{i,j}}{g^*_{i,j}F^*_{i,j}}\right] - \\ p'_i\left[\dfrac{1}{s_{i,j}g^*_{i,j}F^*_{i,j}} + \dfrac{a_{i,j}H_{i,j}f^*_{i,j}G^*_{i,j}}{g^*_{i,j}F^*_{i,j}}\right]\end{array}\right)\end{array}\right) = -d_i \tag{C.12}$$

After a fair amount of algebraic manipulation, the pressure equation is derived as

$$p'_i = \frac{\left(\sum_{j=1}^{J}\left(c_{i,j}p'_{n_{i,j}}\right) + b_i\right)}{c_{i,i}} \tag{C.13}$$

where,

$$c_{i,i} = \sum_{j=1}^{J}\left(\frac{\rho^{*}_{i,j}}{g^{*}_{i,j}F^{*}_{i,j}} + s_{i,j}H_{i,j}a_{i,j}\left(\frac{\rho^{*}_{i,j}f^{*}_{i,j}G^{*}_{i,j}}{g^{*}_{i,j}F^{*}_{i,j}} - \left|Q^{*}_{i,j}\right|\right)\right)$$

$$c_{i,j} = \frac{\rho^{*}_{i,j}}{g^{*}_{i,j}F^{*}_{i,j}} - s_{i,j}H_{i,j}a_{i,j}\left(\frac{\rho^{*}_{i,j}f^{*}_{i,j}G^{*}_{i,j}}{g^{*}_{i,j}F^{*}_{i,j}} - \left|Q^{*}_{i,j}\right|\right)$$

$$b_i = d_i + \sum_{j=1}^{J}\left(\rho_{i,j}Q_{i,j}s_{i,j}\right)$$

with $i = 1,2,\ldots, I$

Appendix C.

SOLUTION METHODS FOR LINEAR SYSTEMS.

THE ENVELOPE METHOD.

In order to understand the envelope method, one firstly has to look at the band method. The task of the band method is to order the matrix in such a way that the non-zeros in $\boldsymbol{PAP}^T$ are collected near the main diagonal [34, (61)]. Although these orderings are often far from optimal, it is a reasonable compromise in a practical sense.

Letting **A** be a n x n symmetric positive definite matrix with the *i*th row of **A**, *i*=1,2,…,n.

$$f_i(\mathbf{A}) = \min \{\mathrm{j} \mid a_{ij} \neq 0\}$$

and

$$\beta_i(\mathbf{A}) = i - f_i(\mathbf{A})$$

Since the diagonal elements are larger than zero

$$f_i(\mathbf{A}) \leq i \quad \text{and} \quad \beta_i(\mathbf{A}) \geq 0$$

If the bandwidth of **A** is defined by

$$\beta_i(\mathbf{A}) = \max \{|\mathrm{i} - \mathrm{j}| \mid a_{ij} \neq 0\}$$

then $\beta_i(\mathbf{A})$ is the *i*th bandwidth of **A**. The band of **A** may then be defined as

$$Band(\mathbf{A}) = \max \{(i,j) \mid 0 < i - j \leq \beta_i(\mathbf{A})\}$$

Zeros outside the Band **A** are ignored and zeros inside the band are stored.

The envelope method is a more sophisticated method following the band method but with the ability to let the bandwidth vary. It is identical to the Gauss elimination method mathematically and without row interchanges, **A** maybe factored into

$$\mathbf{A} = \mathbf{LU}$$

where **L** is the lower triangular matrix and **U** the upper triangular matrix. The idea of the envelope method is to preserve all the leading zeros in a particular row of **A** in **L**. Therefore, only the elements between the first non-zero and the diagonal need to be considered. The envelope of **A** is defined as

$$Env(\mathbf{A}) = \{(i, j) | 0 < i - j \le \beta_i(\mathbf{A})\}$$

and the size of the envelope is defined as

$$|Env(\mathbf{A})| = \sum_{i=1}^{n} \beta_i(\mathbf{A})$$
$$Env(\mathbf{A}) = Env(\mathbf{L} + \mathbf{L}^{\mathrm{T}})$$

From the definitions of the band and the envelope one can see that they are equivalent. The envelope of matrix $\mathbf{PAP}^{\mathrm{T}}$ is illustrated in Figure D.1 below.

$$Env(PAP^T) = \begin{bmatrix} a_{11} & & & & & & & \\ a_{21} & a_{22} & & & & & & \\ 0 & 0 & a_{33} & & & & & \\ 0 & a_{42} & 0 & a_{44} & & & & \\ & a_{52} & a_{53} & 0 & a_{55} & & & \\ & & a_{63} & 0 & a_{65} & a_{66} & & \\ & & & 0 & a_{75} & a_{76} & a_{77} & \\ & & & & 0 & a_{76} & a_{87} & a_{88} \end{bmatrix}$$

Figure D.1 The envelope of matrix $\mathbf{PAP}^{\mathrm{T}}$

Appendix D.

In 1969, Cuthill and McKee developed an algorithm to reduce the bandwidth of a sparse symmetric matrix. It essentially reduces the bandwidth of the matrix via a local minimization of the computed bandwidths, β_is. Therefore the scheme may be used as a method to reduce the profile $\sum\beta_i$ of a matrix. In his studies of profile methods, George [33,37] discovered that reversing the Cuthill-McKee method was much better than the original method in terms of profile reduction, and named this the reversed Cuthill-McKee (RCM) ordering. Liu [33,37] later established that the method posed some disadvantages as far as envelope storage and envelope operation counts are concerned. Nevertheless, the method is very successful and is perhaps the most widely used profile-reduction ordering method. The method may be summarized as follows [8,33]

1. Start at any node, and find the node furthest removed from it (i.e. with the largest number of other nodes along the simplest path connecting these nodes). Repeat from the new node until the path lengths stop increasing. Choose the last of these nodes as number one. All other nodes remain unnumbered and unvisited.
2. Visit the lowest-numbered unvisited node as follows: order all the unnumbered neighbours of this node in increasing order of the number of elements attached to each node and give the next available numbers to these nodes. Repeat until all nodes are numbered.

Reverse the ordering (i.e. node one is now node number n while node n is now node number one. The number of nodes is, $n = 1,2,\ldots,n$)

Appendix E

Consider Equation (4.9) with assumptions as described in the text:

i.e. $$\sum_{j=1}^{J} s_{i,j}\left(\rho^{*}_{i,j}Q^{*}_{i,j} + \rho'_{i,j}Q^{*}_{i,j} + \rho^{*}_{i,j}Q'_{i,j}\right) = -d_i \qquad (4.3)$$

$\therefore$ $$\sum_{j=1}^{J} s_{i,j}\left(\rho^{*}_{i,j}Q'_{i,j} + \rho'_{i,j}Q^{*}_{i,j}\right) = -d_i - \rho^{*}_{i,j}Q^{*}_{i,j} = -b_i$$

$$\sum_{j=1}^{J} s_{i,j}\left(Term1 + Term2\right) = -b_i \qquad (A)$$

Consider Term1:

i.e. $$\sum_{j=1}^{J} s_{i,j}\left(\rho^{*}_{i,j}Q'_{i,j}\right)$$

An expression for $Q'_{i,j}$ in terms of p'_o is now needed. Utilizing Equation (4.34) such an expression may be derrived as follows. Consider Equation (4.34):

$$Q'_{i,j} = \frac{p'_{0j} - p'_{0i}}{s_{i,j}H_{i,j}\left(2Q_{i,j}\varphi + Q^{2}_{i,j}\dfrac{\partial\varphi}{\partial Q_{i,j}}\right)} \qquad (4.34)$$

Group terms and create a new term η such that

$$\eta = H_{i,j}\left(2Q^{*}{}_{i,j}\varphi + Q^{*2}{}_{i,j}\frac{\partial\varphi}{\partial Q^{*}{}_{i,j}}\right)$$

Therefore Equation (4.34) becomes

$$Q'_{i,j} = \frac{p'_{0j} - p'_{0i}}{s_{i,j}\eta}$$

Substitute the expression above into Term1

$\therefore$ $$\sum_{j=1}^{J} s_{i,j}\left(\rho^{*}_{i,j}Q'_{i,j}\right) = \sum_{j=1}^{J} s_{i,j}\rho^{*}_{i,j}\frac{p'_{0j} - p'_{0i}}{\eta} \qquad (B)$$

Consider Term2:

i.e. $$\sum_{j=1}^{J} s_{i,j}\left(\rho'_{i,j} Q^*_{i,j}\right)$$

An expression for $\rho'_{i,j}$ in terms of p'_o is now needed. Utilizing Equation (4.35) such an expression may be derrived as follows. Consider Equation (4.35):

$$\rho'_{i,j} = \frac{1}{2}\left(\rho'_j + \rho'_i\right) \tag{4.35}$$

Expressions for the density corrections at the node points are now needed. Following from the definition of total pressure (Equation 3.21) the following; for node *i*:

$$p'_{0i} = p'_{i_{dyn}} + p'_{i_s} \tag{3.21}$$

$$p'_{0i} = \frac{1}{2}\rho'_i u_i^2 + \rho'_i RT_i$$

Utilizing the conservation of mass principle, an expression for nodal velocity can be obtained.

$$u_i = \frac{\rho^*_{i,j} Q^*_{i,j}}{\rho^*_i A_i}$$

Substituting this expression in the Equation 3.21 and rearranging the terms result in

$$p'_{0i} = \rho'_i\left(\frac{1}{2}\left(\frac{\rho^*_{i,j} Q^*_{i,j}}{\rho^*_i A_i}\right)^2 + RT_i\right)$$

Create a new α and group the terms such that

$$\alpha_a = 1\Big/\left(RT_{i,j} + \frac{1}{2}\left(\frac{\rho^*_{i,j} Q^*_{i,j}}{\rho^*_a A_a}\right)^2\right)$$

$$with \quad a = i \; or \; j \quad and \quad i = 1,2,\ldots,I$$

Therefore

$$\rho'_i = p'_{0i}\,\alpha_i$$

The same holds true for $\rho'_j = p'_{0j}\,\alpha_j$. Substitute ρ_i and ρ_j in Term2.

$$\therefore \quad \sum_{j=1}^{J} s_{i,j}\left(\rho'_{i,j} Q^*_{i,j}\right) = \frac{1}{2}\sum_{j=1}^{J} s_{i,j}\left(p'_{0i}\,\alpha_i + p'_{0j}\,\alpha_j\right)\cdot Q^*_{i,j} \tag{C}$$

Substitute Equations (B) & (C) into (A)

$$\sum_{j=1}^{J} s_{i,j}\rho^{*}_{i,j}\frac{p'_{0j}-p'_{0i}}{\eta}+\frac{1}{2}\sum_{j=1}^{J} s_{i,j}\left(p'_{0i}\ \alpha_i+p'_{0j}\ \alpha_j\right)\cdot Q^{*}_{i,j}=-b_i$$

$$\sum_{j=1}^{J}\left(\rho^{*}_{i,j}\frac{p'_{0j}-p'_{0i}}{\eta}+\frac{1}{2}s_{i,j}\left(p'_{0i}\ \alpha_i+p'_{0j}\ \alpha_j\right)\cdot Q^{*}_{i,j}\right)=-b_i$$

$$\sum_{j=1}^{J}\left(\frac{\rho^{*}_{i,j}}{\eta}p'_{0j}-\frac{\rho^{*}_{i,j}}{\eta}p'_{0i}+\frac{1}{2}s_{i,j}p'_{0j}\ \alpha_j Q^{*}_{i,j}+\frac{1}{2}s_{i,j}p'_{0i}\ \alpha_i Q^{*}_{i,j}\right)=-b_i$$

Rearrange and regroup terms

$$\therefore\quad \sum_{j=1}^{J}\left[\frac{\rho^{*}_{i,j}}{\eta}+\frac{1}{2}s_{i,j}p'_{0j}\ \alpha_j Q^{*}_{i,j}\right]p'_{0j}-\left[\frac{\rho^{*}_{i,j}}{\eta}-\frac{1}{2}s_{i,j}p'_{0i}\ \alpha_i Q^{*}_{i,j}\right]p'_{0i}=-b_i$$

Create terms c_{ii} and c_{ij} such that

$$\sum_{j=1}^{J} c_{i,j}p'_{0j}-c_{i,i}p'_{0i}=-b_i$$

which becomes Equation (4.36)

$$p'_{0i}=\frac{\left(\sum_{j=1}^{J}\left(c_{i,j}p'_{0j}\right)+b_i\right)}{c_{i,i}}$$

$$c_{i,i}=\sum_{j=1}^{J}\left(\frac{\rho^{*}_{i,j}}{\eta}-\frac{1}{2}\alpha_j Q^{*}_{i,j}\right)s_{i,j}$$

$$c_{i,j}=\left(\frac{\rho^{*}_{i,j}}{\eta}+\frac{1}{2}\alpha_i Q^{*}_{i,j}\right)s_{i,j}$$

$$b_i=d_i+\sum_{j=1}^{J}\left(\rho^{*}_{i,j}Q^{*}_{i,j}s_{i,j}\right)$$

$$\eta=H_{i,j}\left(2Q^{*}_{i,j}\varphi+Q^{*2}_{i,j}\frac{\partial\varphi}{\partial Q^{*}_{i,j}}\right)$$

$$\alpha_a=1\Big/\left(RT_{i,j}+\frac{1}{2}\left(\frac{\rho^{*}_{i,j}Q^{*}_{i,j}}{\rho^{*}_{a}A_a}\right)^2\right)$$

$$with\quad a=i\ or\ j\ \ and\ \ i=1,2,\ldots,I$$

Note: if $\eta=s_{i,j}H_{i,j}\ldots$, then $s_{i,j}$ is on the outside in the expression for c_{ii} and c_{ij}.

Appendix F.

VALIDITY OF THE EMPLOYED STRONG FORM OF THE GOVERNING EQUATIONS (EQUATIONS (3.16) AND (3.20))

The text to follow is to prove that the strong form of the governing equations employed in this dissertation, is in fact in agreement with that used by others [20]. The difference is merely due to others employing a form in which all terms (p, u and ρ) have been reduced to 1-D.

FIGURE

Cross-flow Area: $A(x_1)$

- Compressible
- Viscous flow
- Steady State
- $dA=1dx_1$
- $A=2h$

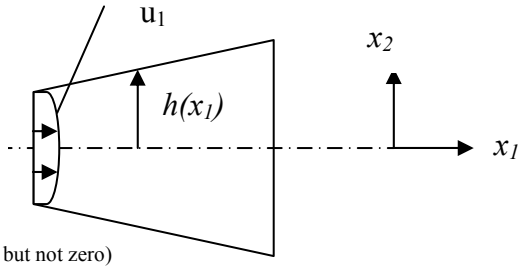

(u_2 not shown, but not zero)

MASS CONSERVATION

The continuity equation for a point in the flow field is given by

$$\frac{\partial}{\partial x_1}(\rho u_1)+\frac{\partial}{\partial x_2}(\rho u_2)=0 \qquad \text{(F1)}$$

Average each term over the cross-sectional area:

$$\int_{-h(x_1)}^{h(x_1)} \frac{\partial}{\partial x_1}(\rho u_1)dx_2 + \int_{-h(x_2)}^{h(x_2)} \frac{\partial}{\partial x_2}(\rho u_2)dx_2 = 0 \qquad \text{(F2)}$$

Consider the first term on the LH side of Equation (F2) and implement the Leibnitz's rule for $x_1;i=1,2$:

$$\int_{-h(x_1)}^{h(x_1)} \frac{\partial}{\partial x_1}(\rho u_1)dx_2 = \frac{\partial}{\partial x_i}\int_{-h(x_1)}^{h(x_1)}(\rho u_i)dx_2 - \rho(x_1,h)u_i(x_1,h)\frac{dh}{dx_1} + \rho(x_1,-h)u_i(x_1,-h)\frac{d(-h)}{dx_1} \tag{F3}$$

For viscous flow $u_i(x_i,h) = u_i(x_i,h) = 0$. Substitute this into the RH side of Equation (F3) and reduce it to

$$\begin{aligned}\int_{-h(x_1)}^{h(x_1)} \frac{\partial}{\partial x_1}(\rho u_1)dx_2 &= \frac{\partial}{\partial x_i}\int_{-h(x_1)}^{h(x_1)}(\rho u_i)dx_2 \\ &= \frac{d}{dx_i}\left[\overline{\rho u_i}\int_{-h(x_1)}^{h(x_1)}dx_2\right] \\ &= \frac{d}{dx_i}\left(\overline{\rho u_i}A\right)\end{aligned}$$

where $\overline{\rho u_i}$ denotes $\frac{1}{A}\int_{-h(x_1)}^{h(x_1)}(\rho u_i)dA$. Note that mathematically $\overline{\rho u_i} \neq \overline{\rho}\,\overline{u}_i$. Therefore,

$$\frac{d}{dx_1}\left(\overline{\rho u_1}A\right) + \frac{d}{dx_2}\left(\overline{\rho u_2}A\right) = 0 \tag{F4}$$

As $\overline{\rho u_2} = 0$ for symmetrical ducts

$$\frac{d}{dx_2}\left(\overline{\rho u_2}A\right) = 0$$

$$\frac{d}{dx_1}\left(\overline{\rho u_1}A\right) \neq \frac{d}{dx_1}\left(\overline{\rho}.\overline{u}_1 A\right) \tag{F5}$$

MOMENTUM CONSERVATION

The momentum equation in the direction of flow reads

$$\frac{\partial p}{\partial x_1} + \frac{\partial}{\partial x_1}\rho u_1 u_j = Fr \tag{F6}$$

Where x_1 is aligned wit the duct axisymmetric axis[1]. Average each term over the cross-sectional area:

[1] The averaged momentum equation in other directions is identically zero. This is trivial to prove and is left for to the reader.

$$\int_{-h(x_1)}^{h(x_1)} \frac{\partial p}{\partial x_1} dx_2 + \int_{-h(x_1)}^{h(x_1)} \frac{\partial}{\partial x_1} \left(\rho u_1 u_j\right) dx_2 = \int_{-h(x_1)}^{h(x_1)} Fr dx_2 \tag{F7}$$

Consider the pressure term on the LH side of Equation (F7) and apply the Leibnitz's rule. Assume $d(h)/dx_1 = d(-h)/dx_1$ and $p(x_1,h) = p(x_1,-h)$ due to symmetry:

$$\begin{aligned}
&\int_{-h(x_1)}^{h(x_1)} \frac{\partial p}{\partial x_1} dx_2 = \frac{\partial}{\partial x_1} \int_{-h(x_1)}^{h(x_1)} p dx_2 - p(x_1,h)\frac{dh}{dx_1} + p(x_1,-h)\frac{d(-h)}{dx_1} \\
&= \frac{d}{dx_1}\bar{p}A - p(x_1,h)\frac{dh}{dx_1} + p(x_1,-h)\frac{d(-h)}{dx_1} \\
&= 2h\frac{d}{dx_1}(\bar{p}) + 2\bar{p}\frac{d}{dx_1}(h) - p(x_1,h)\frac{dh}{dx_1} - p(x_1,h)\frac{d(h)}{dx_1} \\
&= 2h\frac{d}{dx_1}(\bar{p}) + 2\bar{p}\frac{dh}{dx_1} - 2p(x_1,h)\frac{dh}{dx_1} \\
&= A\frac{d\bar{p}}{dx_1} + \frac{dA}{dx_1}\left(\bar{p}(x_1) - p(x_1,h)\right)
\end{aligned} \tag{F8}$$

In the case that $\bar{p}(x_1) = p(x_1,h)$

$$\begin{aligned}
&\int_{-h(x_1)}^{h(x_1)} \frac{\partial p}{\partial x_1} dx_2 = A\frac{d\bar{p}}{dx_1} \\
&or \\
&\frac{d\bar{p}}{dx_1} = \frac{1}{A}\int_{-h(x_1)}^{h(x_1)} \frac{\partial p}{\partial x_1} dx_2
\end{aligned} \tag{F9}$$

In the case that $\bar{p}(x_1) \neq p(x_1,h)$

$$\begin{aligned}
&\int_{-h(x_1)}^{h(x_1)} \frac{\partial p}{\partial x_1} dx_2 = A\frac{d\bar{p}}{dx_1} + \frac{dA}{dx_1}\left(\bar{p}(x_1) - p(x_1,h)\right) \\
&or \\
&\frac{d\bar{p}}{dx_1} = \frac{1}{A}\left[\int_{-h(x_1)}^{h(x_1)} \frac{\partial p}{\partial x_1} dx_2 - \frac{dA}{dx_1}\left(\bar{p}(x_1) - p(x_1,h)\right)\right] \\
&\frac{d\bar{p}}{dx_1} \neq \frac{1}{A}\int_{-h(x_1)}^{h(x_1)} \frac{\partial p}{\partial x_1} dx_2
\end{aligned} \tag{F10}$$

Consider the second term in Equation (F6). Then, as previously

$$\frac{1}{A}\int_{-h(x_1)}^{h(x_1)}\frac{\partial}{\partial x_1}\rho u_1 u_j dx_2 = \frac{1}{A}\frac{d}{dx_1}\left(\overline{\rho u_1 u_j} A\right) \neq \frac{1}{A}\frac{d}{dx_1}\left(\overline{\rho}.\overline{u}_1.\overline{u}_j A\right) \tag{F11}$$

Substituting Equations (F10) and (F11) into the LH side of Equation (F7)

$$LH = \frac{d\overline{p}}{dx_1} + \frac{1}{A}\frac{dA}{dx_1}\left(\overline{p}(x_1) - p(x_1,h)\right) + \frac{1}{A}\frac{d}{dx_1}\left(\overline{\rho u_1 u_j} A\right) \tag{F12}$$

Fundamentally then

$$\frac{d\overline{p}}{dx_1} + \frac{1}{A}\frac{dA}{dx_1}\left(\overline{p}(x_1) - p(x_1,h)\right) + \frac{1}{A}\frac{d}{dx_1}\left(\overline{\rho u_1 u_j} A\right) \neq \frac{d\overline{p}}{dx_1} + \frac{1}{A}\frac{d}{dx_1}\left(\overline{\rho}.\overline{u}_1.\overline{u}_j A\right)$$

However, if the following approximation is made that $\overline{p}(x_1) \approx p(x_1,h)$

$$\frac{d\overline{p}}{dx_1} + \frac{1}{A}\frac{dA}{dx_1}\left(\overline{p}(x_1) - p(x_1,h)\right) + \frac{1}{A}\frac{d}{dx_1}\left(\overline{\rho u_1 u_j} A\right) \approx \frac{d\overline{p}}{dx_1} + \frac{1}{A}\frac{d}{dx_1}\left(\overline{\rho}.\overline{u}_1.\overline{u}_j A\right)$$

The above governing equation is identical to that of the other's report as well as that by Greyvenstein [20]. This proves that the strong form of the governing equation as employed in this dissertation must be supported by the examiner if considered clearly. Finally, it is noted that over the duct cross-sectional area A, it is clear that $\overline{u}_j = 0$. In passing, we note that even for laminar flow, there is an error made with this approximation.

Appendix G.

VALIDITY OF EQUATION (4.29)

In this appendix, a proof is documented to show that the proposed discreet momentum equation of others [20], which describes the elemental (global) momentum conservation pertaining to flow through a duct of constant cross-sectional area, is in fact an approximation and not exact. It will further be proven that the discreet equation employed in this dissertation represents the exact expression. This will be done with the proposed momentum Equation (23) of others as starting point such that there is no room left for doubt.

VALIDITY OF THE MOMENTUM EQUATION

Equation (23) of others;

$$\frac{\partial p}{\partial x} + \rho u \frac{\partial u}{\partial x} = -Fr \tag{23}$$

refers and is valid for both compressible and incompressible flow with variable cross-sectional area in a infinitesimal one-dimensional control volume. We will start at

$$\frac{dp}{dx_1} + \rho u \frac{du}{dx_1} = -Fr \tag{G1}$$

Applying the quotient rule

$$\frac{dp}{dx_1} + \frac{du}{dx_1} \rho u^2 - u \frac{du}{dx_1} \rho u = -Fr \tag{G2}$$

Consider the third term on the LH side. By introducing area, applying the quotient rule and ensuring mass conservation over the element, the latter term can be expressed as

$$u\frac{du}{dx_1}\rho u = \frac{u}{A}\left(A\frac{d}{dx_1}(\rho u)\right)$$
$$= \frac{u}{A}\left(\frac{d}{dx_1}(\rho u A) - \rho u\frac{dA}{dx_1}\right)$$
$$= \frac{u}{A}\left(0 - \rho u\frac{dA}{dx_1}\right)$$
$$= \chi$$

Thus, Equation (G2) becomes

$$\frac{dp}{dx_1} + \frac{du}{dx_1}\rho u^2 - \chi = -Fr \tag{G3}$$

Equation (G3) can now be integrated over the element

$$\int_{x_i}^{x_j}\frac{dp}{dx_1}dx + \int_{x_i}^{x_j}\frac{d}{dx_1}\rho u^2 dx - \int_{x_i}^{x_j}\chi dx = -\int_{x_i}^{x_j} Fr dx$$

$$\therefore p_j - p_i + \rho_j u_j^2 - \rho_i u_i^2 - \int_{x_i}^{x_j}\chi dx = -\overline{Fr}\Delta x \tag{G4}$$

where Δx denotes the length of the element. Implementing the total pressure concept as explained in this dissertation, i.e. Equation (3.21) and treating the subsequent dynamic pressure terms, Equation (G4) may be rewritten as

$$p_{0j} - p_{0i} + \frac{1}{2}\frac{A_i}{A_j}\left(1 - \frac{\rho_j A_j^2}{\rho_i A_i^2}\right)\rho_i u_i u_j - \int_{x_i}^{x_j}\chi dx = -\overline{Fr}\Delta x \tag{G5}$$

The expression above, as derived, is valid for both compressible and incompressible flow with variable cross-sectional area. In the case where the cross-sectional area remains constant, therefore $\chi=0$, Equation (G5) reduces to

$$p_{0j} - p_{0i} = -\overline{Fr}\Delta x + \frac{1}{2}\left(\frac{\rho_j}{\rho_i} - 1\right)\rho_i u_i u_j \tag{G6}$$

Equation (G6) is identical to that of others, i.e. equation (30), which was an area of concern. The latter equation is identical to that which the examiner obtained derived from Equation (4.24). Consequently Equation (G6) is then mathematically identical to Equation (4.29). As the aforementioned equations (Equation (G6) and (4.29)) were obtained via exact integration (no approximations made), these must be more accurate than that of others. This will be demonstrated in the following section. One may conclude that the latter expression is therefore more accurate than that of others.

VALIDATION OF THE ABOVE

Regarding the accuracy of the dissertation's formulation, the following comparative analysis was done to further validate which of the conflicting expressions (i.e. Equation (23) above and Equation (G6)) is in error (an approximation). This was done by choosing arbitrary functions (polynomials) for ρ and u and then calculating the resulting Δp_0 exactly. This can then be compared to that obtained via the expressions proposed by others as well as the author.

We commence by selecting the following equation for velocity:

$$u = x^2 + 2x + 3$$

Satisfying the continuity equation, i.e. $\frac{\partial}{\partial x}(\rho u) = 0$, the expression for ρ follows as

$$\rho = \frac{5}{x^2 + 2x + 3}$$

The above relations for velocity and density are now substituted into the momentum governing equation (i.e. Eq. (3.20)) for a constant area duct. After differentiation and integration it follows that:

$$dp_0 = Fr\Delta x + \frac{5}{2}(x_i^2 - x_j^2) + 5(x_i - x_j) \qquad \text{(G7)}$$

For the purposes of this response, $Fr\Delta x$ is kept constant at a value of -7.5 in all cases. The values of x are as follows:

$$x_i \in (2,4,6\ldots,40)$$
$$x_j \in (1,2,3\ldots,20)$$

Considering next the expressions for dp_0 proposed by others: a formulae for pressure drop can be derived (Eq.(29):Others) as

$$dp_0 = Fr\Delta x + \frac{1}{2}(\rho_j - \rho_i)\tilde{u}^2 \qquad \text{(G8)}$$

were $\tilde{u}^2 = \dfrac{u_i^2 + u_j^2}{2}$.

Therefore, substituting the relations for velocity and density into eq.(G8), dp_0 becomes:

$$\begin{aligned} dp_0 &= Fr\Delta x + \frac{1}{2}(\rho_j - \rho_i)\tilde{u}^2 \\ &= Fr\Delta x + \frac{1}{2}\left(\frac{5}{x_j^2 + 2x_j + 3} - \frac{5}{x_i^2 + 2x_i + 3}\right)\tilde{u}^2 \qquad \text{(G9)} \\ &= Fr\Delta x + \frac{1}{4}\left(\frac{5}{x_j^2 + 2x_j + 3} - \frac{5}{x_i^2 + 2x_i + 3}\right)\left((x_j^2 + 2x_j + 3)^2 + (x_i^2 + 2x_i + 3)^2\right) \end{aligned}$$

We now plot the Eq.(G9) against the exact solution Eq. (G7):

Appendices

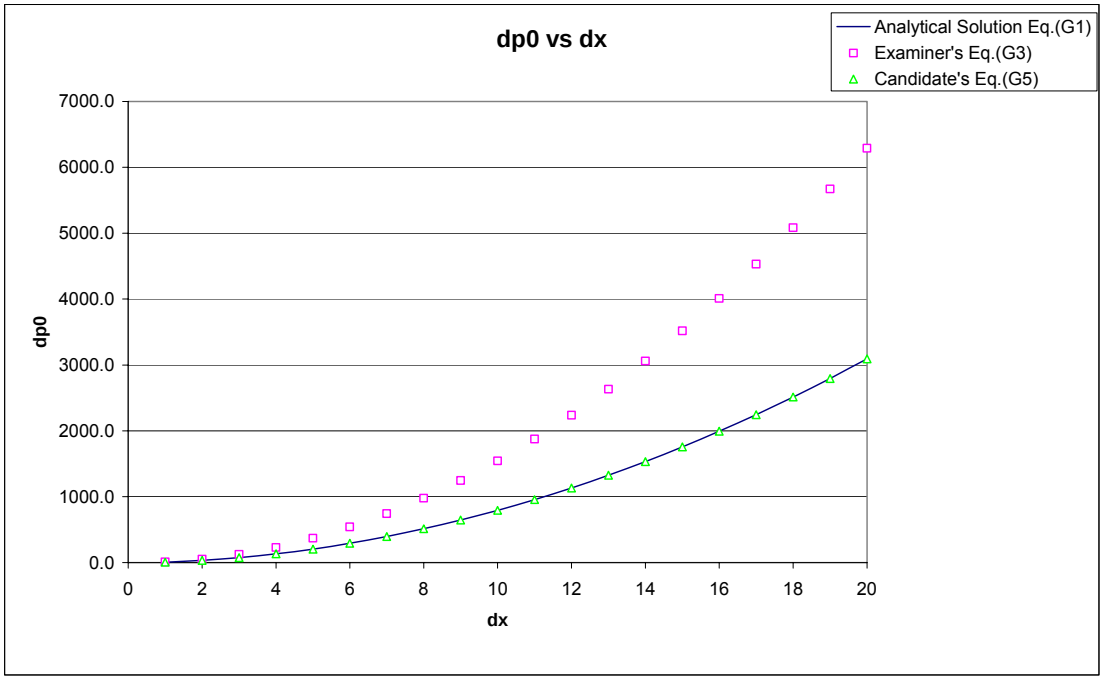

Thus, it is clear that the other's expression is not exact particularly if *dx* becomes large. Considering next the expression for dp_0 proposed by the author: Eq.(4.29) of the author was reduced to the same form to that of the above pressure drop equation (i.e. Eq.(G8)).

$$dp_0 = Fr + \frac{1}{2}(\rho_j - \rho_i)u_i u_j \qquad \text{(G10)}$$

By substituting the relations for velocity and density into Eq.(G10) it can be shown that Eq.(G10) is exactly the same as Eq.(G7):

$$\begin{aligned} dp_0 &= Fr\Delta x + \frac{1}{2}(\rho_j - \rho_i)u_i u_j \\ &= Fr\Delta x + \frac{1}{2}\left(\frac{5}{x_j^2 + 2x_j + 3} - \frac{5}{x_i^2 + 2x_i + 3}\right)\left((x_j^2 + 2x_j + 3)(x_i^2 + 2x_i + 3)\right) \qquad \text{(G11)} \\ &= Fr\Delta x + \frac{5}{2}(x_i^2 - x_j^2) + 5(x_i - x_j) \end{aligned}$$

Therefore, the greater *dx*, the greater the error of other's Eq. (29) becomes compared to the analytical solution. However, it is evident that Eq.(4.24) as described in this dissertation satisfies the analytical solution exactly as shown.